Sistemas deposicionais

Sistema deposicional: conjunto de depósitos sedimentares designado e definido com base em ambientes fisiográficos de sedimentação geneticamente relacionados (ex. sistema deposicional fluvial, eólico, deltaico, barra-barreira etc.).

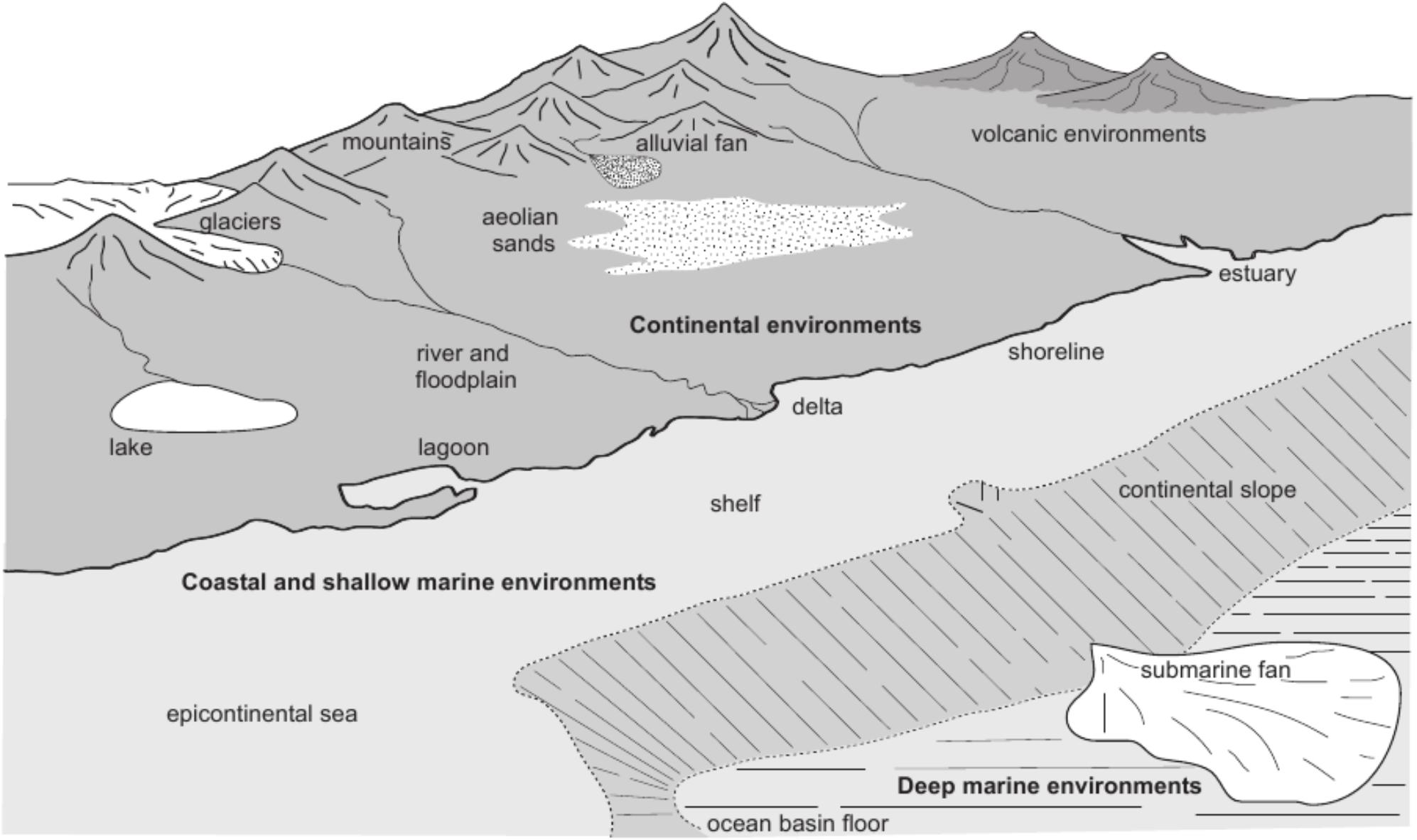
mountains
alluvial fan
volcanic environments
glaciers
aeolian
sands
estuary
Continental environments
river and
floodplain
shoreline
delta
lake
lagoon
shelf
continental slope
Coastal and shallow marine environments
submarine fan
epicontinental sea
Deep marine environments
ocean basin floor

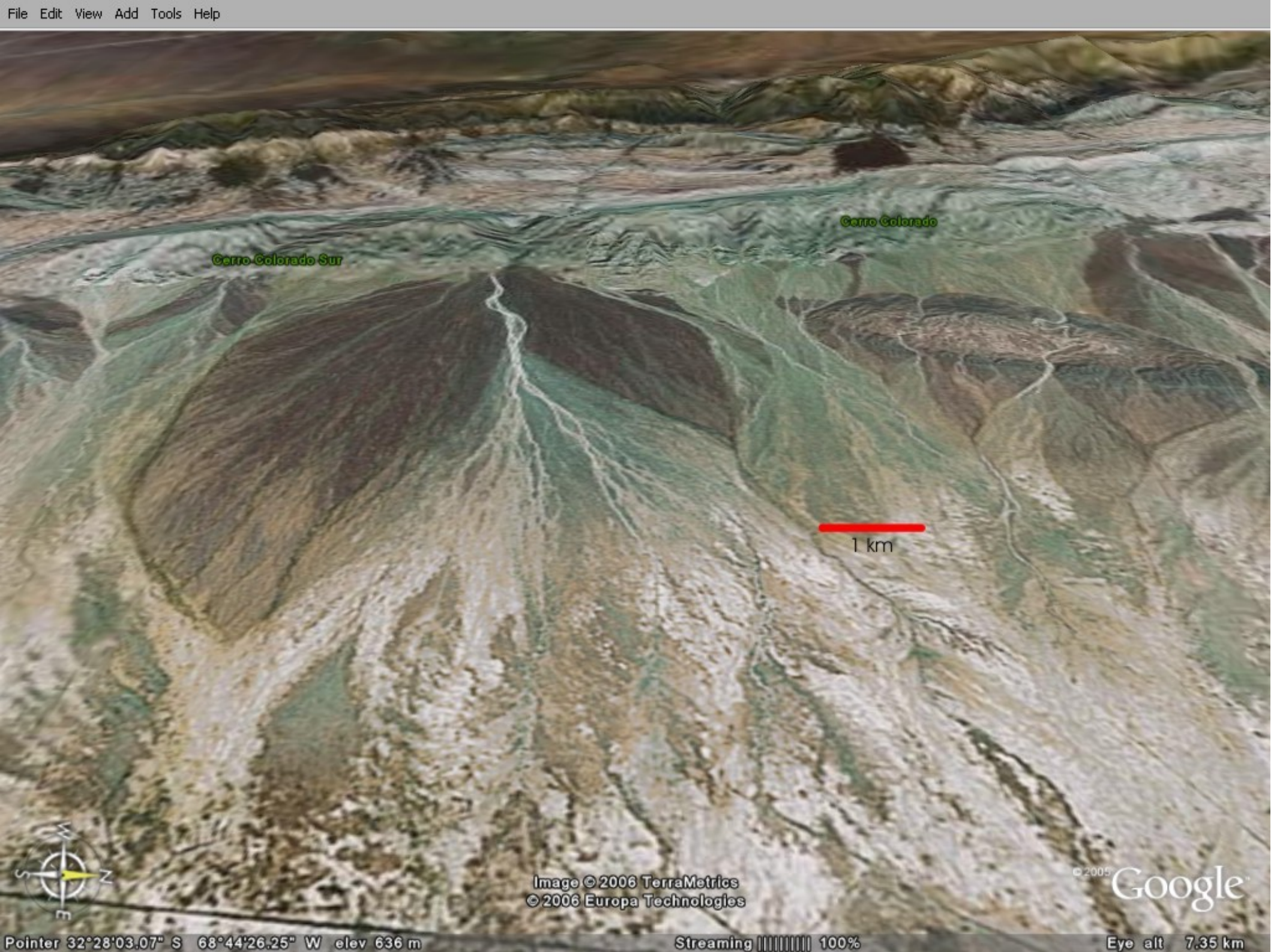
File Edit View Add Tools Help
Cerro Colorado
Cerro Colorado Sur
1 km
Image © 2006 TerraMetrics
© 2006 Europa Technologies
© 2005 Google
Pointer 32°28'03.07" S 68°44'26.25" W elev 636 m
Streaming 100%
Eye alt 7.35 km

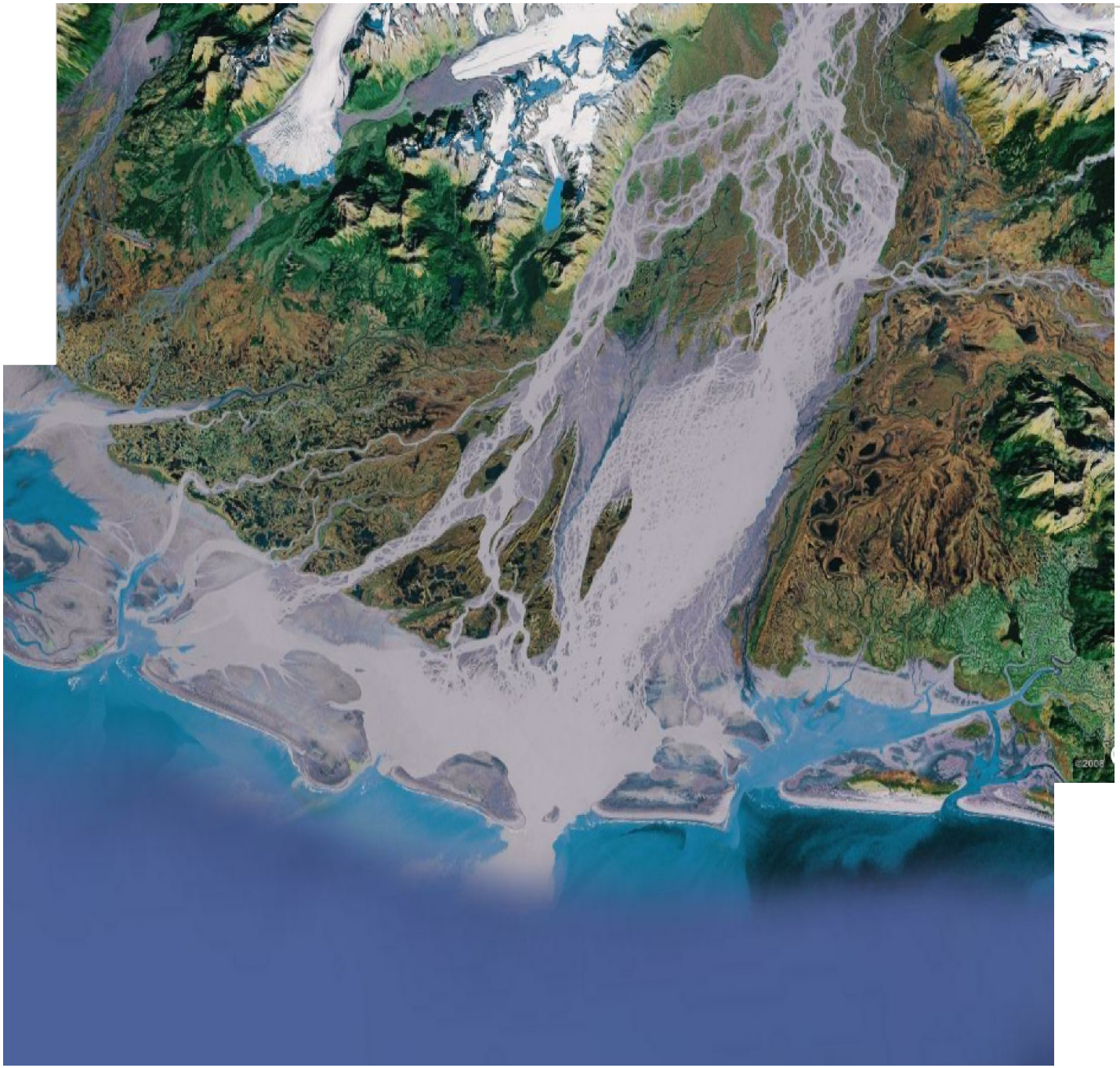
©2008


File Edit View Add Tools Help
N
W
E
S
Image © 2006 TerraMetrics
2 km
© 2005 Google
Pointer 23°08'08.33" S 45°50'18.92" W elev 551 m
Streaming 100%
Eye alt 14.97 km


File Edit View Add Tools Help
N
W
E
S
Image © 2006 TerraMetrics
5 km
©2005 Google
Pointer 29°07'53.53" N 89°14'39.56" W elev 0 m
Streaming ||||||||| 100%
Eye alt 70.15 km

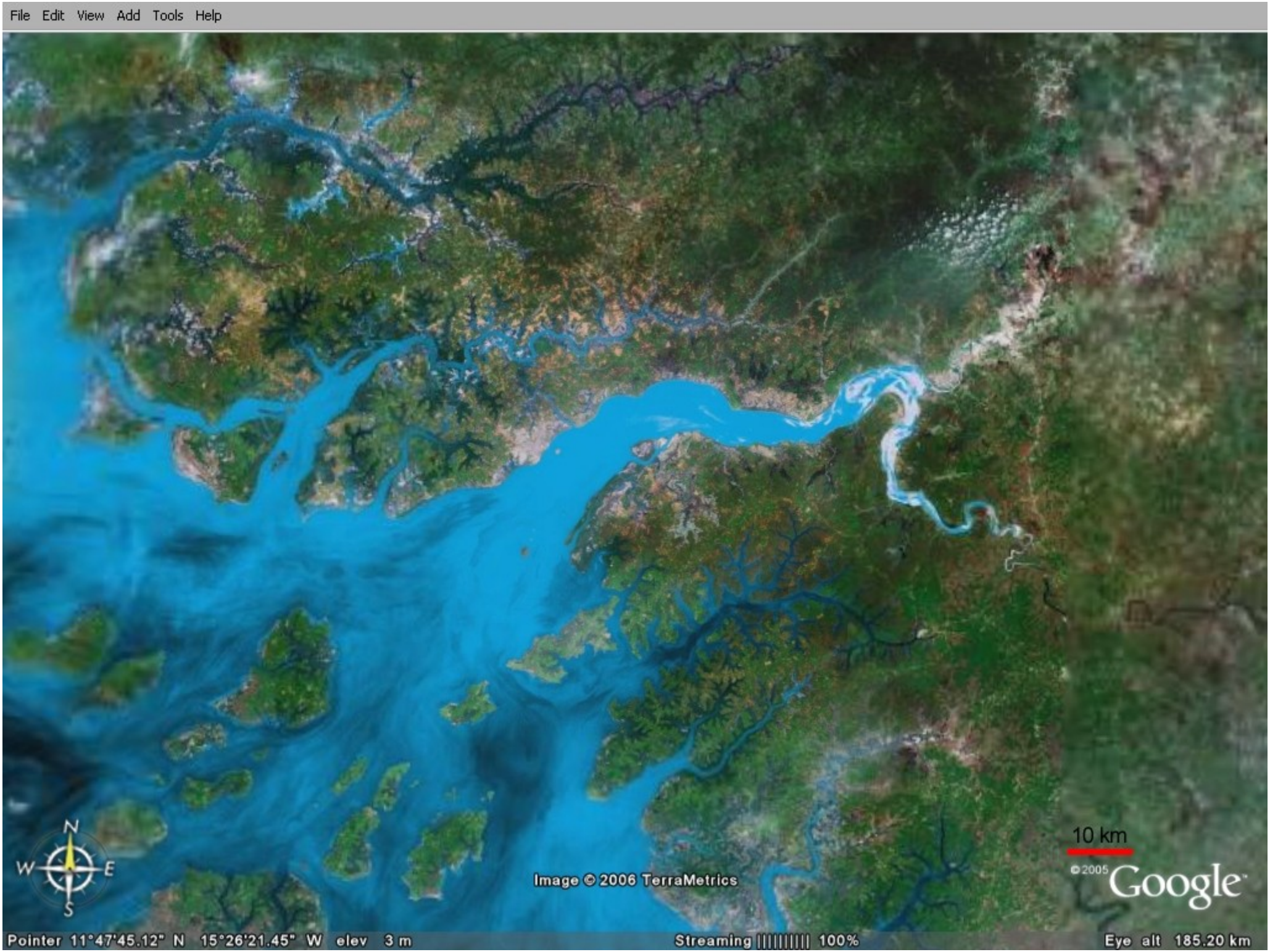
File Edit View Add Tools Help
N
W
E
S
Image © 2006 TerraMetrics
10 km
©2005 Google
Pointer 11°47'45.12" N 15°26'21.45" W elev 3 m
Streaming 100%
Eye alt 185.20 km

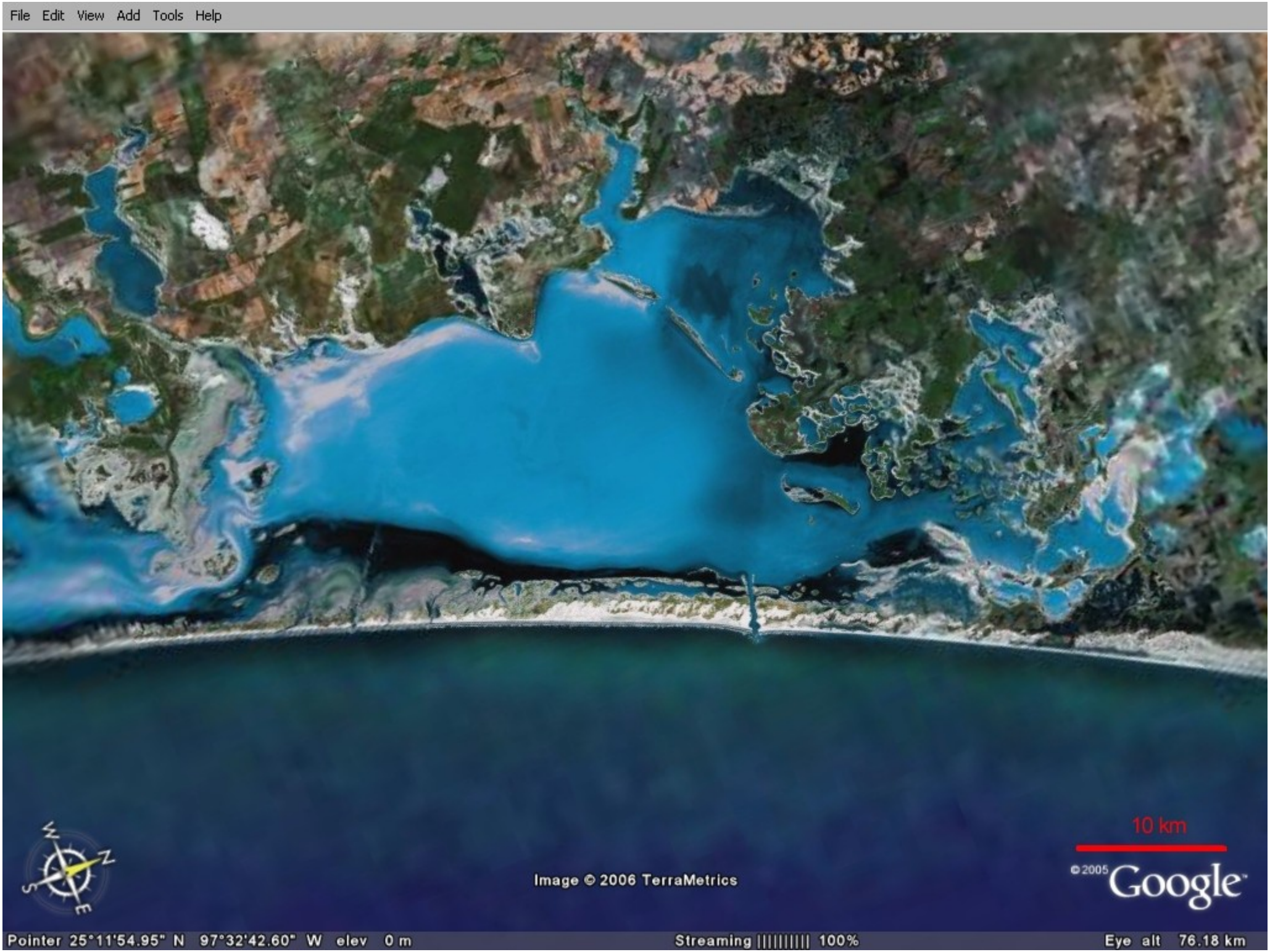
File Edit View Add Tools Help
Image © 2006 TerraMetrics
10 km
© 2005 Google
Pointer 25°11'54.95" N 97°32'42.60" W elev 0 m
Streaming 100%
Eye alt 76.18 km

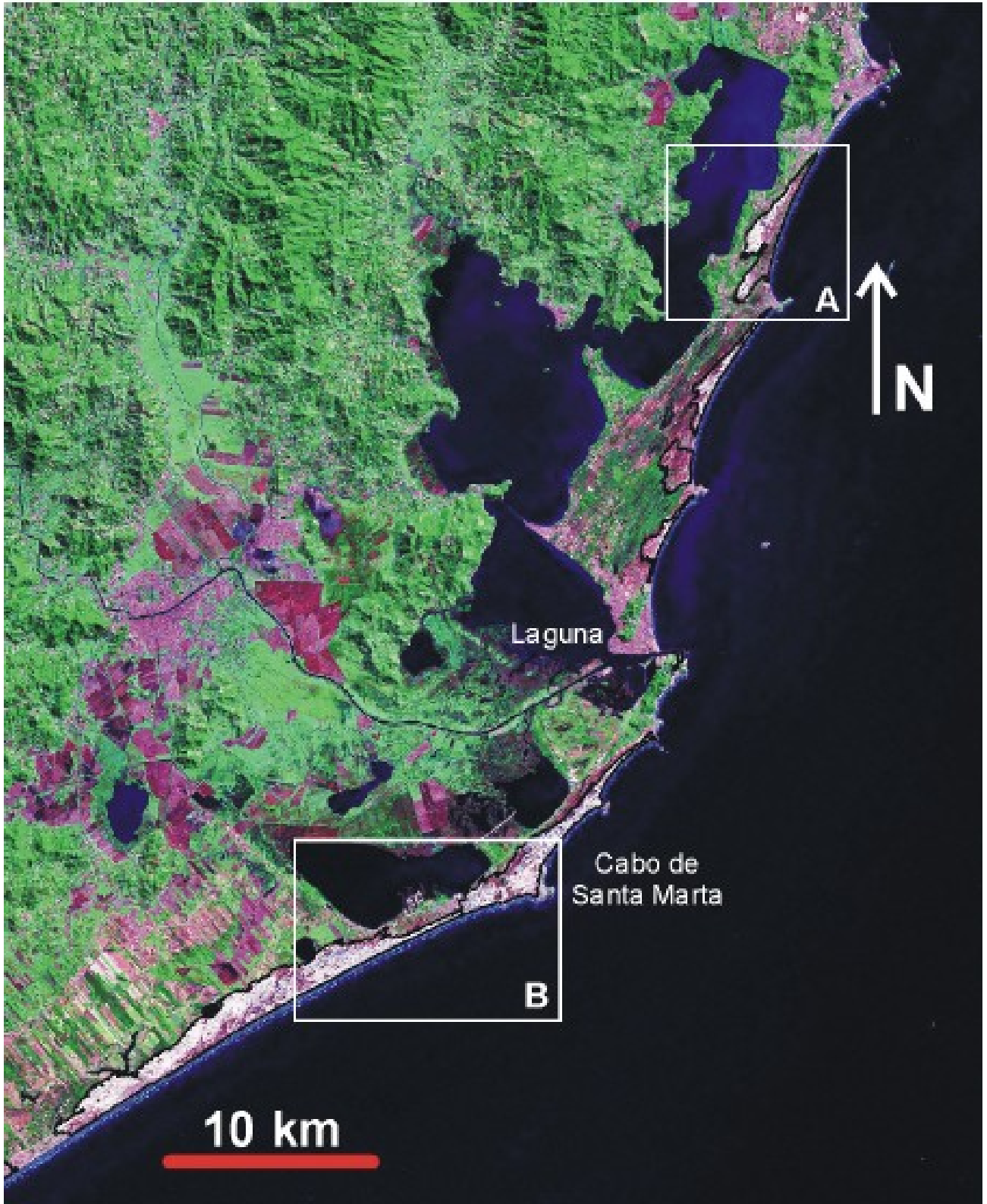

Sistemas deposicionais do litoral centro-sul catarinense


1,5 km
B


File Edit View Add Tools Help
10 km
N
W
E
S
Image © 2006 TerraMetrics
© 2005 Google
Pointer 21°50'51.96" S 41°20'45.73" W elev 4 m
Streaming 100%
Eye alt 137.12 km

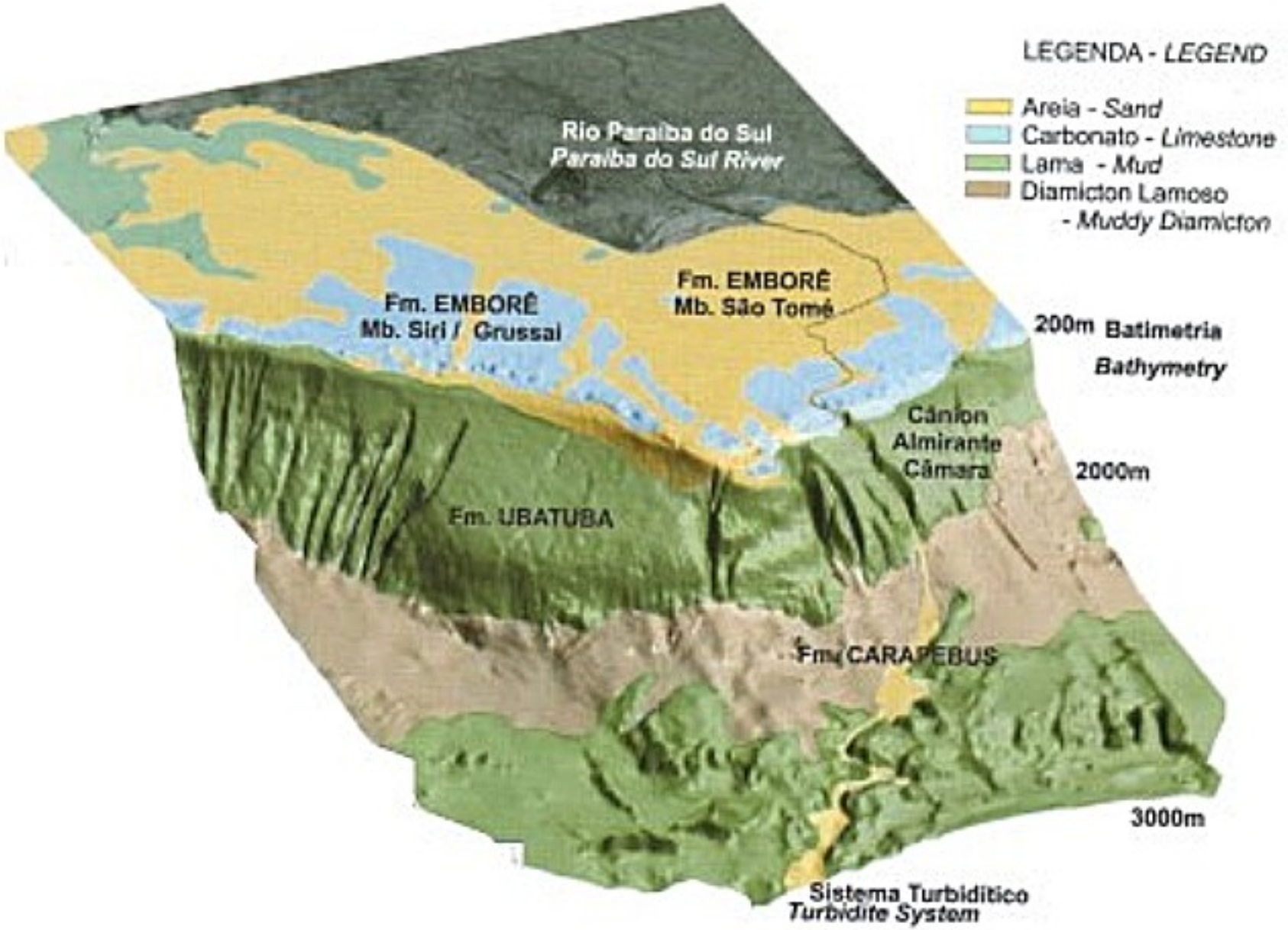
LEGENDA - LEGEND
Areia - Sand
Carbonato - Limestone
Lama - Mud
Diamicton Lamoso
- Muddy Diamicton
Rio Paraíba do Sul
Paraíba do Sul River
Fm. EMBORÊ
Mb. Siri / Grussaí
Fm. EMBORÊ
Mb. São Tomé
200m Batimetria
Bathymetry
Cânion
Almirante
Câmara
2000m
Fm. UBATUBA
Fm. CARAPEBUS
3000m
Sistema Turbidítico
Turbidite System

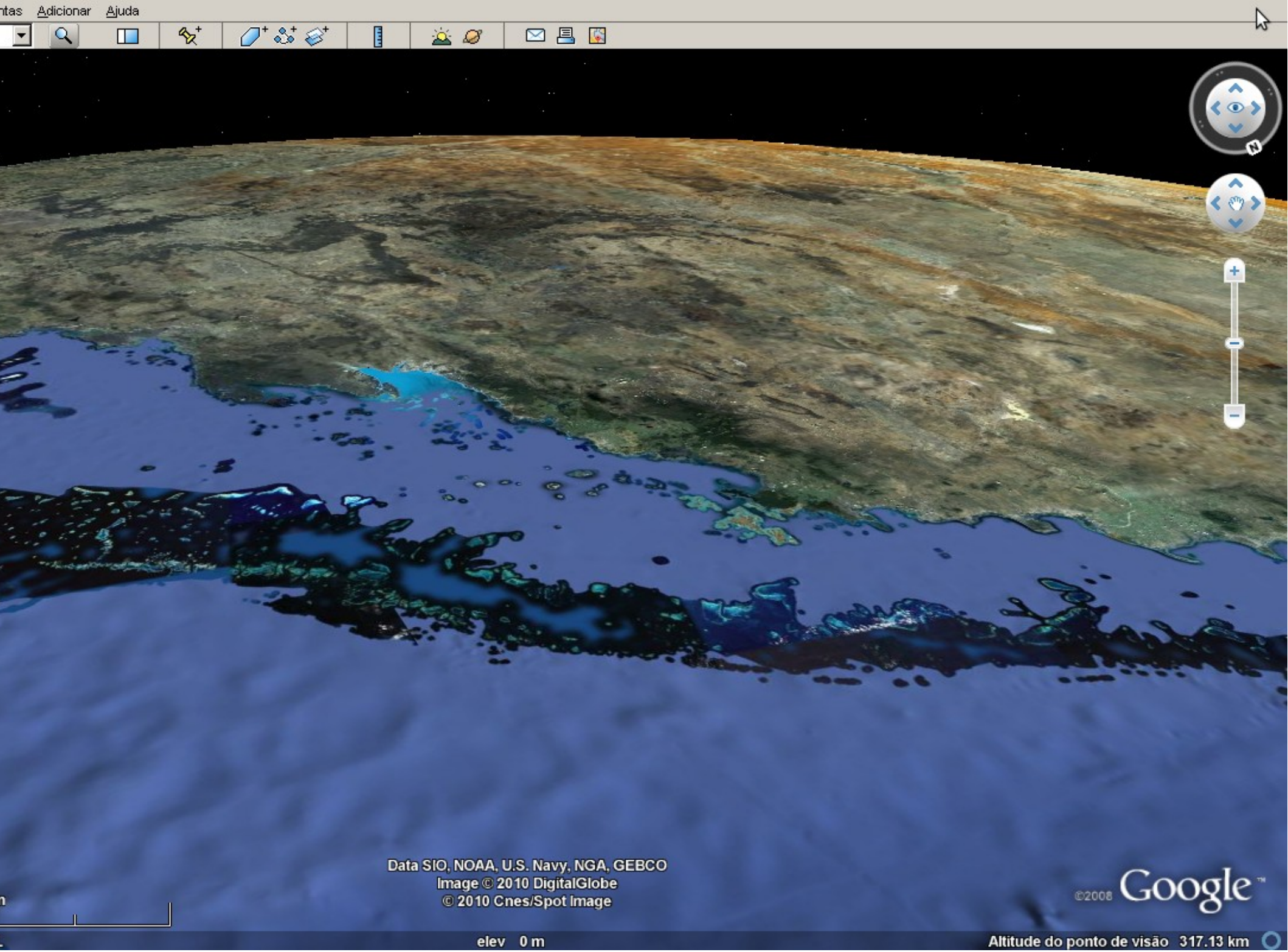
ntas Adicionar Ajuda
Data SIO, NOAA, U.S. Navy, NGA, GEBCO
Image © 2010 DigitalGlobe
© 2010 Cnes/Spot Image
©2008 Google
elev 0 m
Altitude do ponto de visão 317.13 km

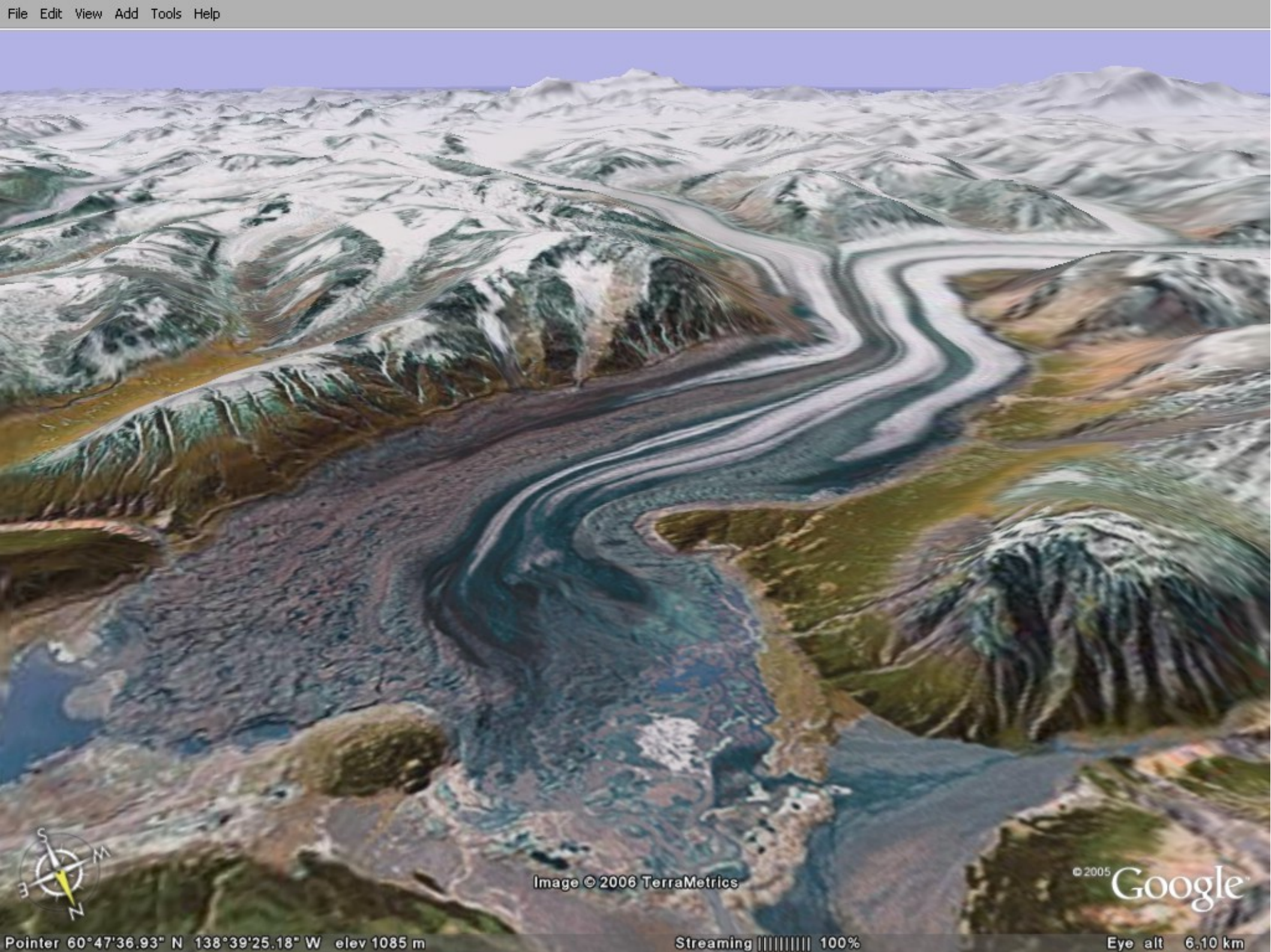
File Edit View Add Tools Help
Image © 2006 TerraMetrics
© 2005 Google
Pointer 60°47'36.93" N 138°39'25.18" W elev 1085 m
Streaming 100%
Eye alt 6.10 km


File Edit View Add Tools Help
Image © 2006 TerraMetrics
Google
Pointer 60°52'47.01" N 149°20'17.23" W elev 675 m
Streaming 100%
Eye alt 30.52 km

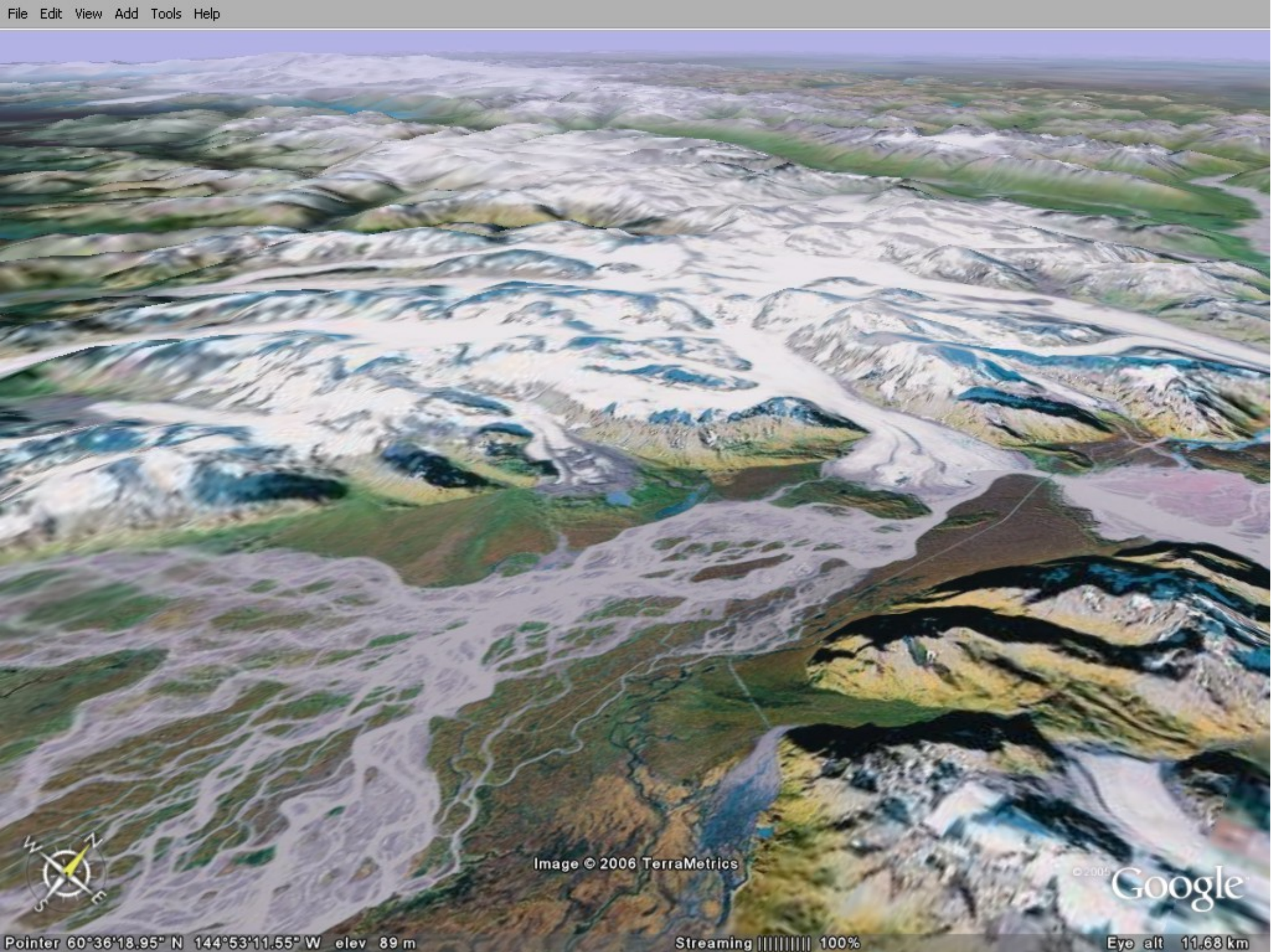
File Edit View Add Tools Help
Image © 2006 TerraMetrics
Google
Pointer 60°36'18.95" N 144°53'11.55" W elev 89 m
Streaming 100%
Eye alt 11.68 km


2010 m
Image © 2010 DigitalGlobe
© 2010 Cnes/Spot Image
Image © 2010 TerraMetrics
Data SIO, NOAA, U.S. Navy, NGA, GEBCO
19°05'50.25" S 12°37'14.08" L
elev 94 m
5 A

Sand dunes in Swakopmund, Namibia
Photograph by Cary Wolinsky

NATIONAL GEOGRAPHIC

Introdução aos sistemas deposicionais fluviais

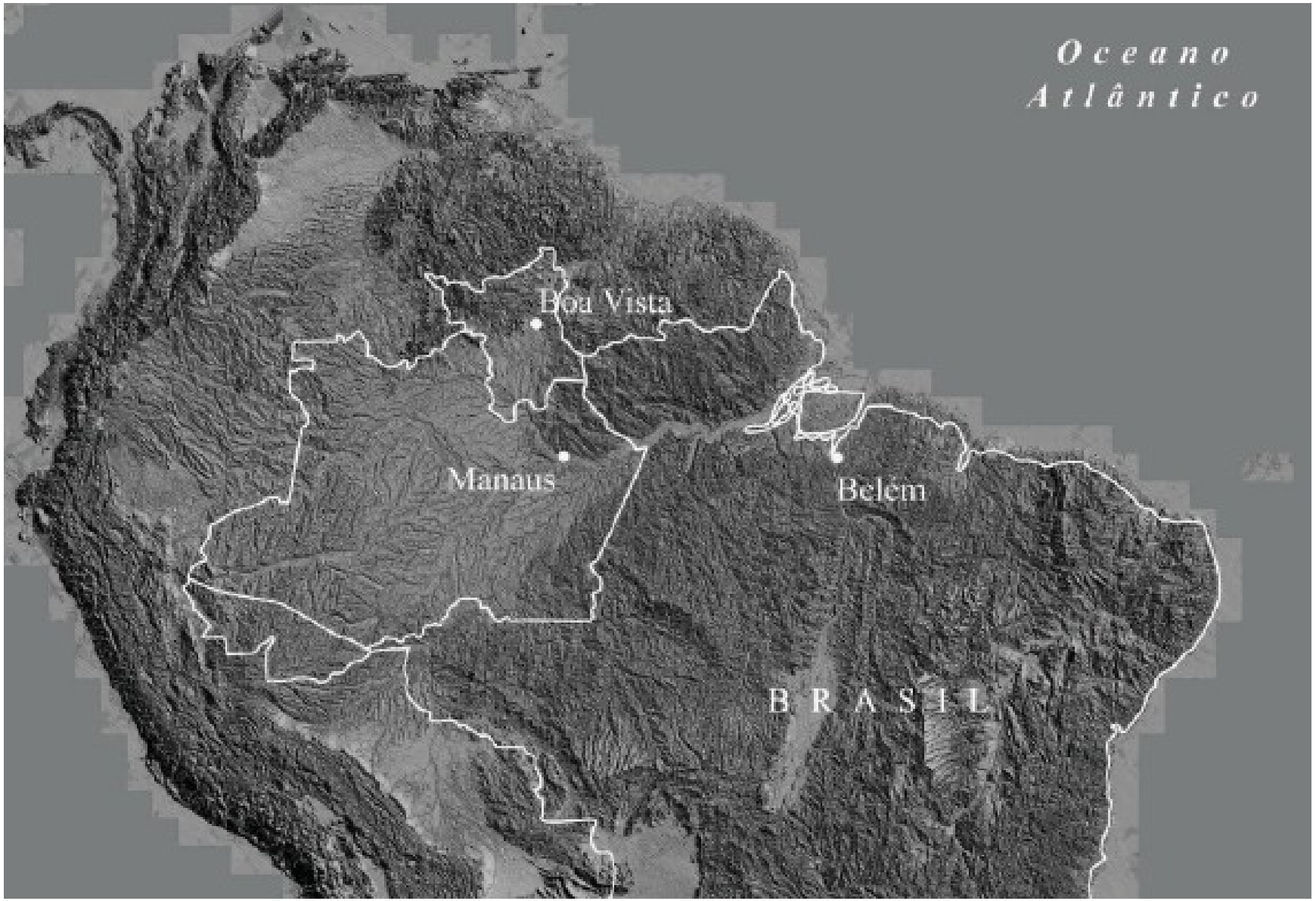
Oceano
Atlântico
Boa Vista
Manaus
Belém
BRASIL


Caracas
VENEZUELA
Georgetown
Atlantic Ocean
Orinoco
GUYANA
Bogotá
COLOMBIA
Boa Vista
Branco
Negro
Vaupés
Apaporis
Caquetá
Japurá
Trombetas
Paru
Jari
Macapá
Para
Belém
Quito
ECUADOR
Putumayo
Amazon
Santarém
Manaus
Napo
Pastaza
Tigre
Iquitos
Marañón
Javary
Juruá
Purus
Madeira
Tapajós
Iriri
Huallaga
Ucayali
Pucallpa
Rio Branco
Porto Velho
Juruena
Teles Pires
Xingu
Tocantins
Acre
Madre de Dios
Machado
Arinos
Tambo
Ene
Mantaro
Apurimac
Guaporé
Lima
Cusco
Beni
Mamoré
Araguaia
PERU
Brasília
La Paz
Grande
Cochabamba
Santa Cruz
BRAZIL
Pacific Ocean
BOLIVIA
Rio de Janeiro
São Paulo

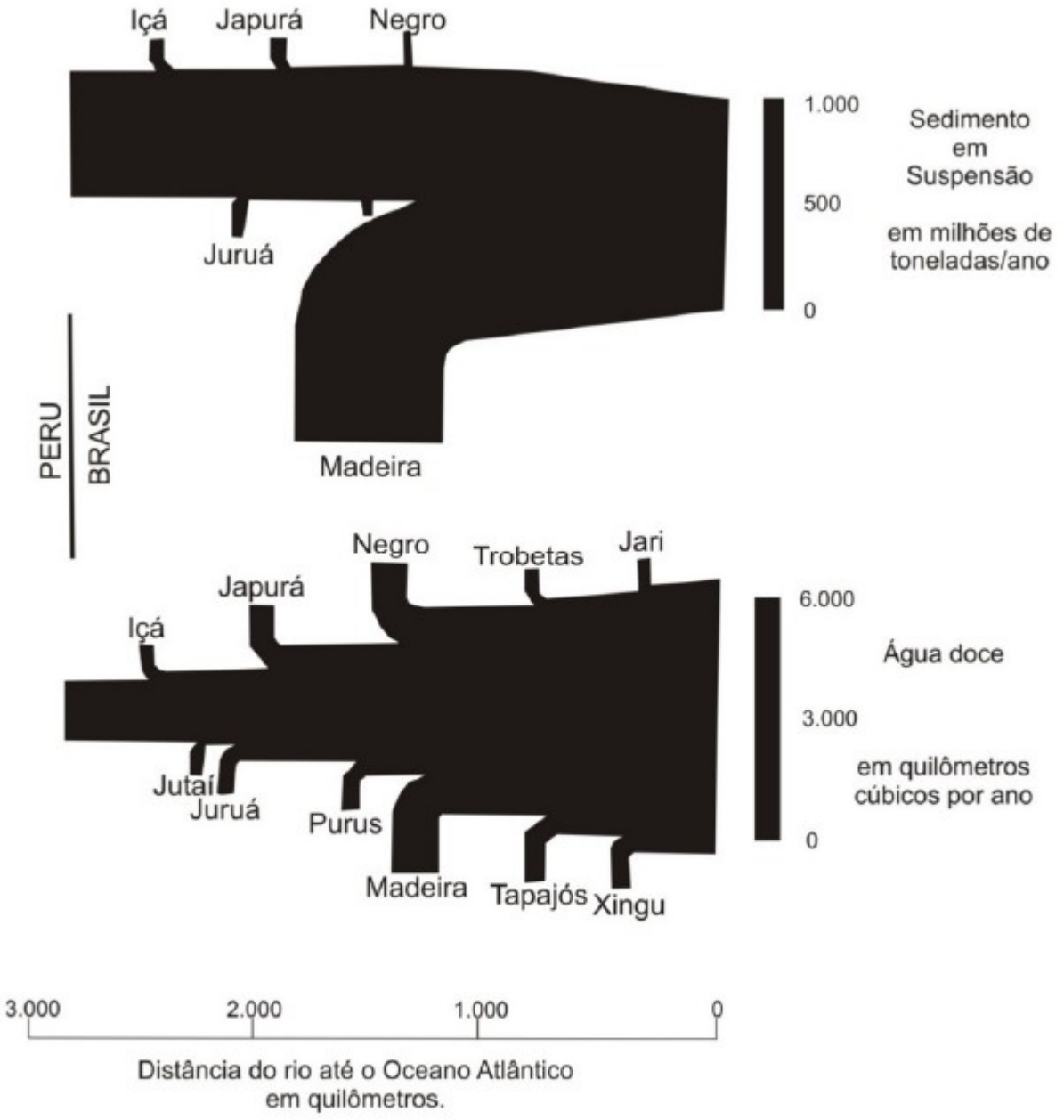

Figura 08 - Descarga média de sedimentos no rio Amazonas (acima) e carga de água doce na calha principal do rio Amazonas (abaixo). Modificado de (Meade, 2007).

Deposição é função da capacidadede transporte – diminuição dadeclividade para jusante (geralmente compensada por aumento da vazão dos rios)

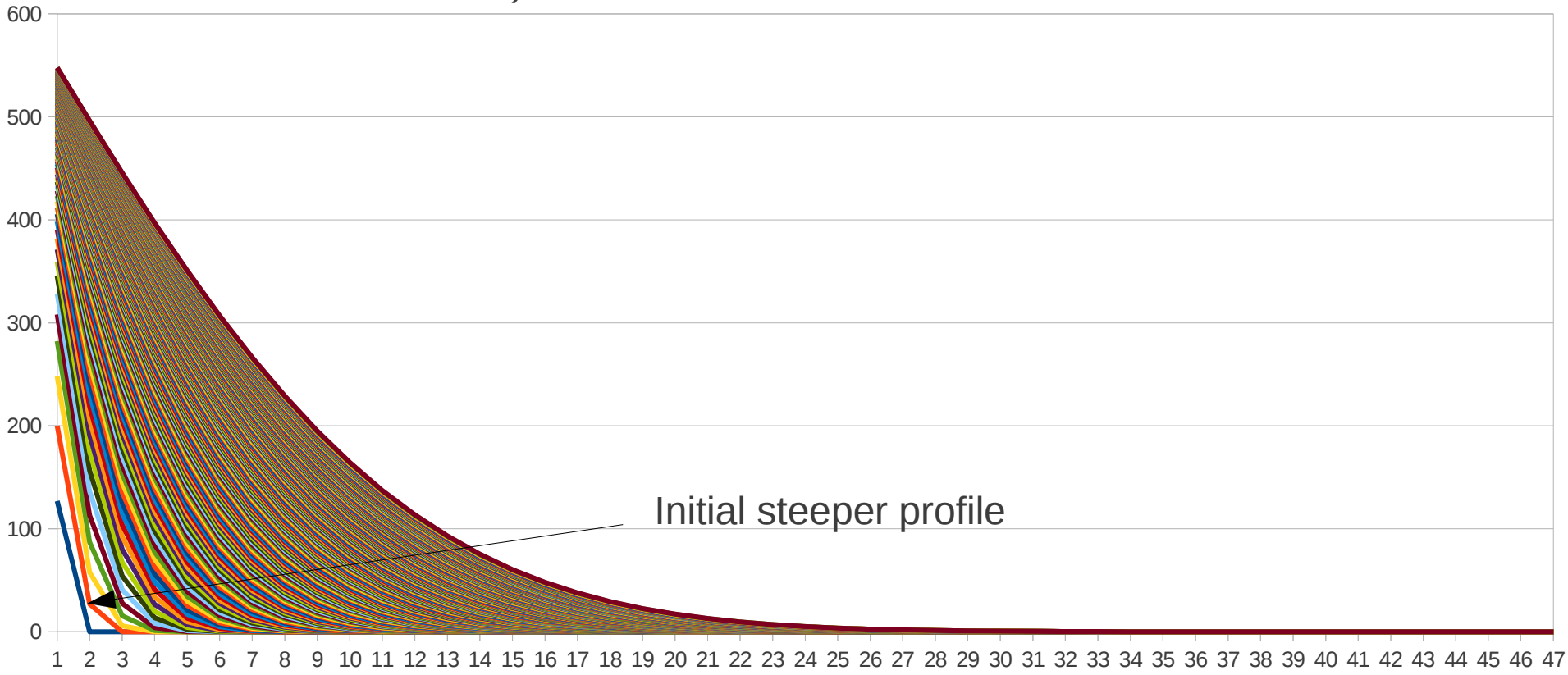

Sistema fluvial – estilos de canal e cinturões de canais

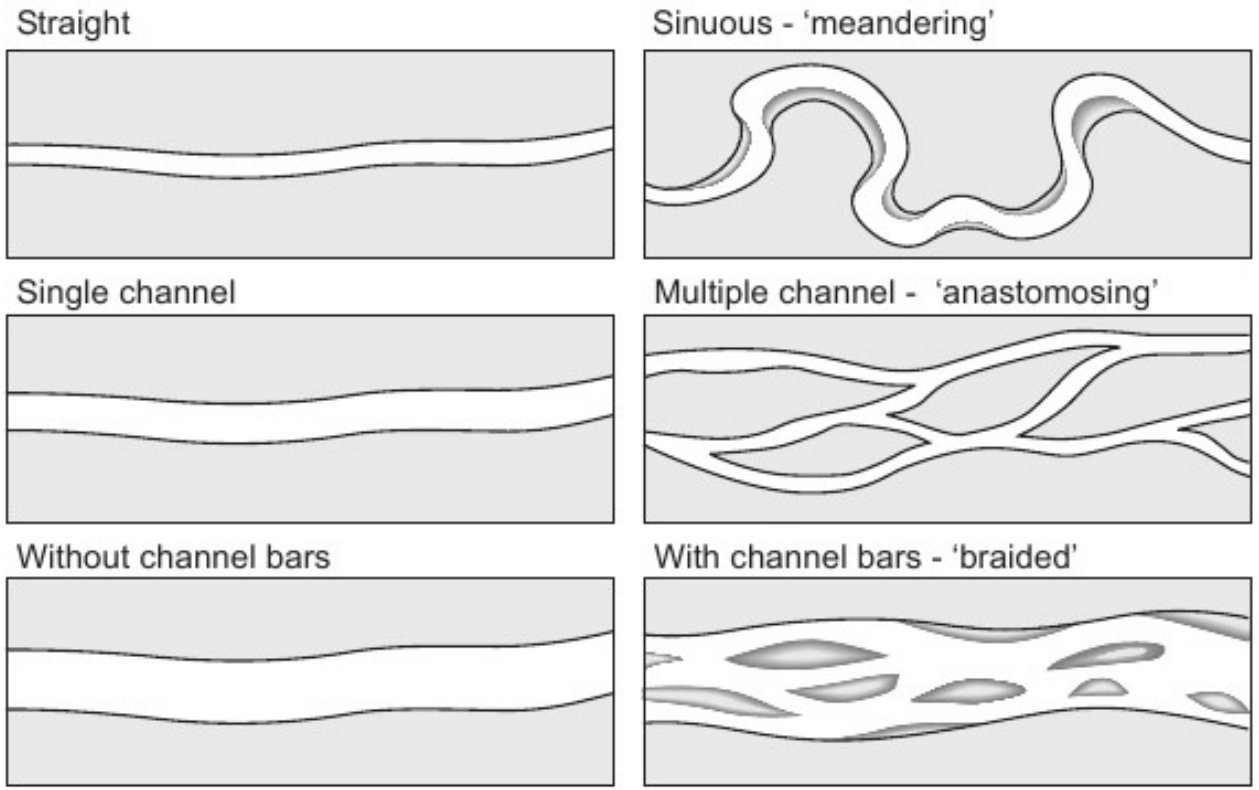

Fig. 9.3 Several types of river can be distinguished, based on whether the river channel is straight or sinuous (meandering), has one or multiple channels (anastomosing), and has in-channel bars (braided). Combinations of these forms can often occur.

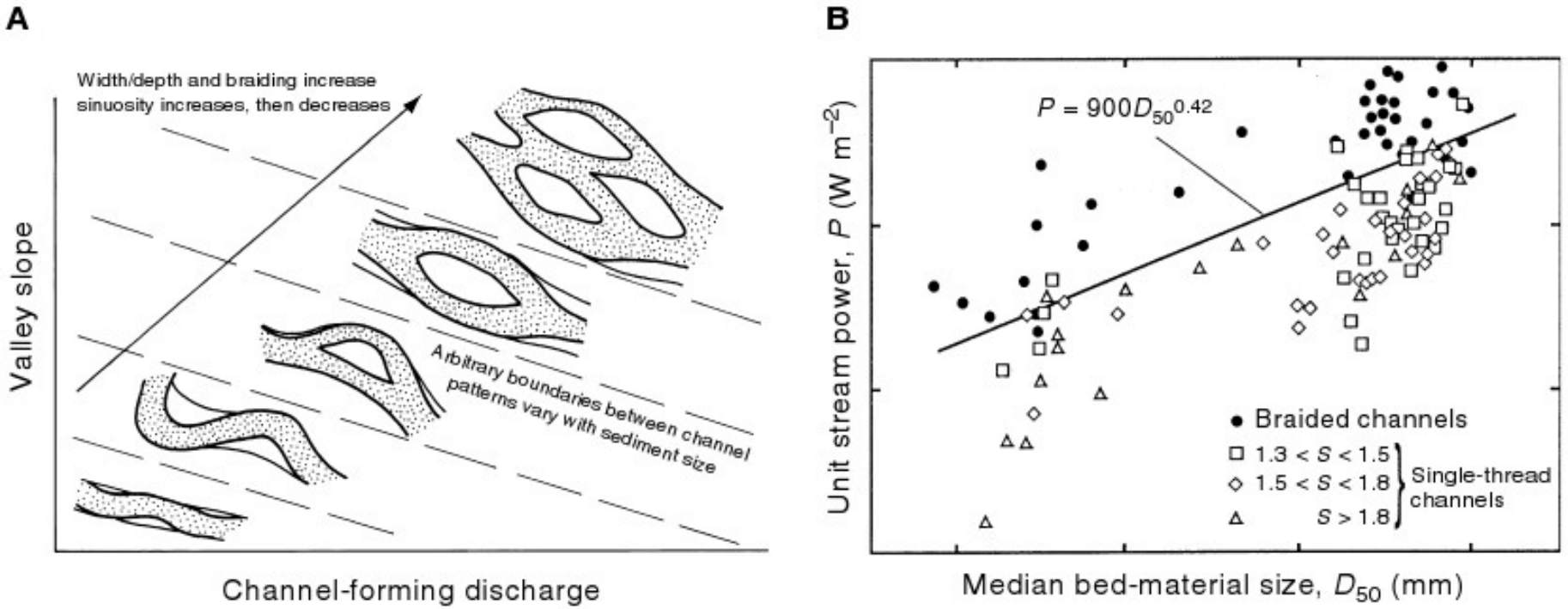

FIGURE 13.17. (A) Gradual variation of equilibrium channel patterns with channel-forming water discharge, valley slope, and sediment size. (B) Prediction of channel patterns as a function of stream power per unit bed area and bed material size; S = sinuosity. After Van Den Berg (1995).

Rios retilíneos

Rios meandrantes

Rio Purus – estável em 30 anos

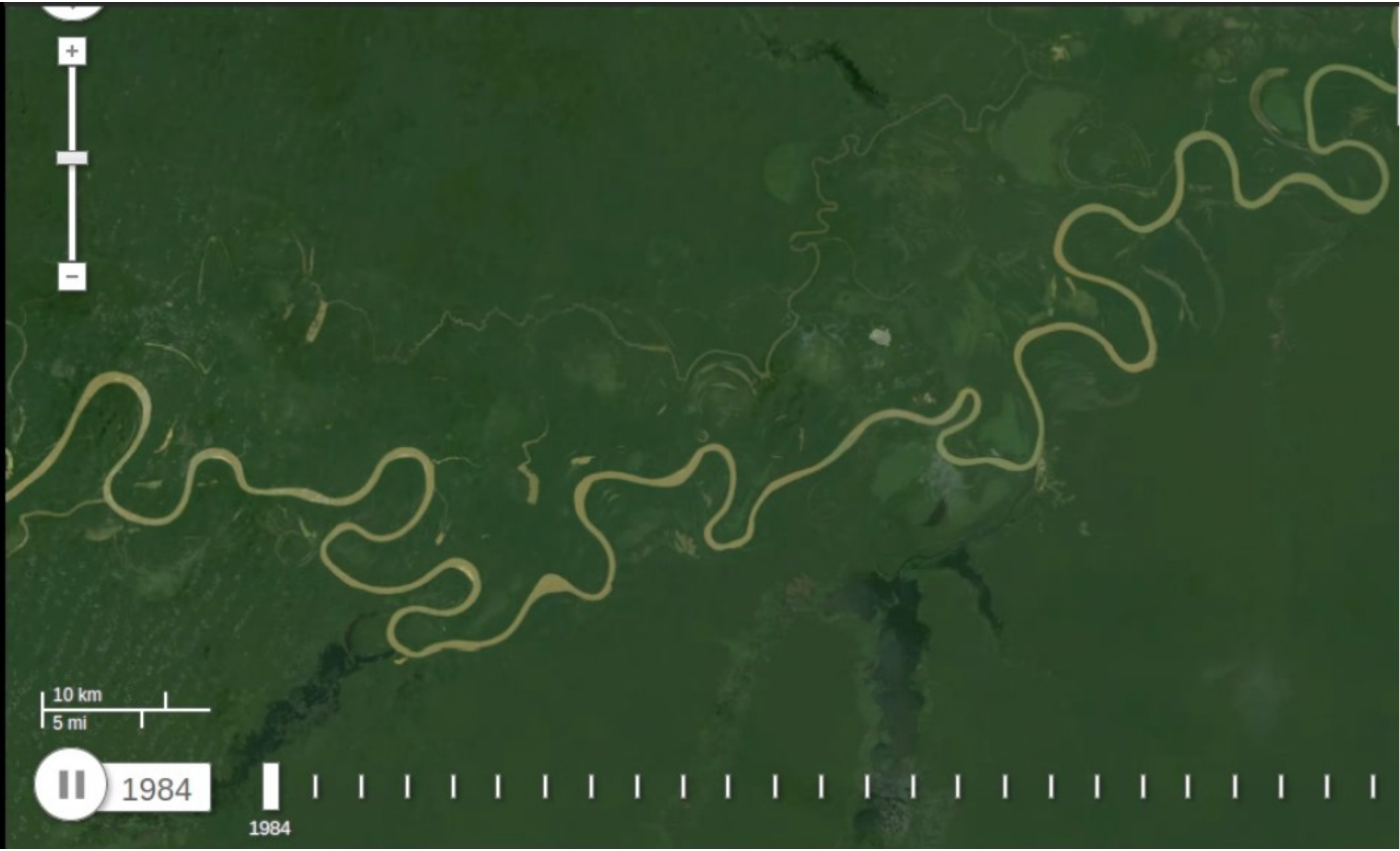

Rios meandrantes

Rio Javari– dinâmica em 20 anos

Rios *wandering*

Meandrantes multicanais
Rio Solimões

Rios *wandering*

Rio Solimões – dinâmica em 20 anos

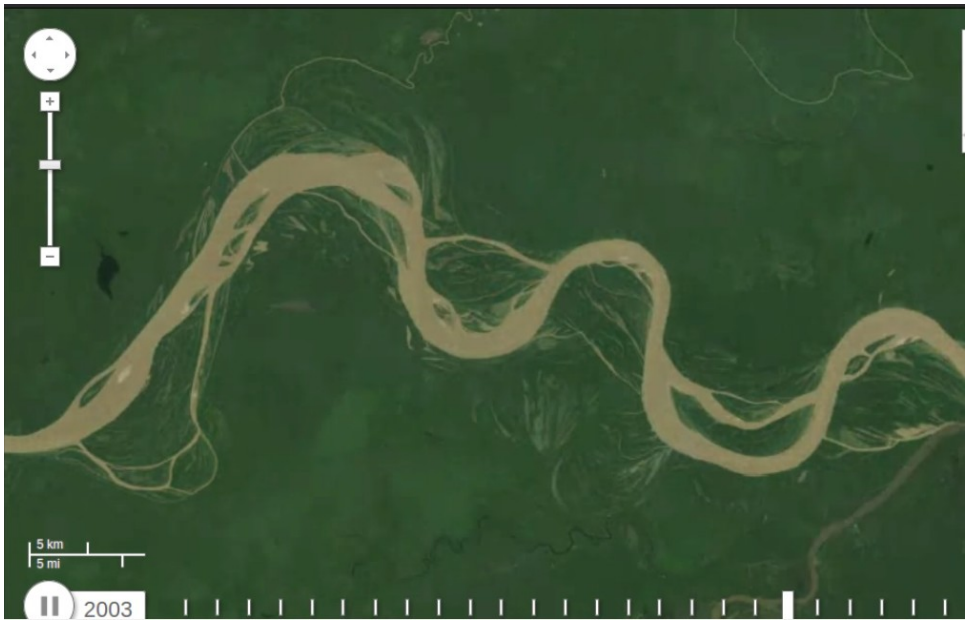

Rios *wandering*

Meandrantes multicanais
Riu Indo – Paquistão
Índice de entrelaçamento 2 a 3.

Rios entrelaçados

Rio Brahmaputra – Índia
Ìndice de entrelaçamento 3 a 5.

Rios entrelaçados

Rio Brahmaputra – Bangladesh – alto índice de entrelaçamento

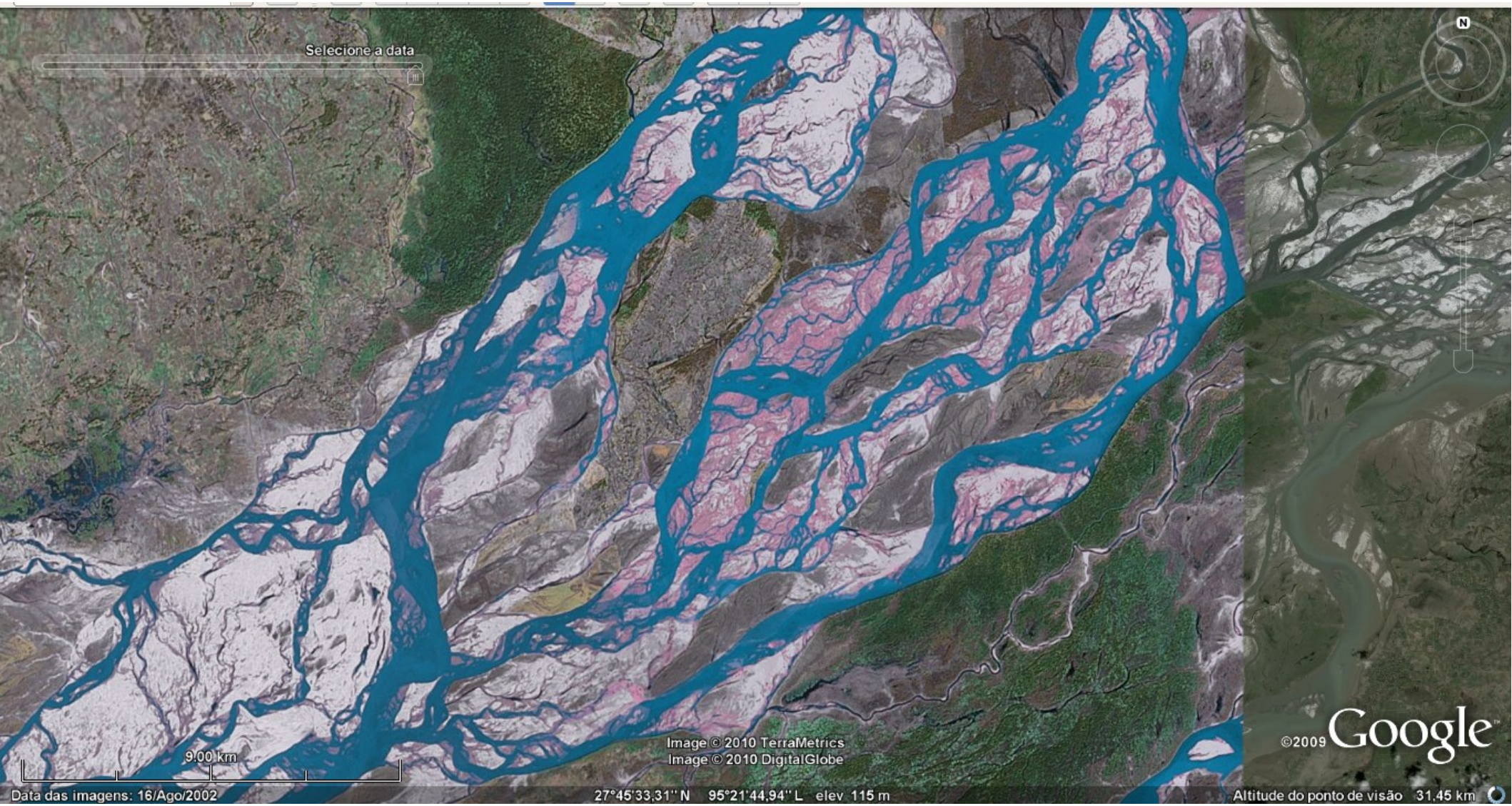

Rios de estilo indefinido

Rio Negro – macroformas de preenchimento de lago barrado?

Um estilo para cada rio?

Três estilos ao longo do Rio Indo – Paquistão.

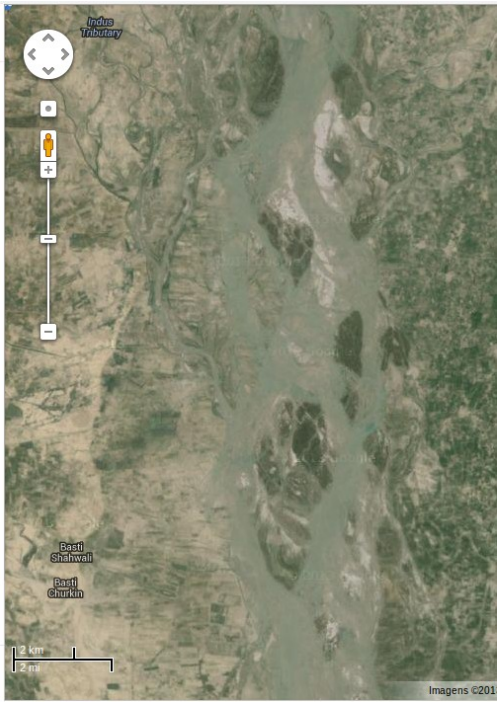

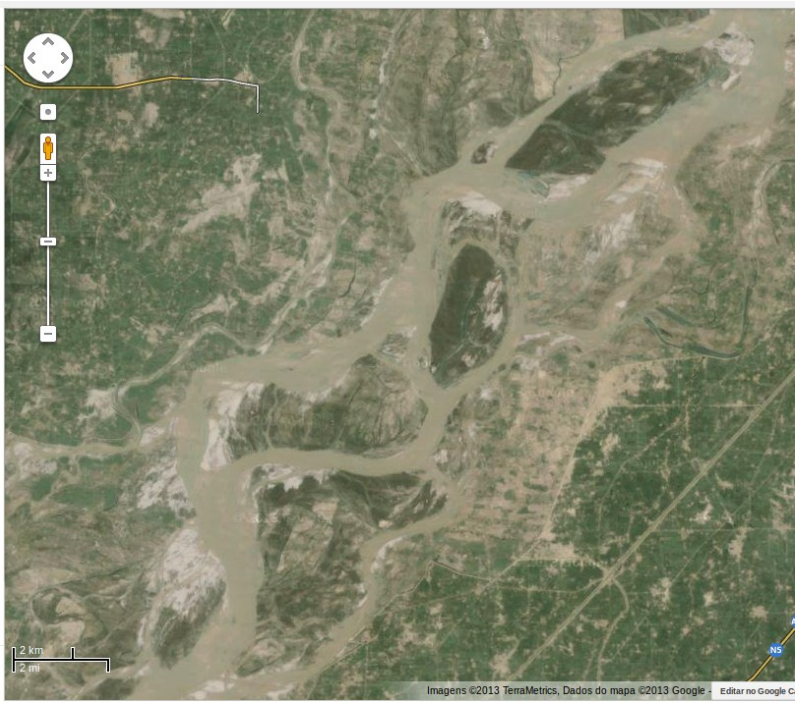

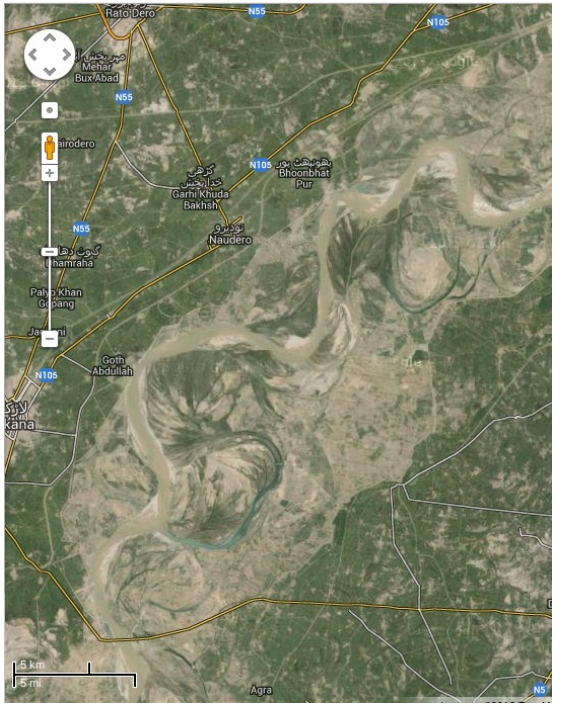

Padrões de canal vs. padrões de cinturões de canais

Padrão contributário em rios meandrantes e wandering – planíce amazônica

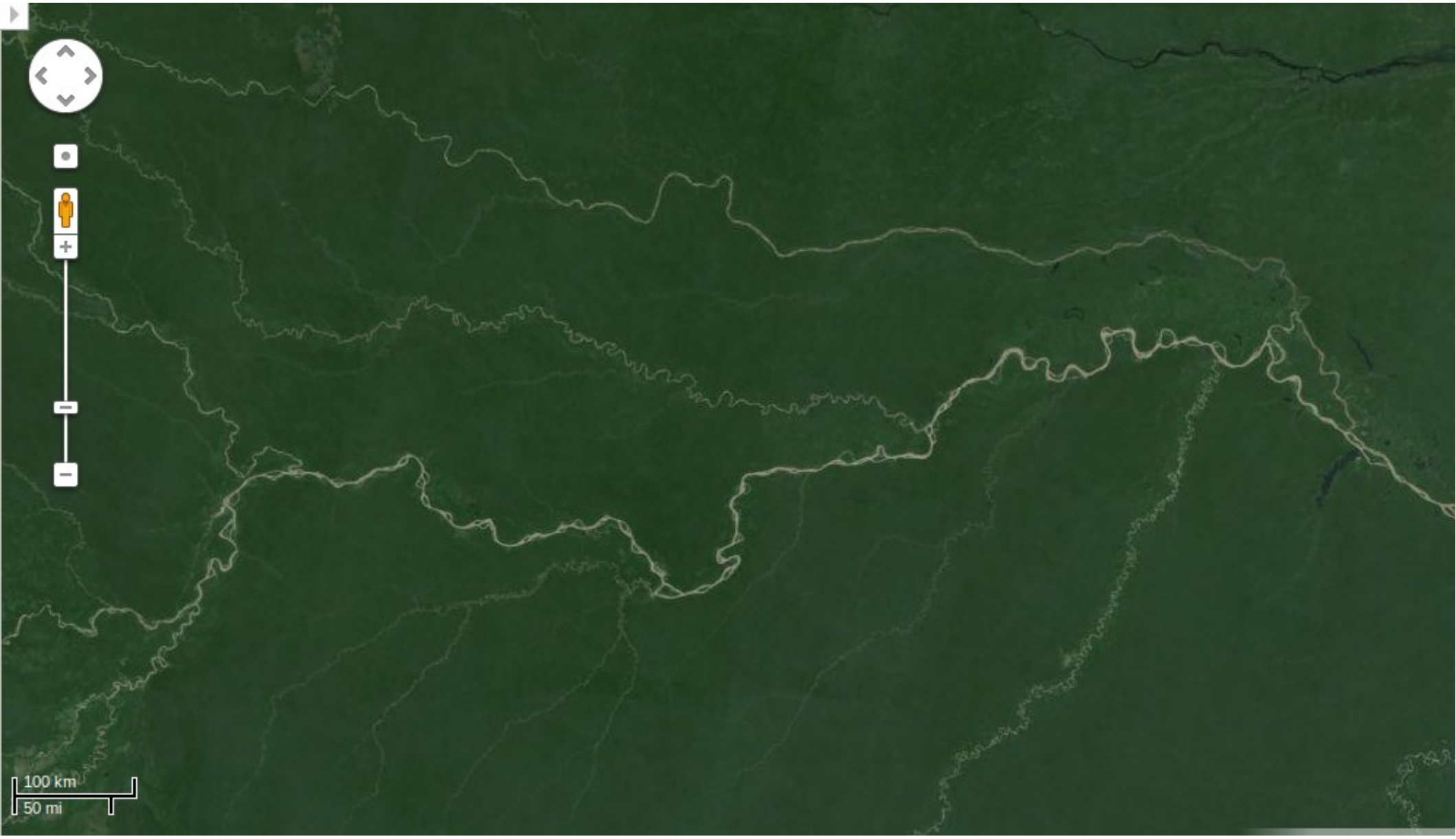

Padrões de canal vs. padrões de cinturões de canais

Padrão distributário Rio Okavango Botswana

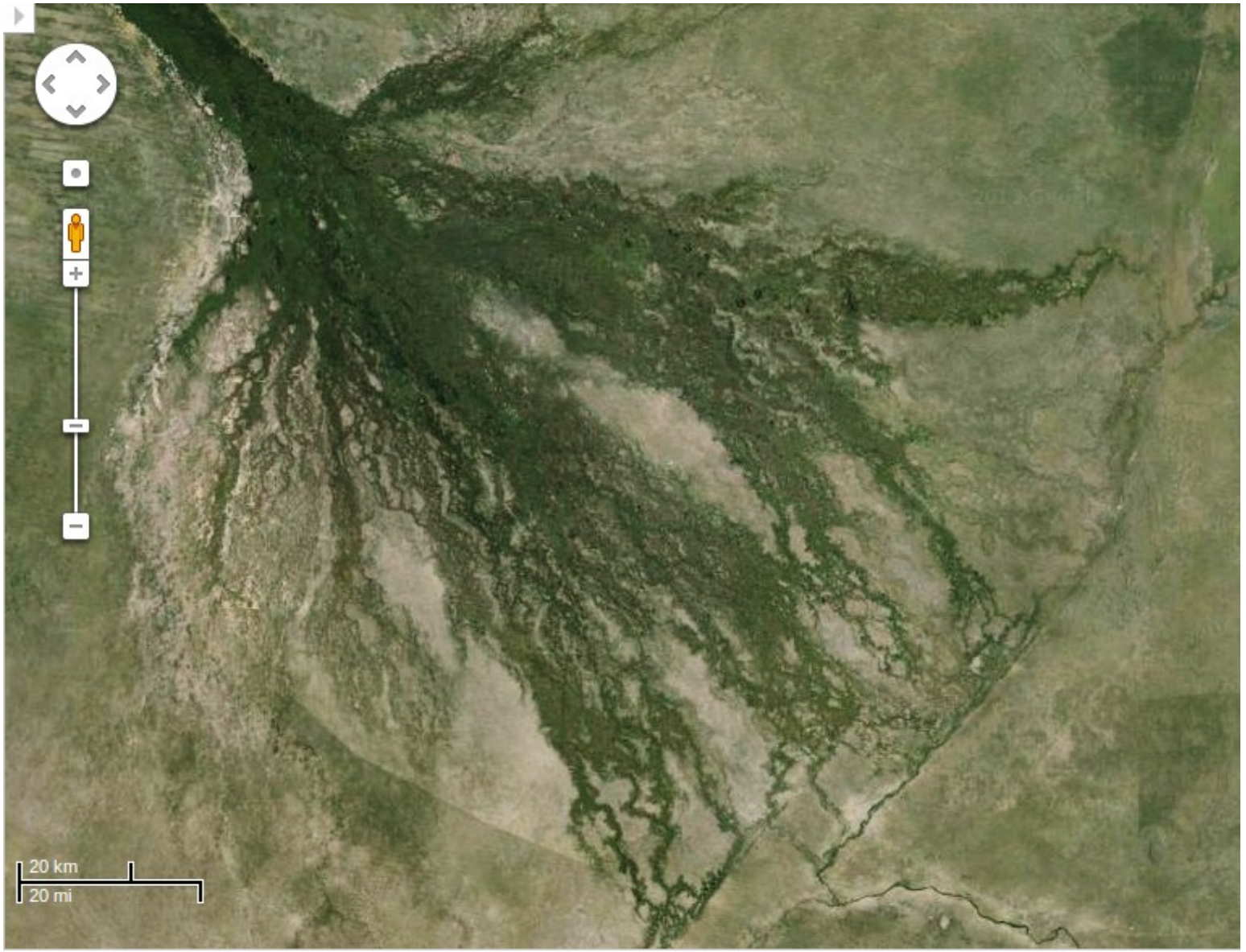

Padrões de canal vs. padrões de cinturões de canais

Padrão anastomosado em rios meandrantes Rio Santo Antonio - BA

Padrões de canal vs. padrões de cinturões de canais

Padrão anastomosado (ou anabranching) em rios entrelaçados Rio Gandak ìndia

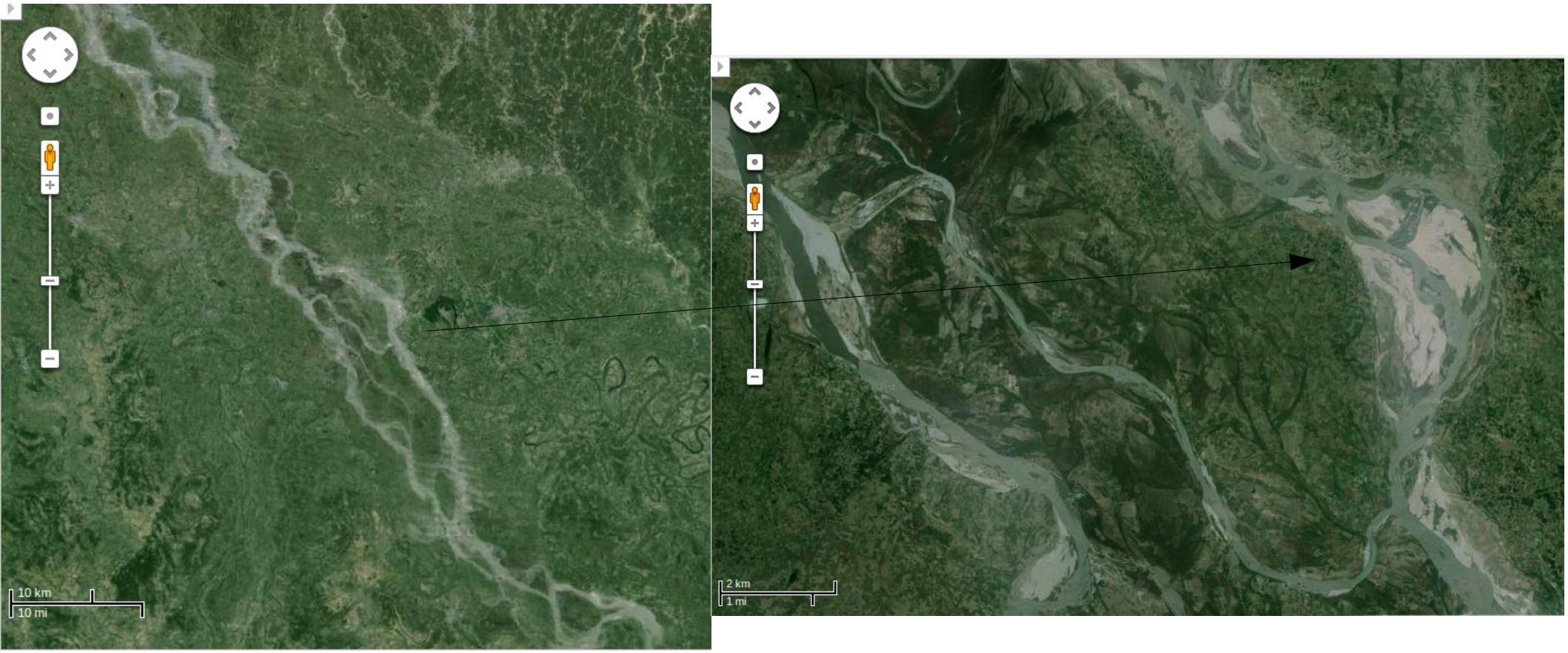

“Rios muito grandes tedem ao anastomosado (anabranching).”

E. Latrubesse

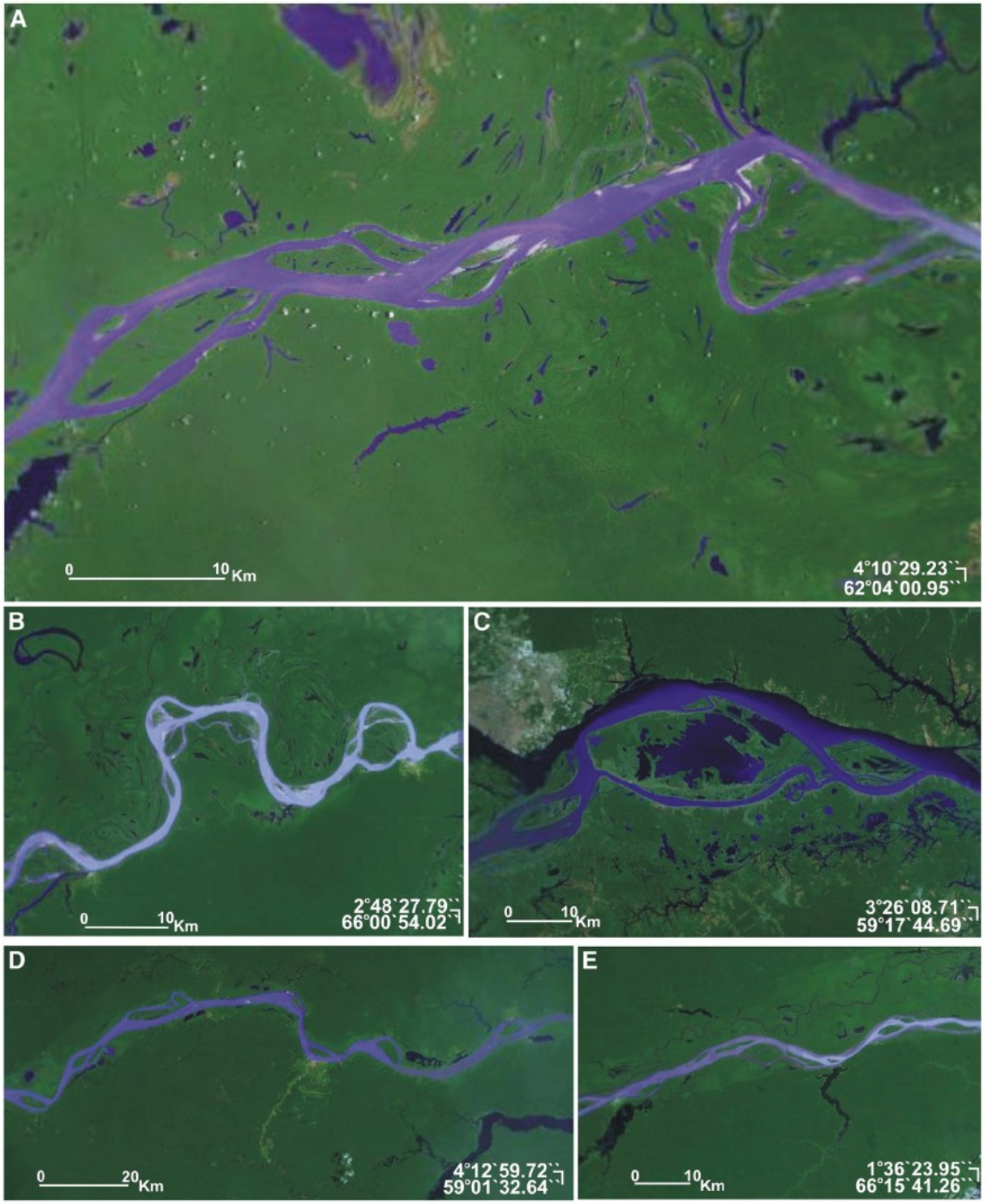

Anabranching de baixa declividade

E.M. Latrubesse / Geomorphology 101 (2008) 130–145

Fig. 5. Low sinuosity anabranching patterns. A) Solimões–Amazon immediately downstream of Itapeua; B) Solimões–Amazon at Fonte Boa downstream of Santo Antonio do Iça (Q_{mean} ~ 55,600 m^3/s); C) Amazon at Careiro Island, Jatuarana station (Q_{mean} = 123,680 m^3/s); D) Madeira River at Fazenda Vista Alegre (Q_{mean} = 31,000 m^3/s); E) Japura River at Acanaui (Q_{mean} = 14,333 m^3/s).

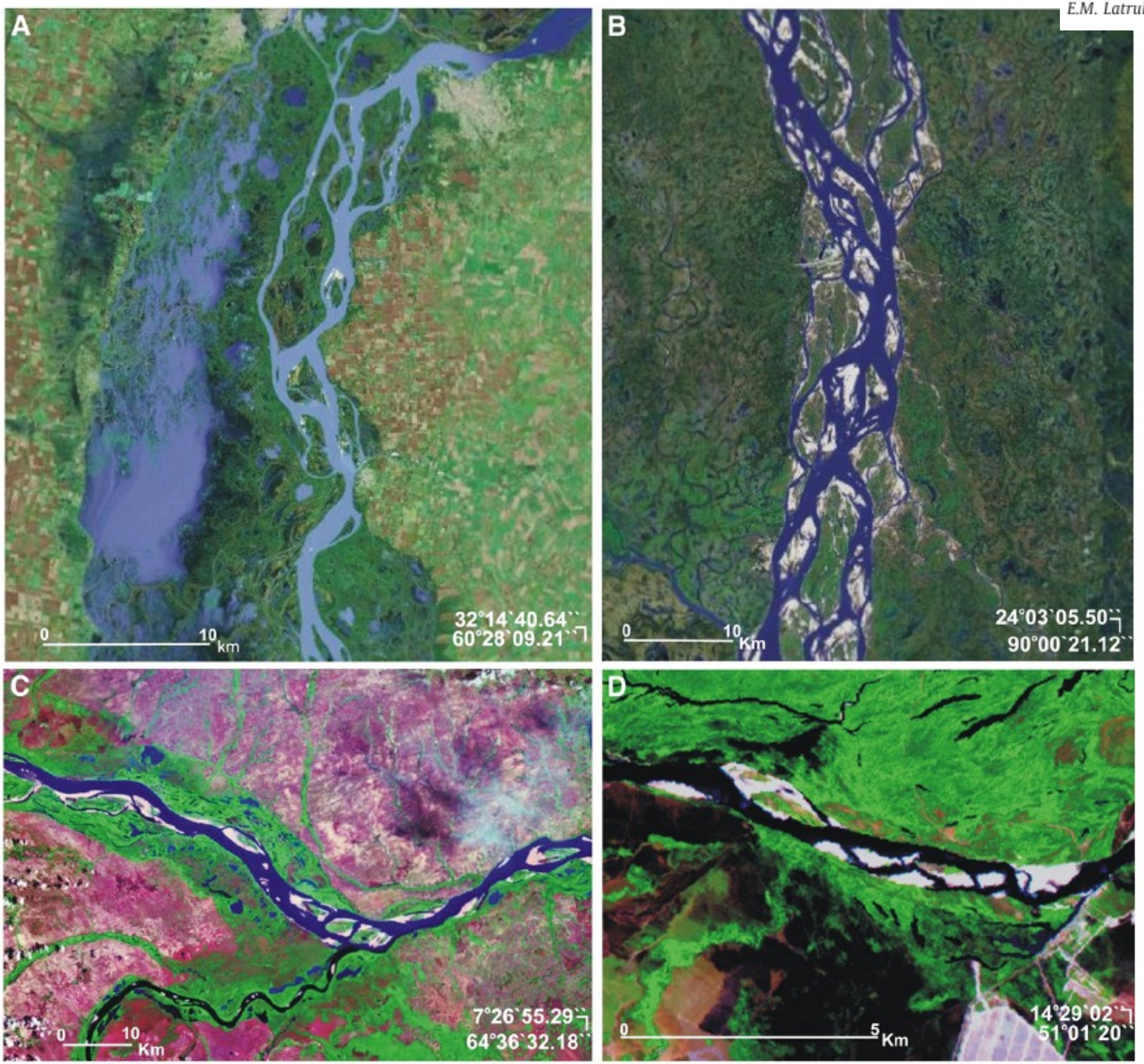

Anabranching de canais entrelaçados

Fig. 7. Anabranching rivers with tendency towards braided pattern. A) lower Parana River downstream of Santa Fe (downstream Villa Urquiza gauge station) (Q_{mean} = 16,400 m^3/s); B) Brahmaputra at Baharudabad (Q_{mean} = 21,261 m^3/s); C) Orinoco River at Musinacio (Q_{mean} = 28,723 m^3/s); D) Araguaia River at Luiz Alves (Q_{mean} = 3700 m^3/s).

Anabranching
mega complexos

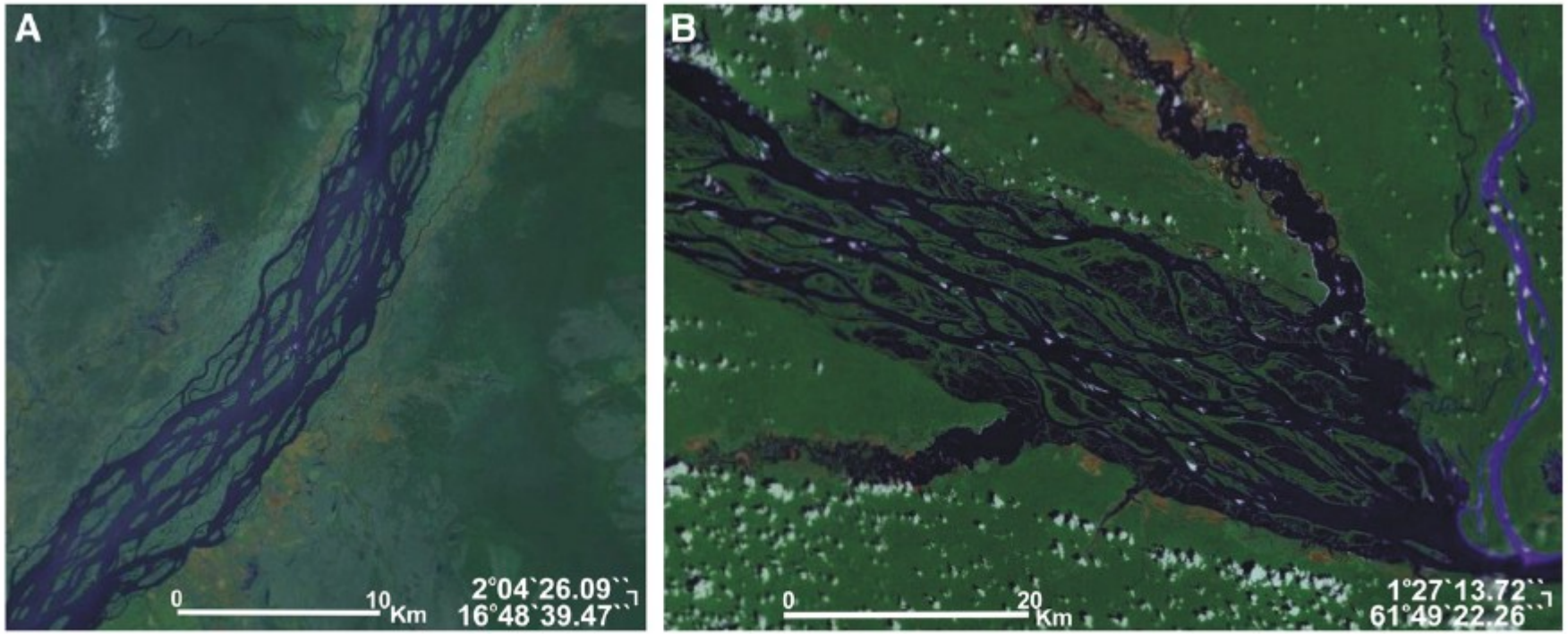

Fig. 9. Mega complex anabranching rivers. A) the Congo River between Mobenga and Mokangamoi B) the Negro river at Barcelos, Mariuá archipelago (no gauging stations available at these reaches, however taking account data from gauging station located upstream and downstream, the river reaches are inside the classification of mega rivers with $Q_{mean} > 17{,}000\ m^3/s$).

Sistemas fluviais distributivos e megaleques aluviais

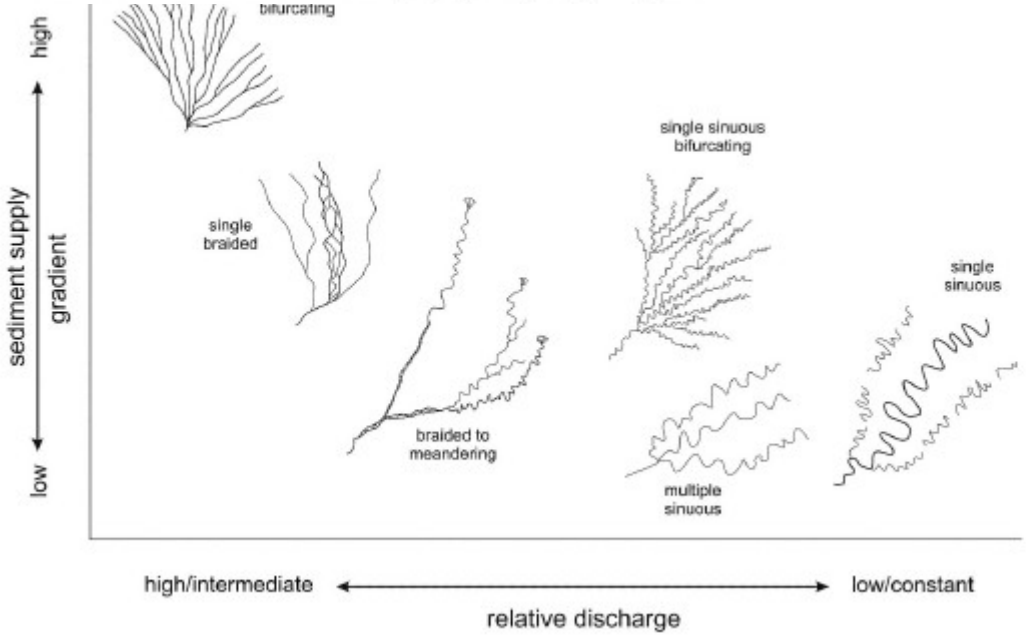

HARTLEY ET AL.

Journal of Sedimentary Research, 2010, v. 80, 167–183

FIG. 12.—Schematic illustration of the continuum in DFS planform type in relation to gradient and relative discharge. Note that these are generalized relationships and that factors inherent to individual DFSs, in particular catchment hydrology, may affect this general relationship.

Tipos de leques aluviais

- Leques *sensu strictu* derivados de escarpas
  - Leques dominados por fluxos de detritos
  - Leques dominados por enchentes em lençol

- Grandes sistemas aluviais distributários


Cerro Colorado
Cerro Colorado Sur
1 km
Image © 2006 TerraMetrics
© 2006 Europa Technologies
© 2005 Google


30 km
© 2006 Europa Technologies
Image © 2006 TerraMetrics
© 2005 Google

Grandes sistemas aluviais distributários

- Diâmetros de dezenas de km.
- Dominados por processos de transporte e deposição fluviais.
- Padrão distributário causado por avulsão
- Exemplos: rios Kosi (Índia), Okavango (África meridional), Taquari (Pantanal).

Leques adjacentes a escarpas

- Diâmetros de poucos km
- Dominados por fluxo gravitacional de sedimento ou enchentes em lençol
- Canais fluviais apenas retrabalham sedimentos na superfície do leque
- Abundantes em bordas de bacias limitadas por falhas

Depósitos Fluviais: fácies e elementos arquitetônicos.

Sistema fluvial – Micro e Mesoformas

Velocidade do fluxo e formas de leito

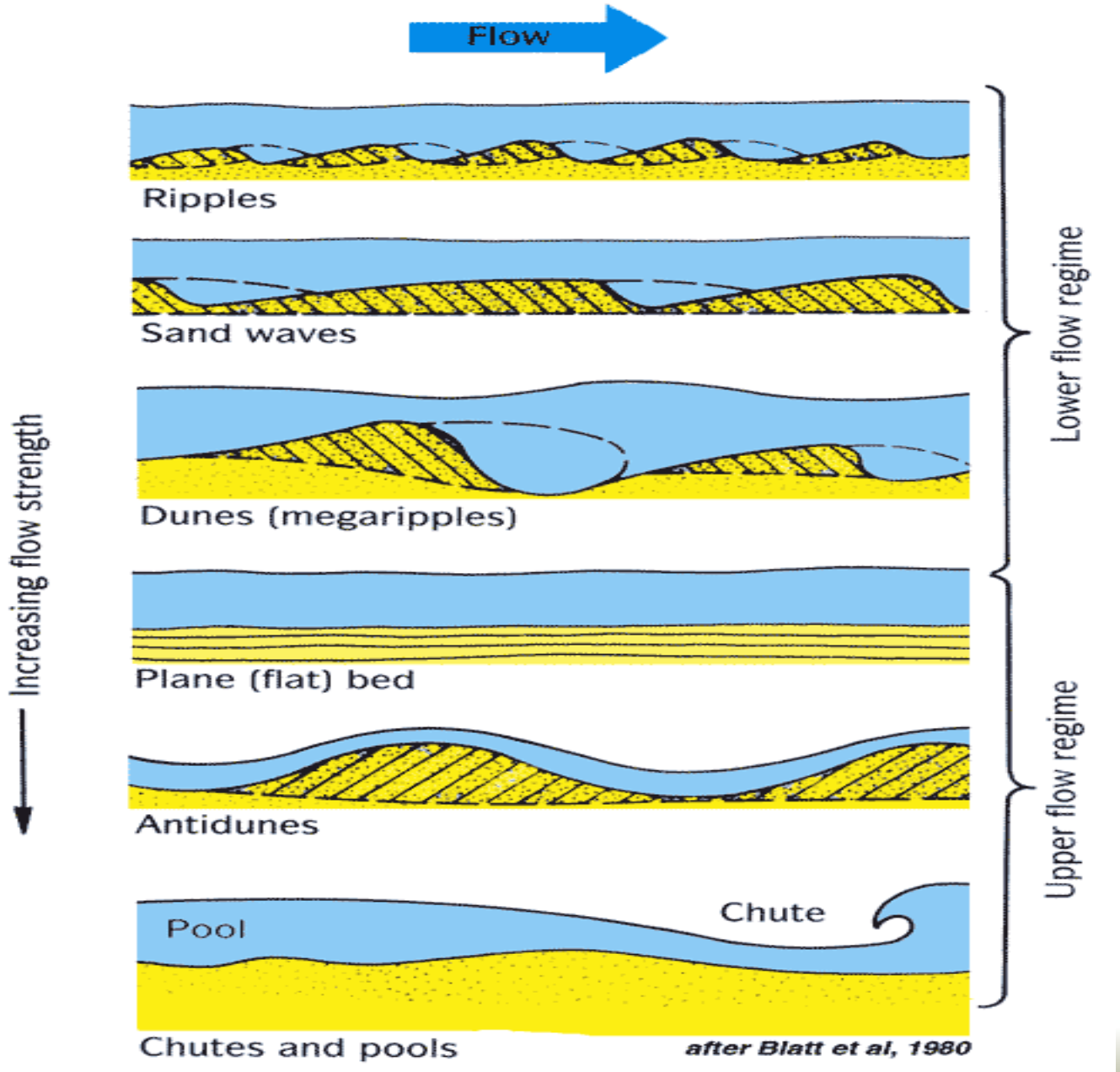

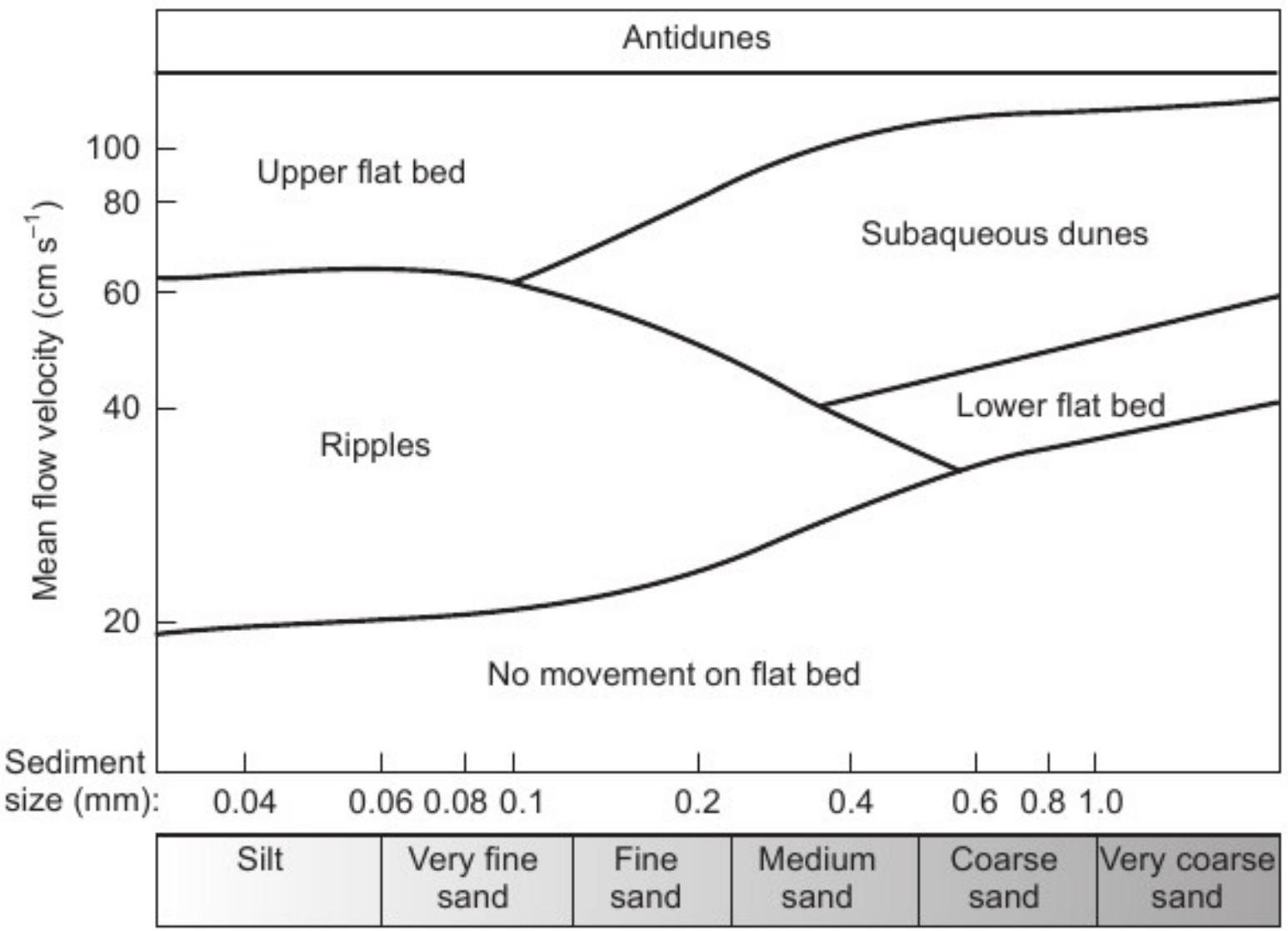
Antidunes
Upper flat bed
Subaqueous dunes
Lower flat bed
Ripples
No movement on flat bed
Mean flow velocity (cm s^{-1})
100
80
60
40
20
Sediment size (mm):
0.04
0.06
0.08
0.1
0.2
0.4
0.6
0.8
1.0
Silt
Very fine sand
Fine sand
Medium sand
Coarse sand
Very coarse sand

Filmes

Migração de ondulações de corrente

Ondulações cavalgantes

Migração de formas de leito e formação de estratificações

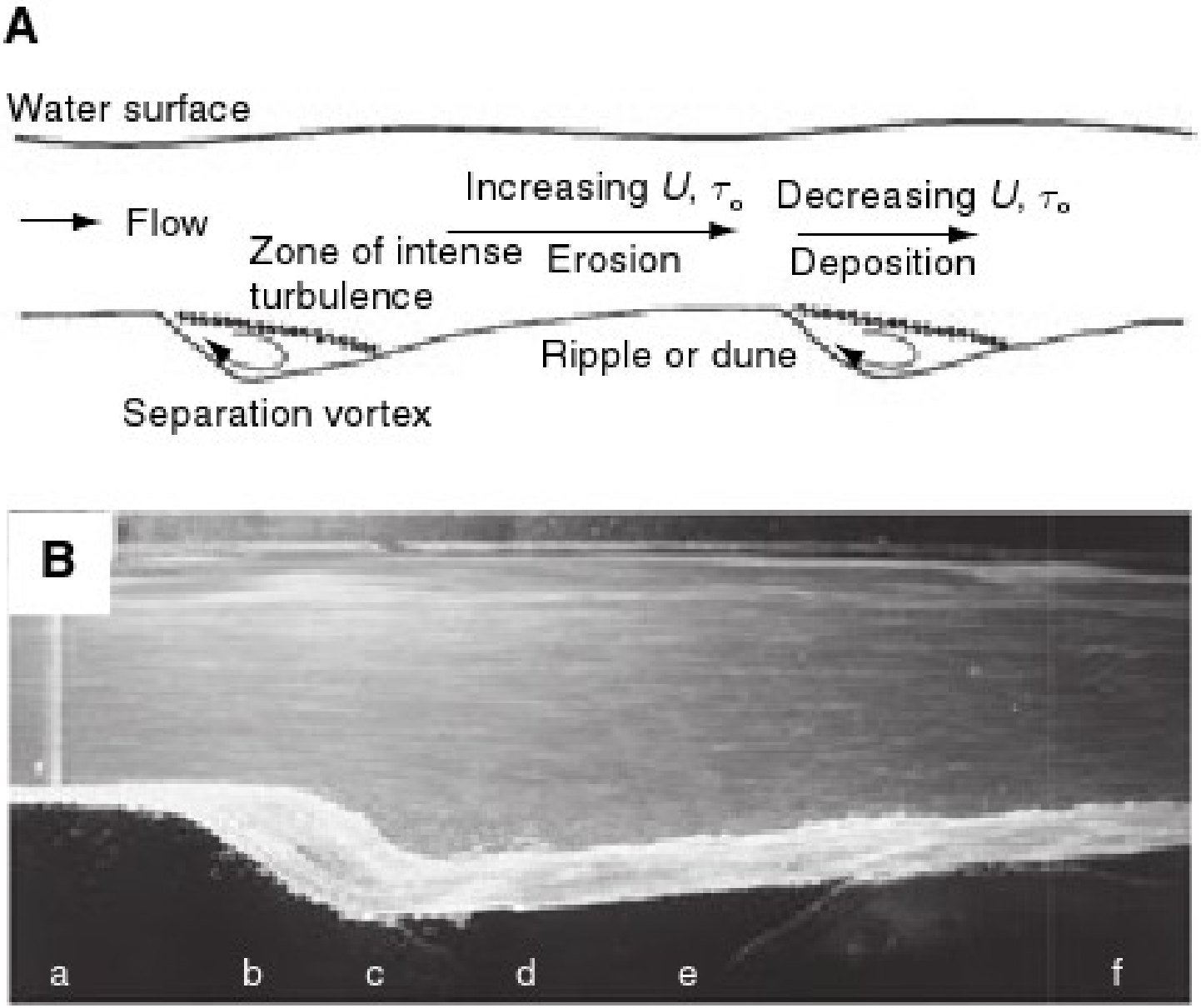
A
Water surface
Flow
Increasing U, τo
Decreasing U, τo
Zone of intense turbulence
Erosion
Deposition
Ripple or dune
Separation vortex
B
a
b
c
d
e
f

A

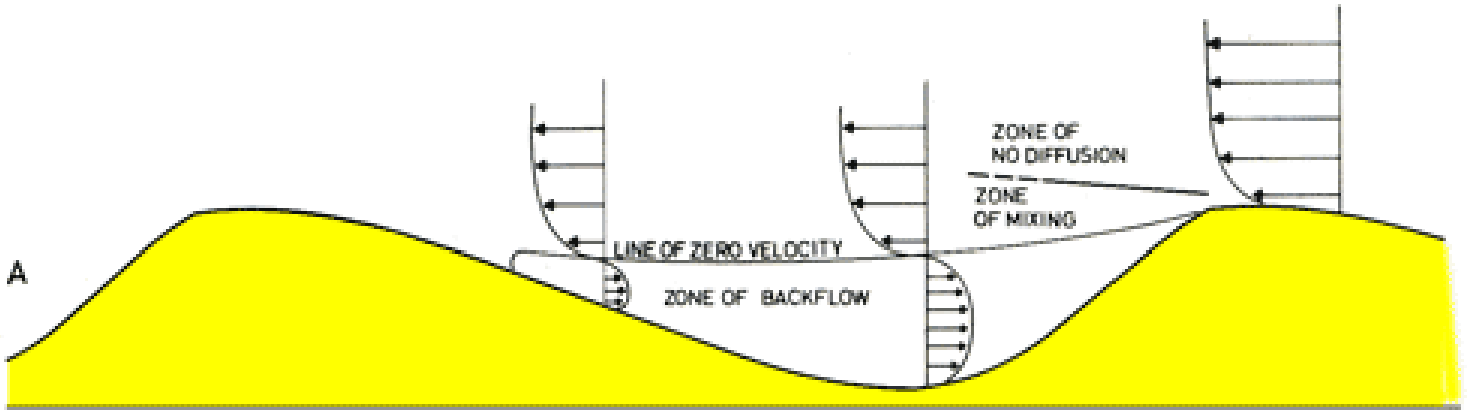

After Reineck & Singh, 1975

B

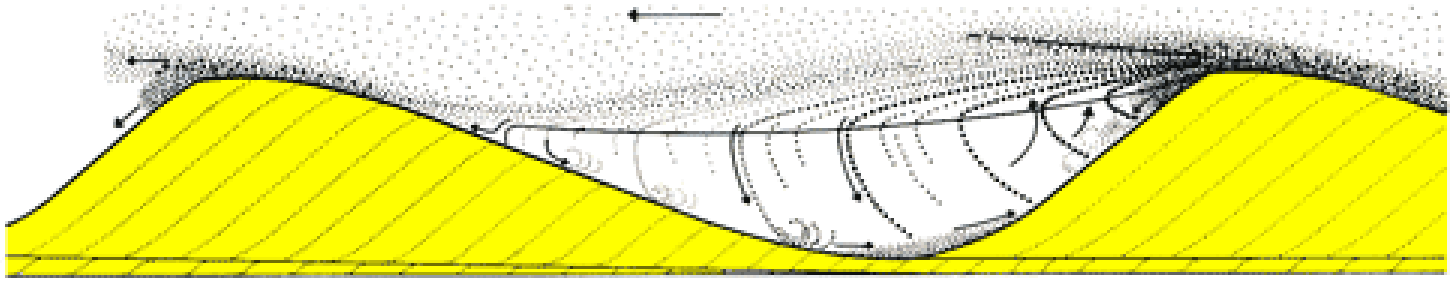

After Reineck & Singh, 1975

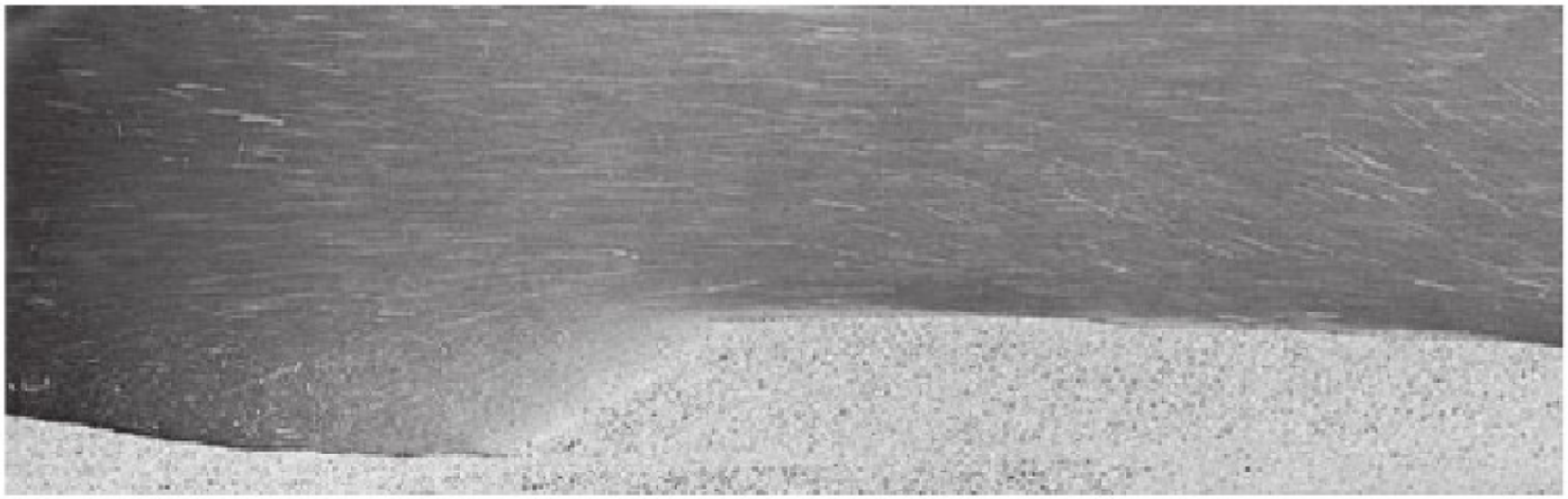

Estruturas sedimentares formadas por migração de formas de leito

-Acamadamento – planos visíveis, marcados por diferença de granulação ou composição.

Estratificação – camadas de mais de 1 cm de espessura.

Laminação – camadas de menos de 1 cm de espessura (lâminas)

Série – conjunto de lâminas ou estratos

Estruturas sedimentares formadas por migração de formas de leito

- Marcas onduladas (preservadas)

  Laminação cruzada
  Laminação cruzada cavalgante

- Dunas subaquáticas – estratificação cruzada

  Acanalada
  Tabular

-Dunas eólicas

  Acanalada Tabular

- Leito plano – laminação plana

- Praia – estratificação inclinada

Leito plano

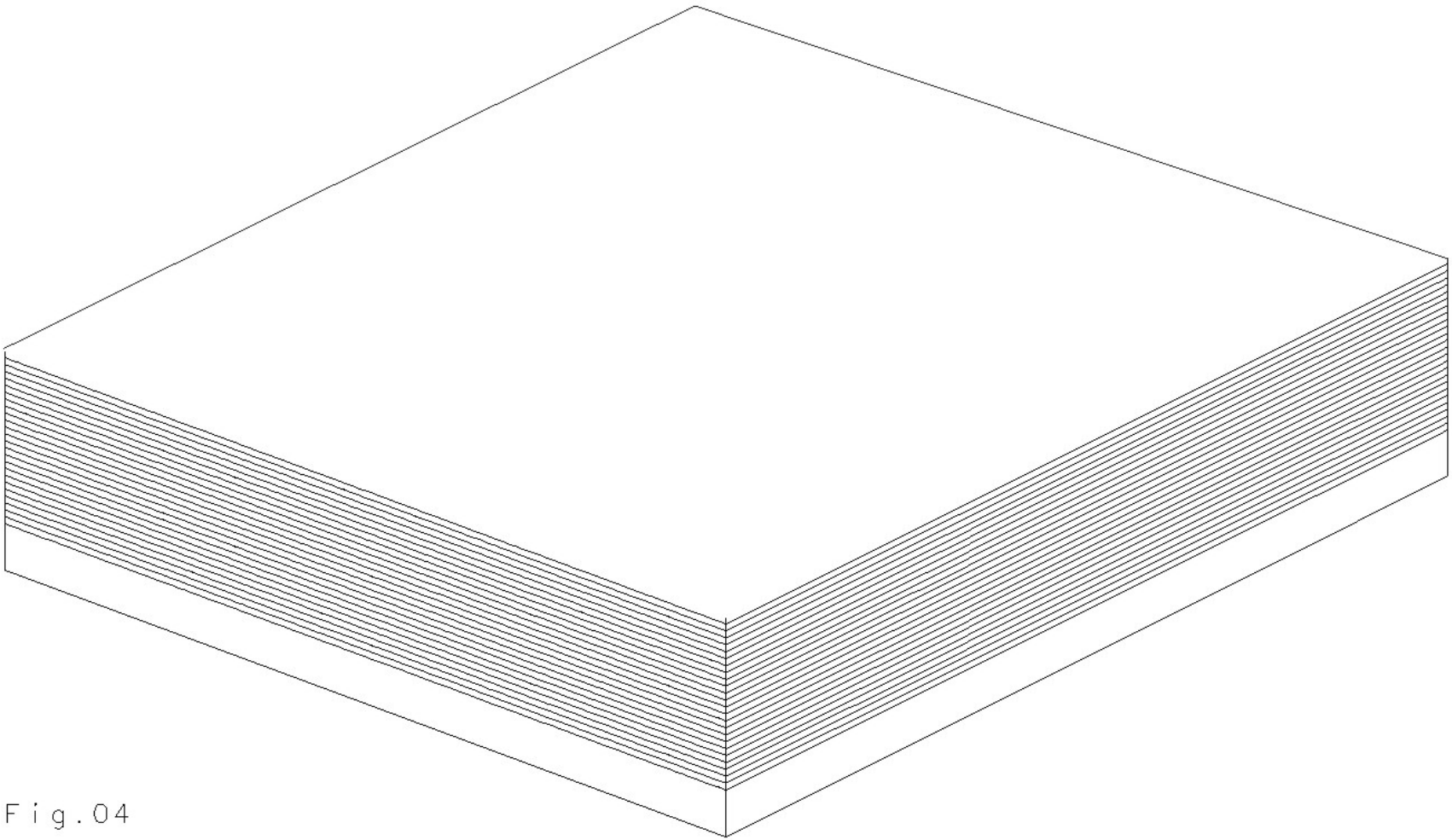

Fig.04

Stoss- and lee-depositional climb

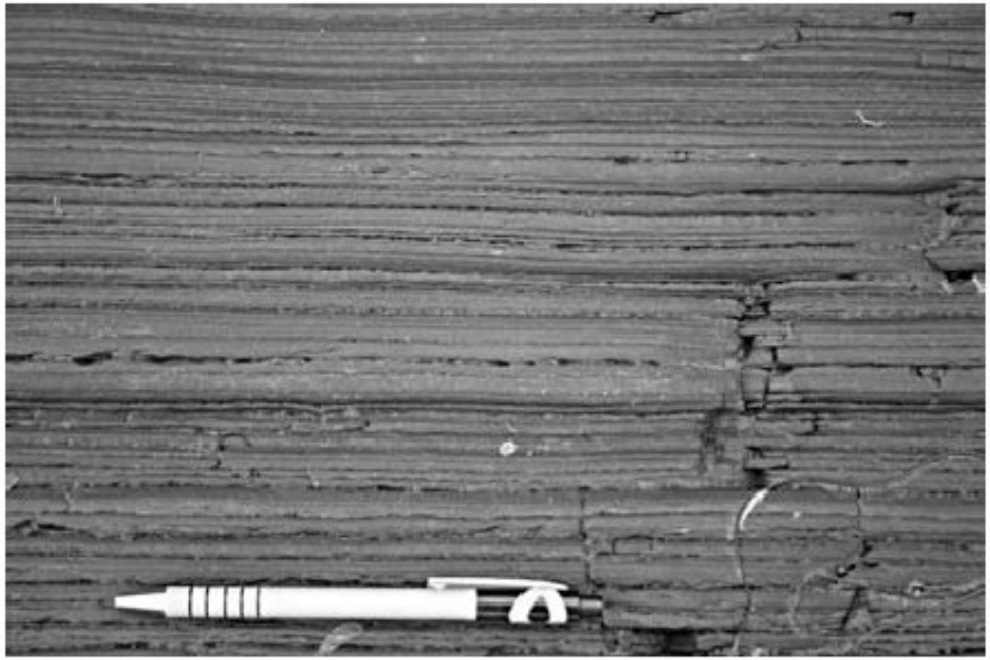

Fig. 4.19 Horizontal lamination in sandstone beds.

Lineação de corrente

Ondulação e laminação cruzada

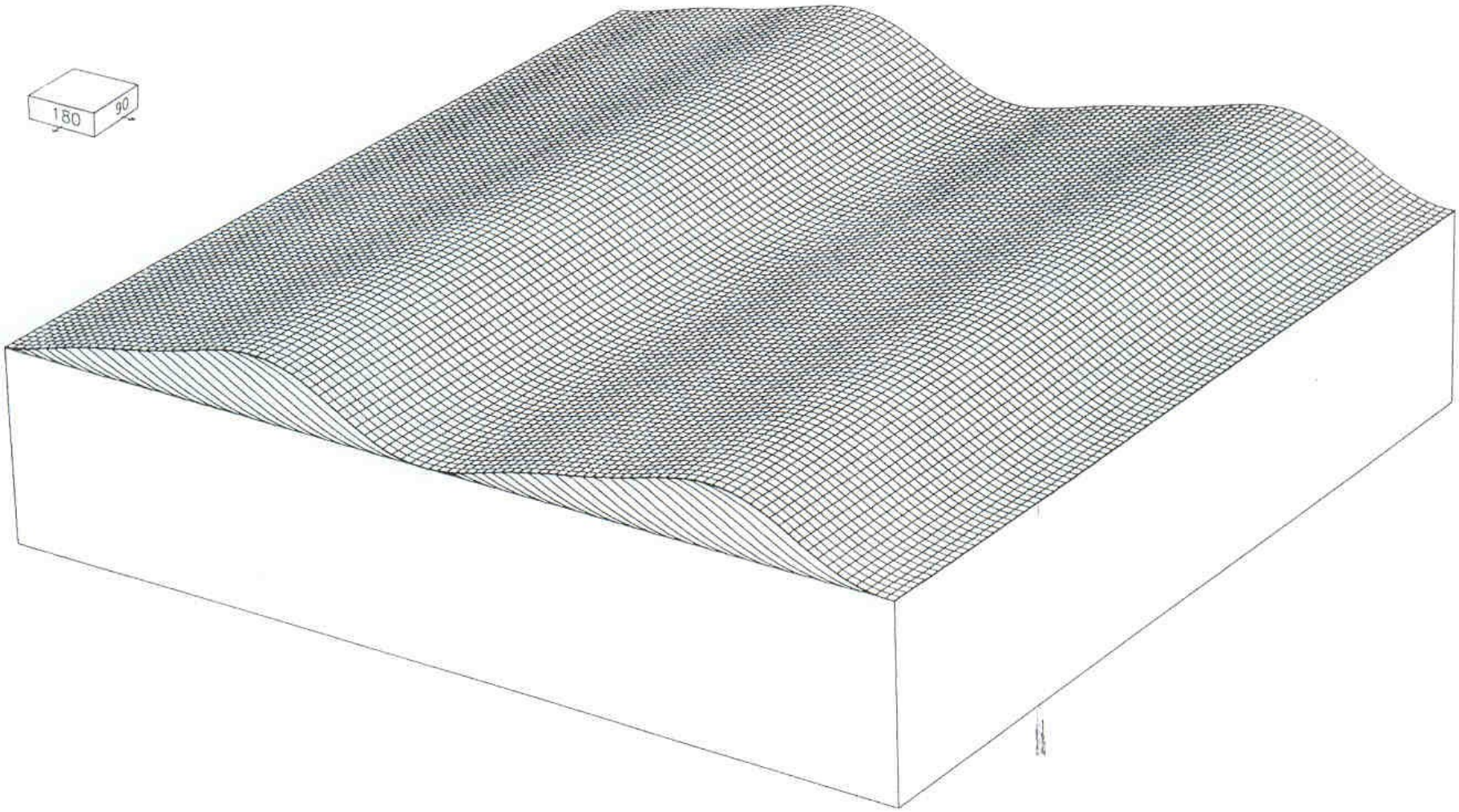

Laminação cruzada cavalgante

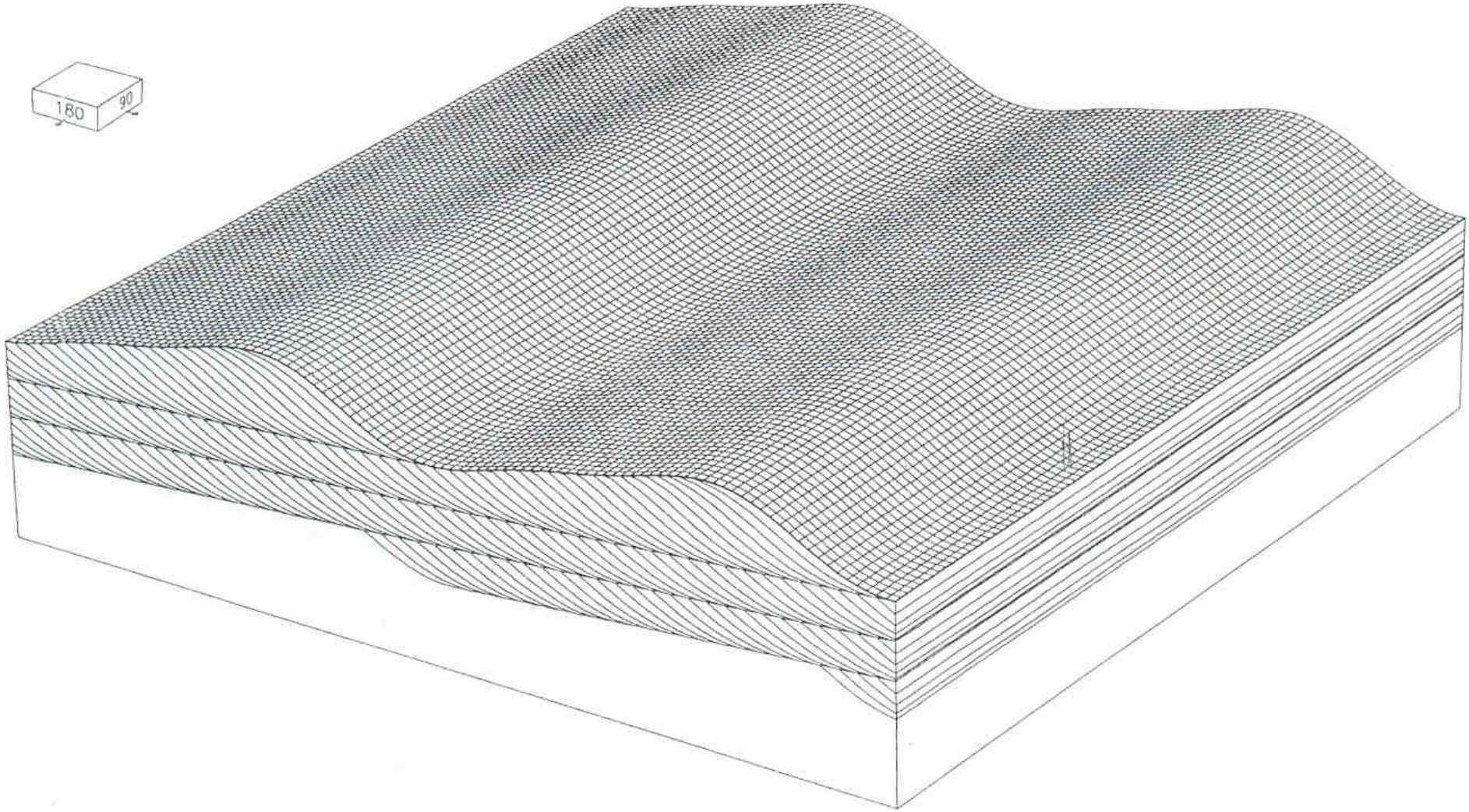


180
90

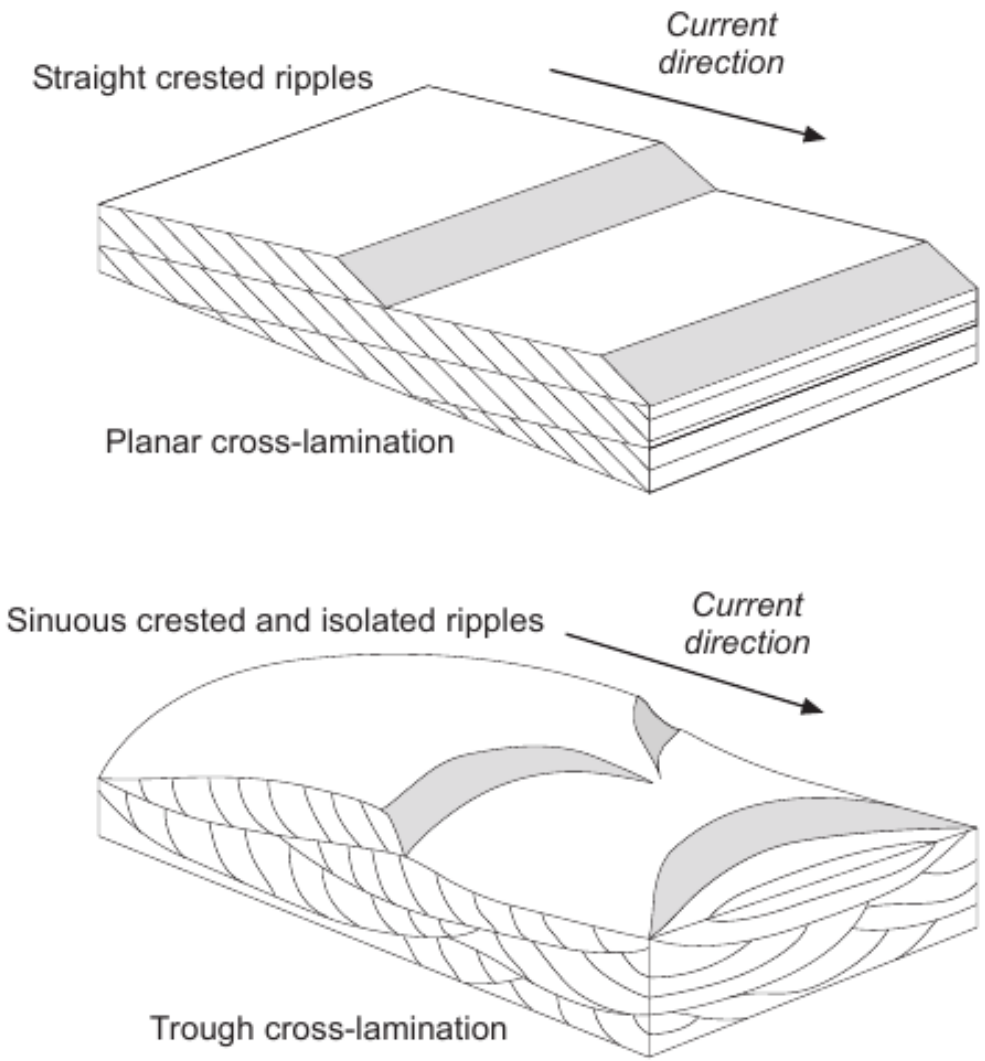

Fig. 4.10 Migrating straight crested ripples form planar cross-lamination. Sinuous or isolated (linguoid or lunate) ripples produce trough cross-lamination. (From Tucker 1991.)

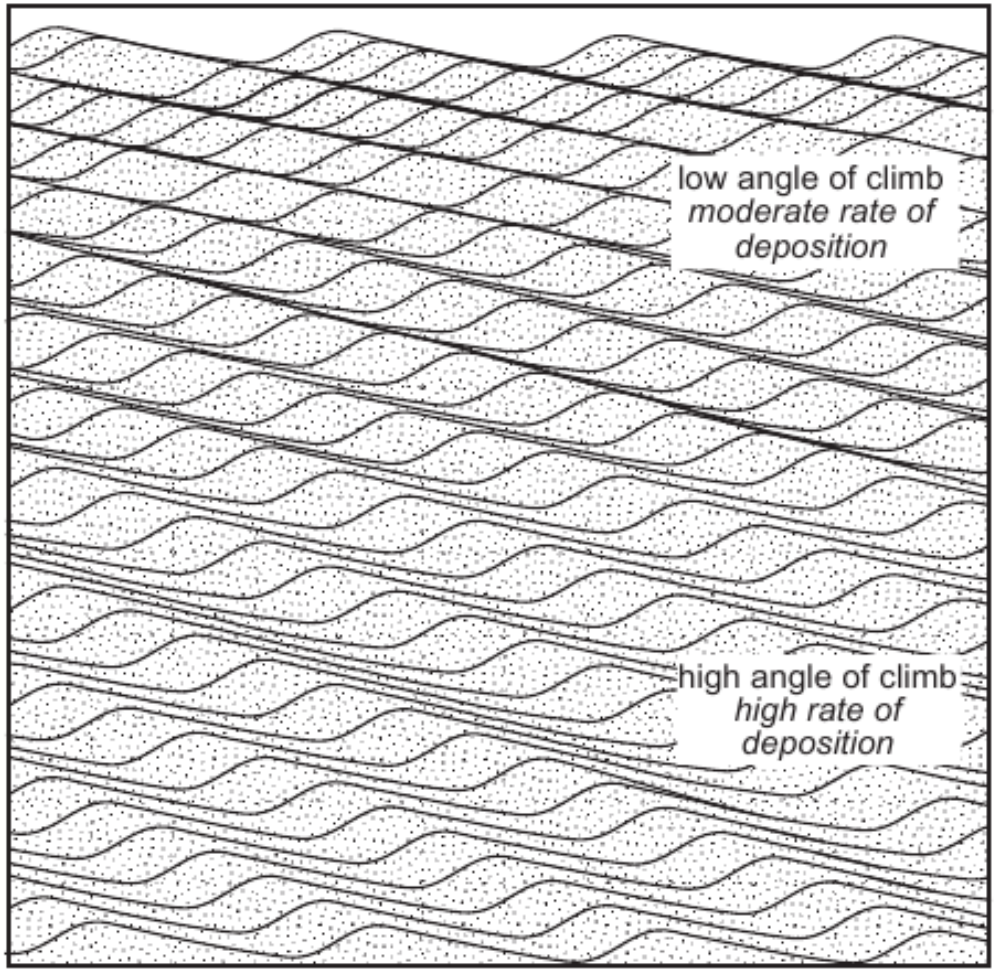

Fig. 4.12 Climbing ripples: in the lower part of the figure, more of the stoss side of the ripple is preserved, resulting in a steeper 'angle of climb'.


24

Cavalgamento crítico

Duna de crista sinuosa

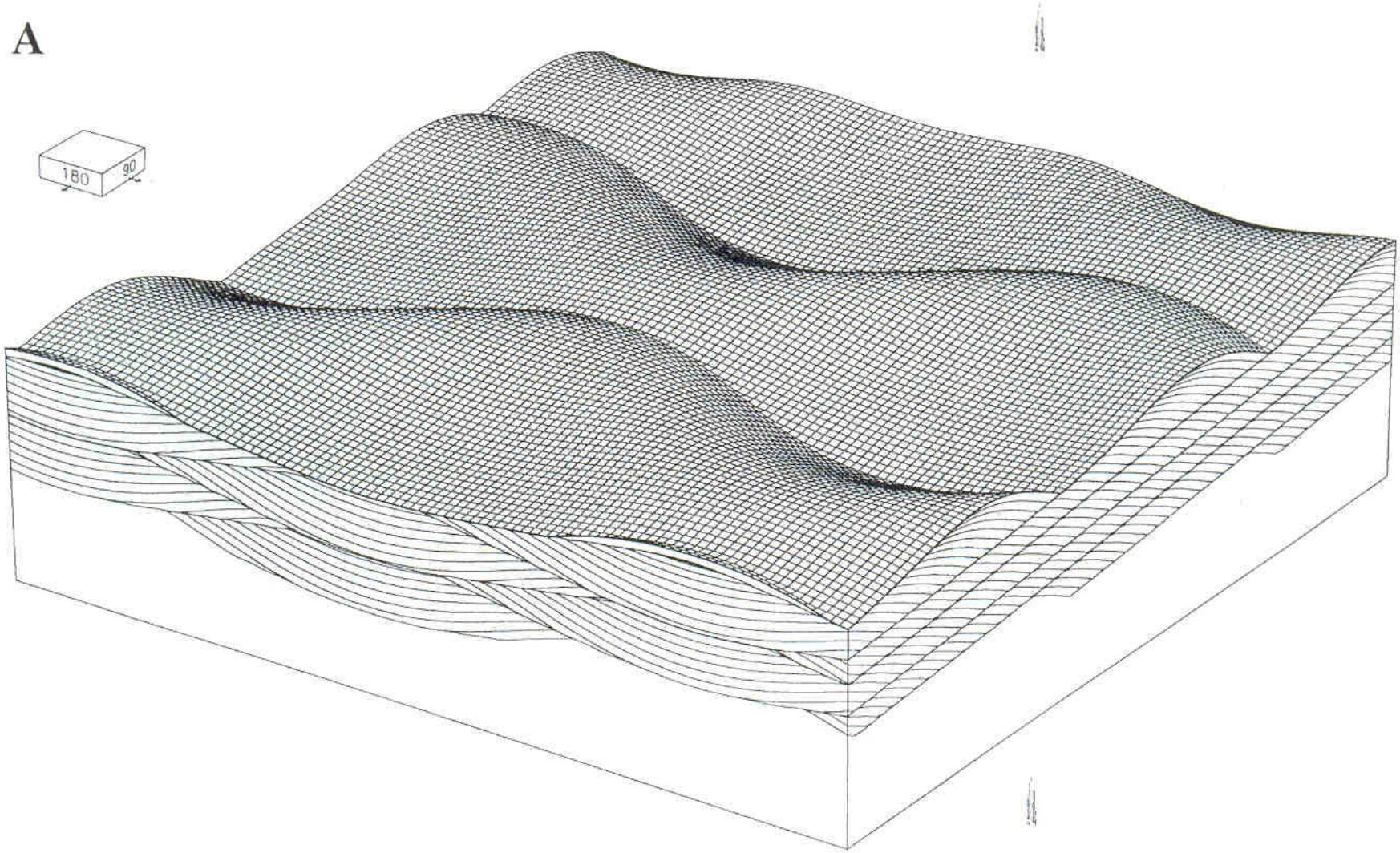

Estratificação cruzada acanalada

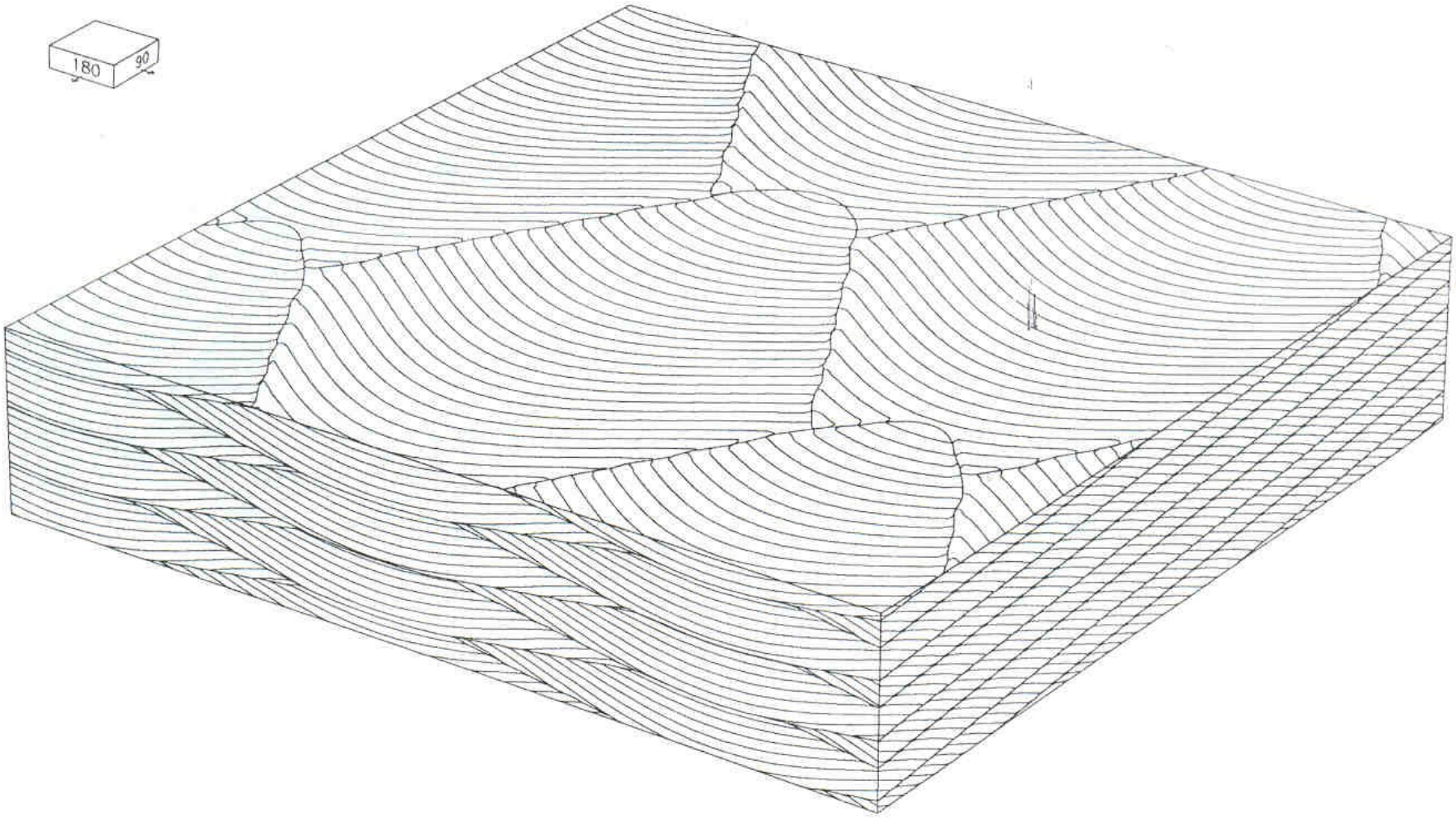

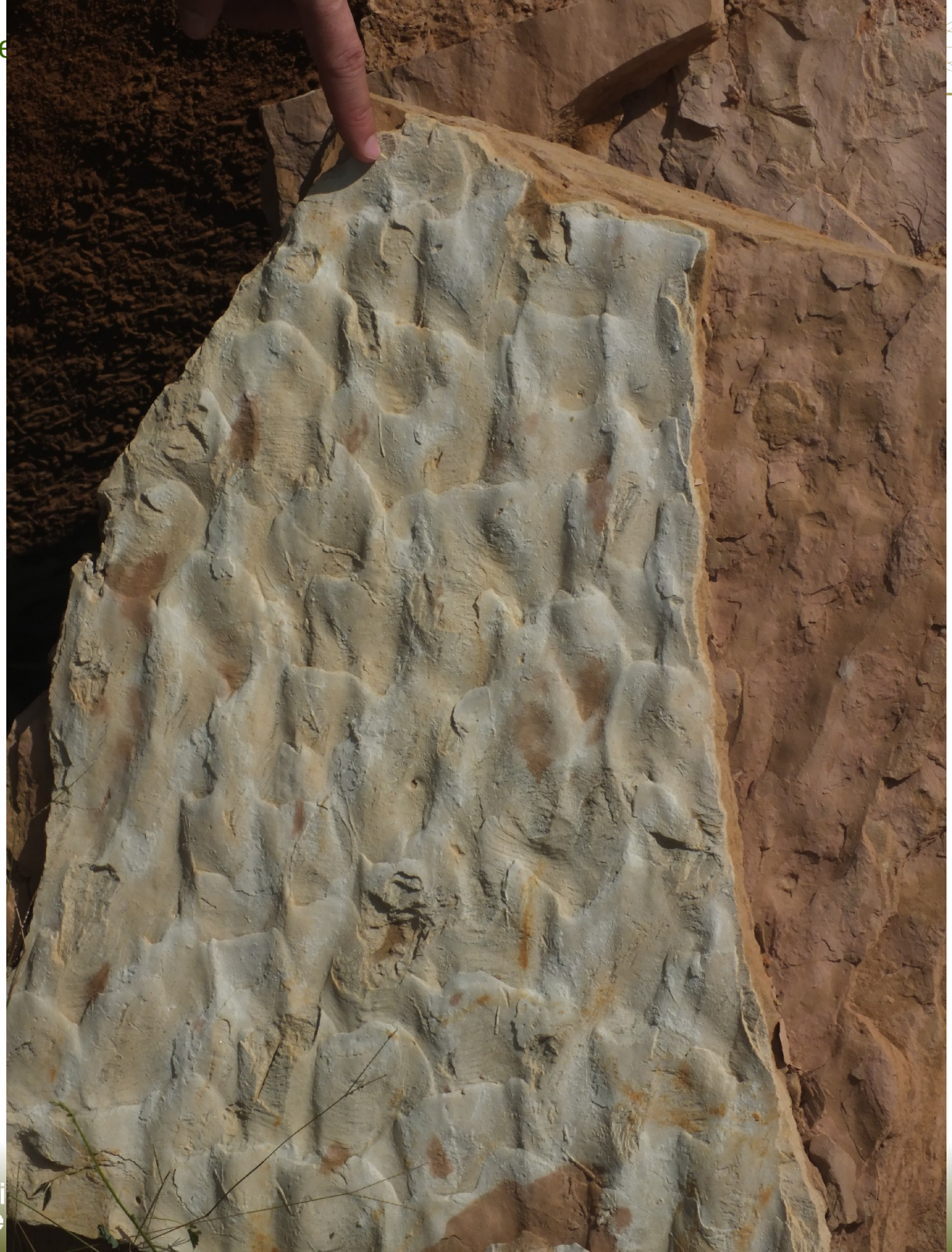


BRASIL

Estratificação cruzada acanalada (Aa)

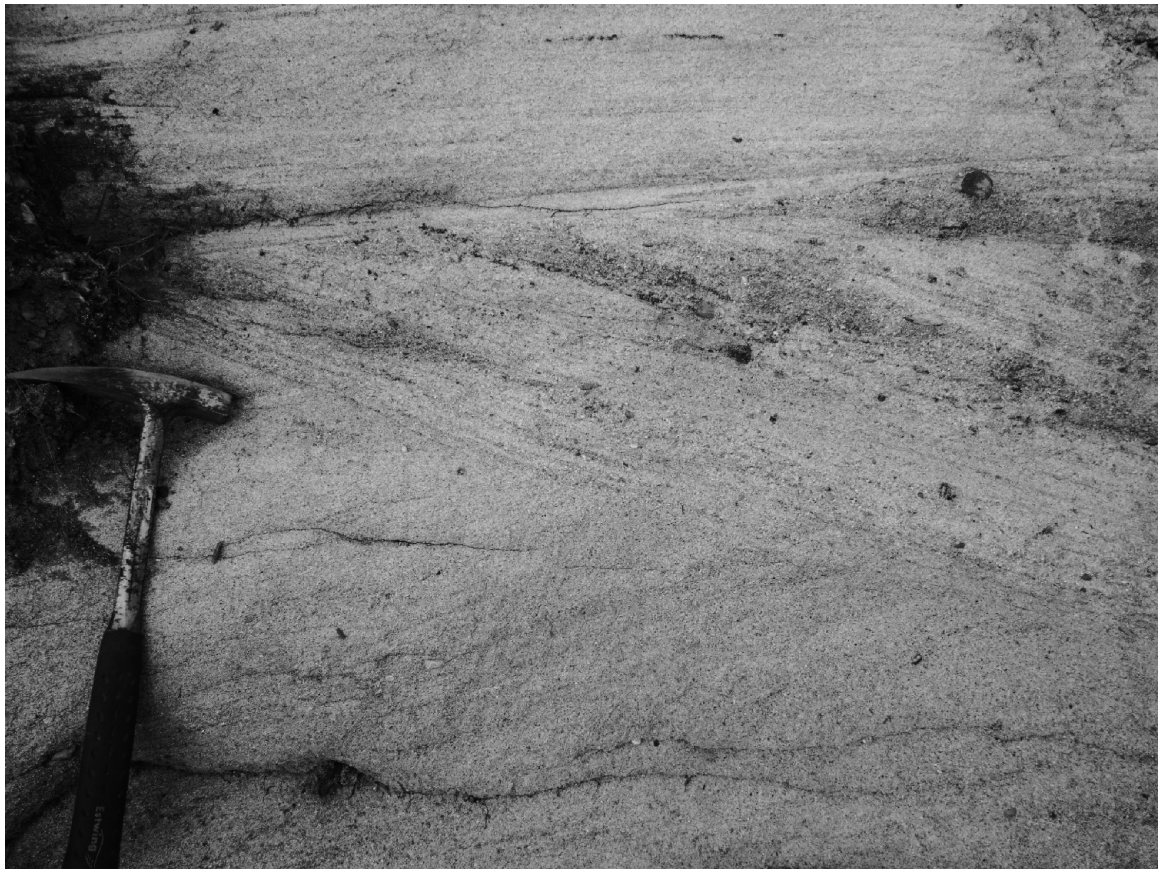

Dunas de cristas retas

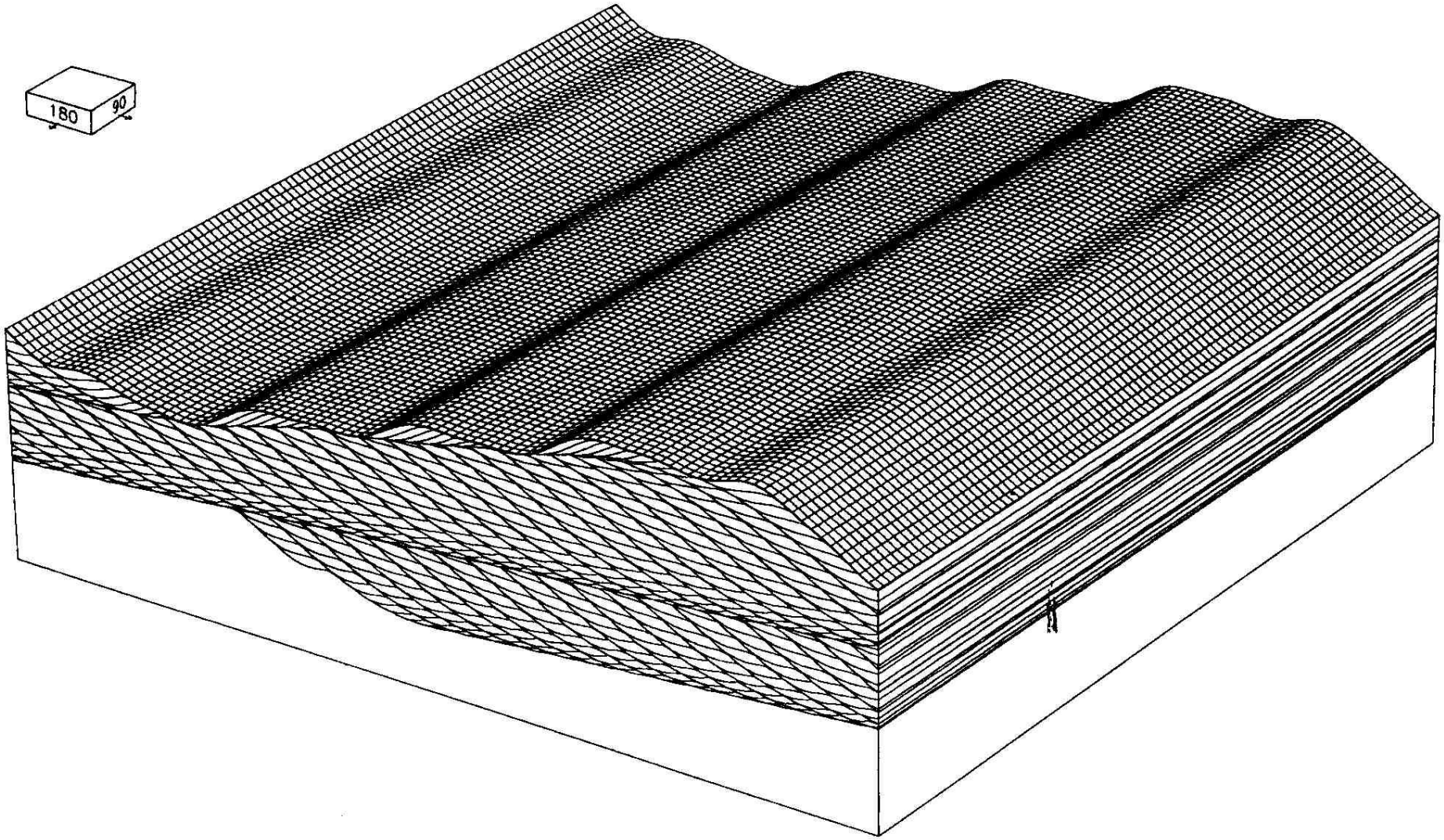

Segregação nos foresets

Fig. 5. Experimental data from Lunt and Bridge (2007) showing cross strata of varying thickness and grain size within a unit bar, associated with deposition from superimposed bedforms of varying height. Peel is 0.5 m across and 0.2 m high.

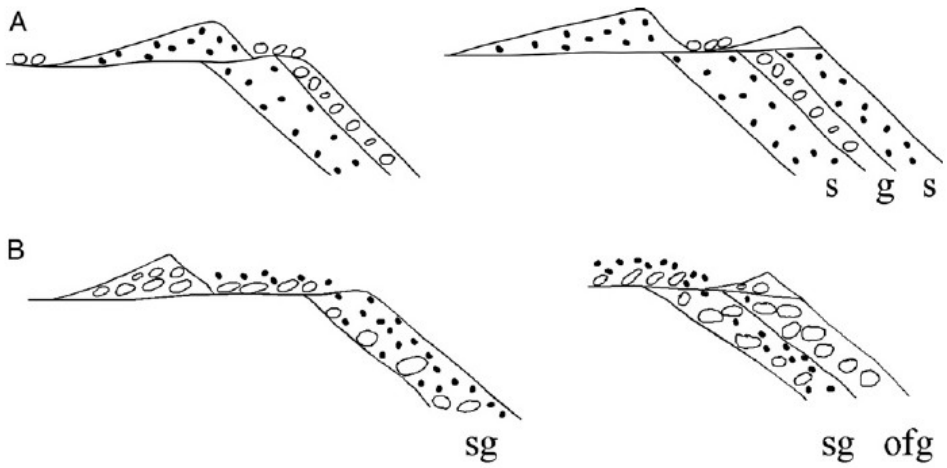

Fig. 4. Grain size sorting in unit bars resulting from size sorting in superimposed dunes, according to (A) Hooke (1968) and Smith (1972), and (B) Rust (1984). s is sand, g is gravel, sg is sandy gravel and ofg is open-framework gravel.

Modelos anteriores

A.J.H. Reesink, J.S. Bridge / Sedimentary Geology 202 (2007) 281–296

Modelo atual

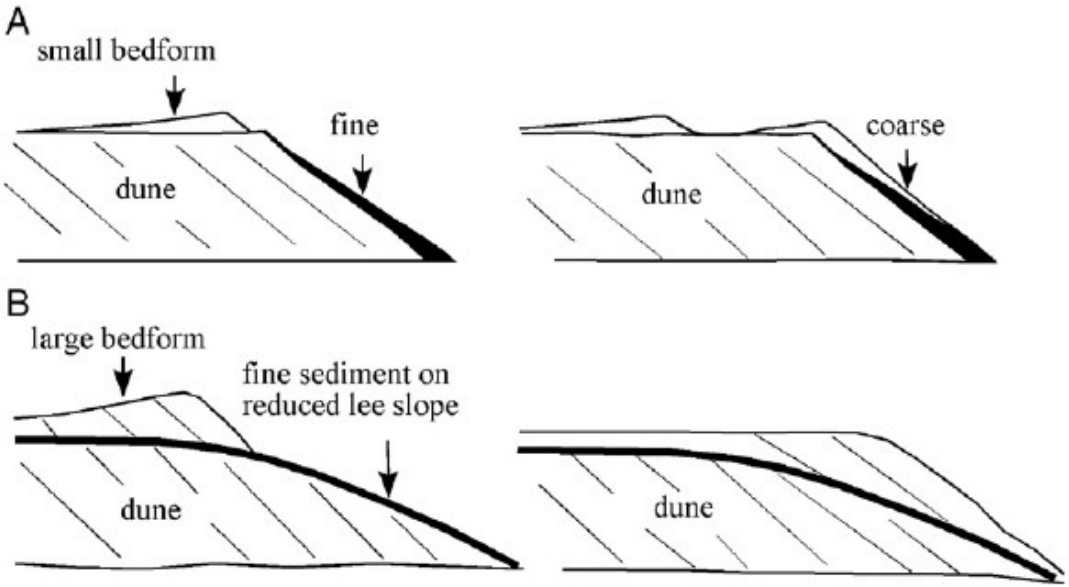

Estratificação cruzada tabular

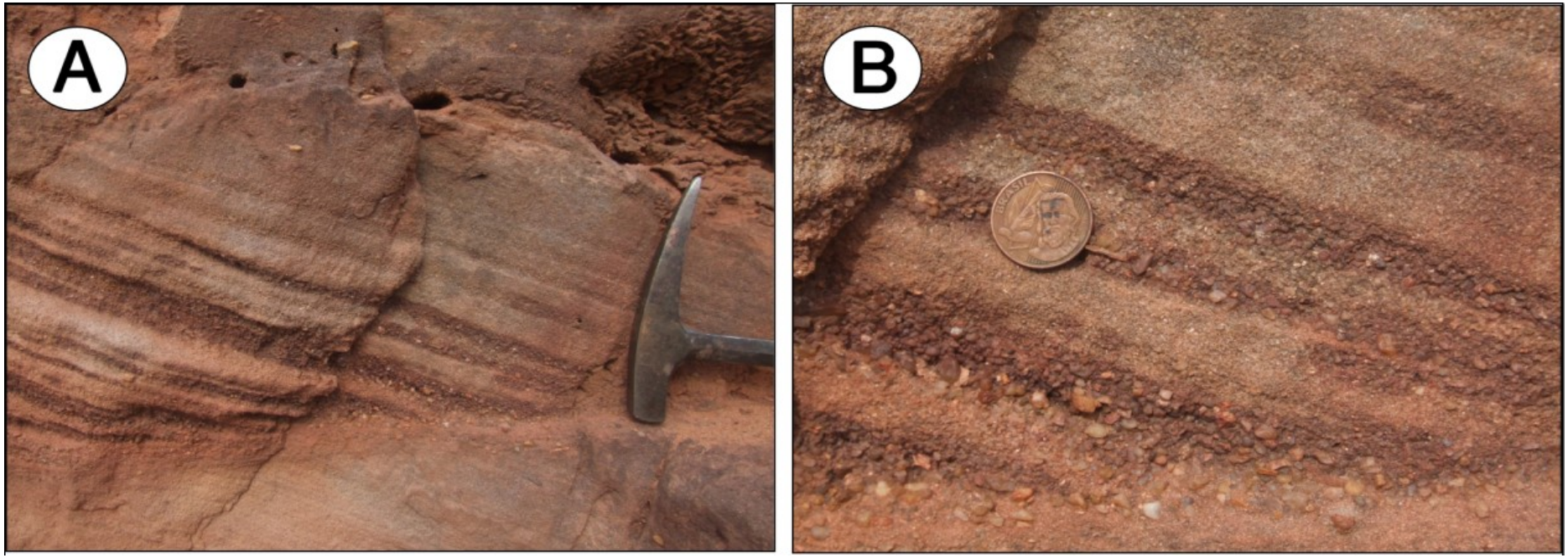

Regimes de Fluxo

Se um fluxo tem velocidade superior à velocidade de propagação de ondas em sua superfície, ele é chamado supercrítico. Se não, é subcrítico.

Esses dois tipos de fluxo têm características diferentes e implicam em formas de leito diferentes.

Para reconhecer o regime de um fluxo, basta determinar seu número de Froude.

Se Fr > 1, o fluxo é supercŕitico.

Se Fr < 1, o fluxo é subcrítico.

$$\mathrm{Fr} = \frac{V}{\sqrt{gh}}$$

Regimes de Fluxo

Deduzindo regimes de fluxo:

$Ek = mv^2/2$
$Ep = mgh$

$Et = hL\rho v^2/2 + hL\rho gh$

V*h é constante para vazão constante = Q

$v = Q/h$

$Et = h*(Q/h)^2*1/2 + h^2*g$

$Et = Q^2/(2h) + h^2g$

Regimes de Fluxo

Comparando com o gráfico do h crítico para froude=1

Vc=1*(gh)^1/2

Et=3/2*h²*g

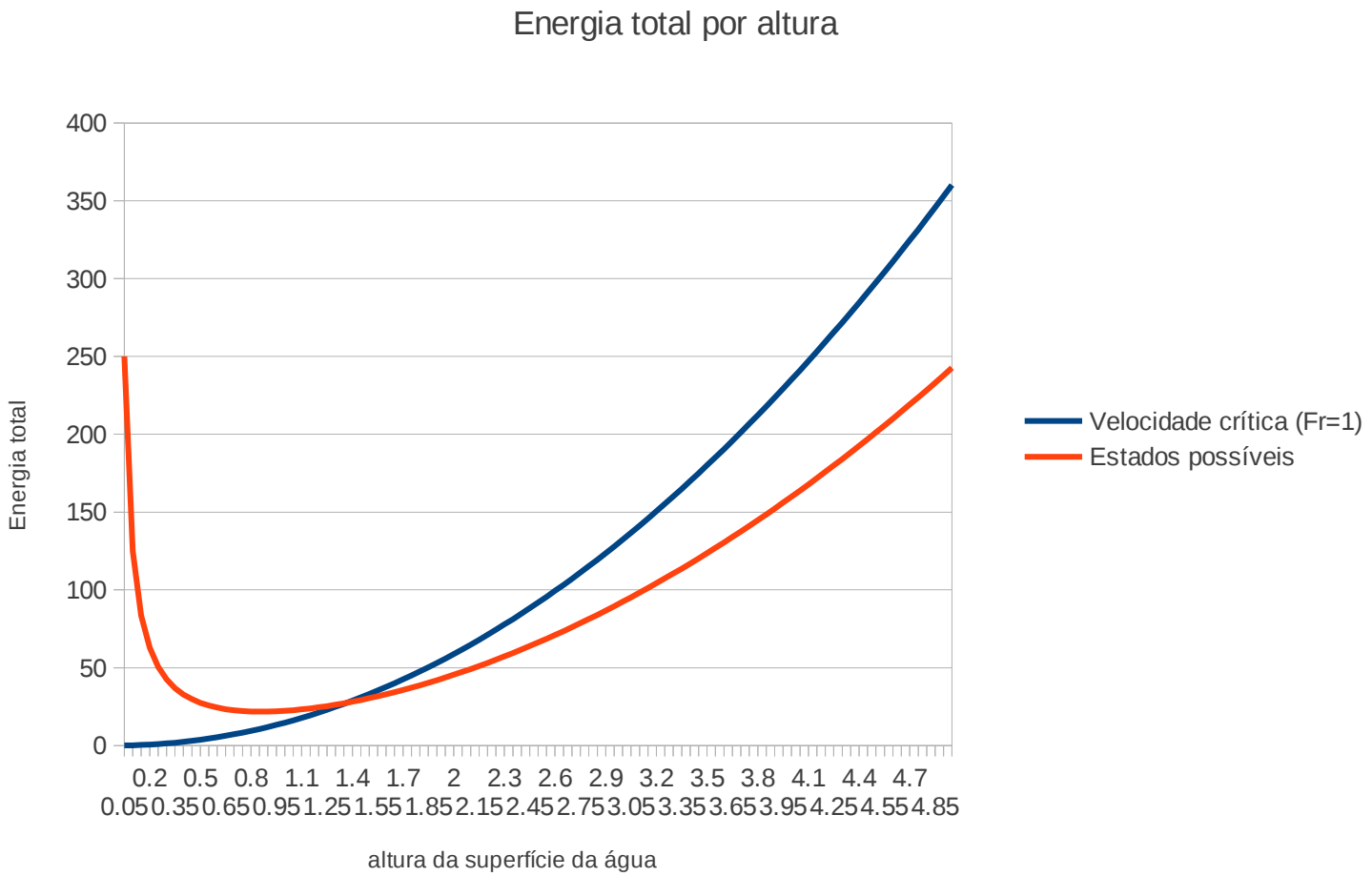

Velocidade de ondas de superfície

Velocidade de ondas de superfície na água:

Se a profundidade é maior que L/2 - Ondas de águas profundas -> $C=(gL/2\pi)^{1/2}$
Onde L é o comprimento de onda.

Se a profundidade é menor que L/2 – Ondas de águas rasas → $C=(gD)^{1/2}$
Onde D é a profundidade

Wave Type	Typical Wavelength	Disturbing Force	Restoring Force
Capillary wave	< 2 cm	Wind	Surface tension
Wind wave	60-150 m (200-500 ft)	Wind over ocean	Gravity
Seiche	Large, variable; a function of basin size	Change in atmospheric pressure, storm surge	Gravity
Seismic sea wave (tsunami)	200 km (125 mi)	Faulting of sea floor, volcanic eruption, landslide	Gravity
Tide	Half the circumference of Earth	Gravitational attraction, rotation of Earth	Gravity

Regimes de Fluxo

Se considerarmos as dusa fórmulas de cisalhamento de fundo:

$\delta c = \rho g h S$, onde S é a declividade e:

$\delta c / \rho = v^2 * Cf$, onde Cf é um coeficiente de fricção = 0.01

Temos que Froude=$(v^2/gh)^{1/2}=(S/Cf)^{1/2}$

Então o que determina o Froude é uma declividade crítica.

Salto Hidráulico

A passagem do fluxo supercríticoc para o subcrítico é brusca, causando o salto hidráulico

Regimes de Fluxo

	Fluxo Superior	Fluxo Inferior
N Froude	> 1	<1
relação superfície da água / topografia do fundo	Em fase	Fora de fase
turbulência	alta	moderada
ocorrência	Águas muito rasas ou grandes enchurradas	Maior parte das correntes naturais

Formas de leito e estratificações geradas por fluxo unidirecional

Velocidade do fluxo e formas de leito

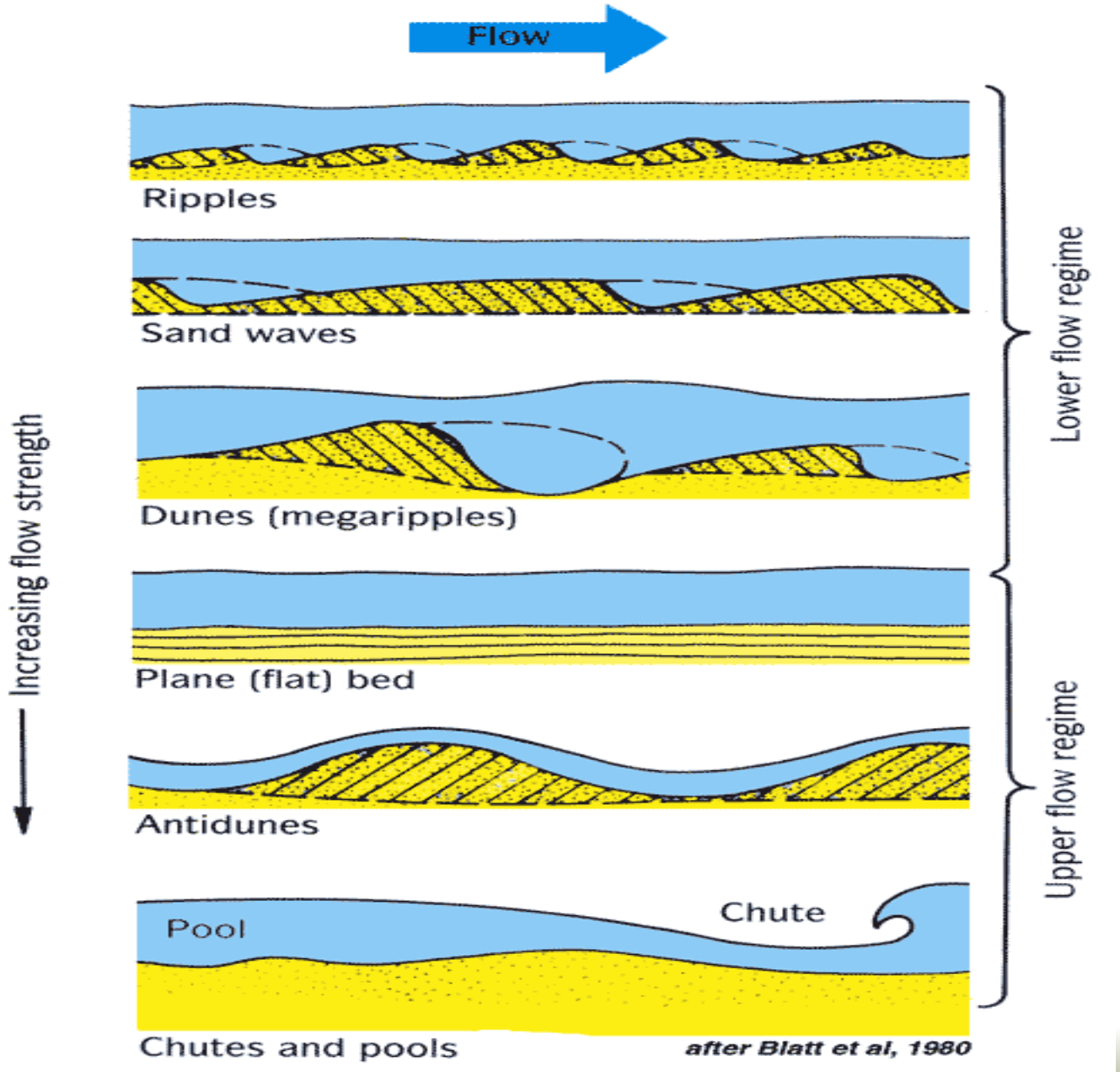

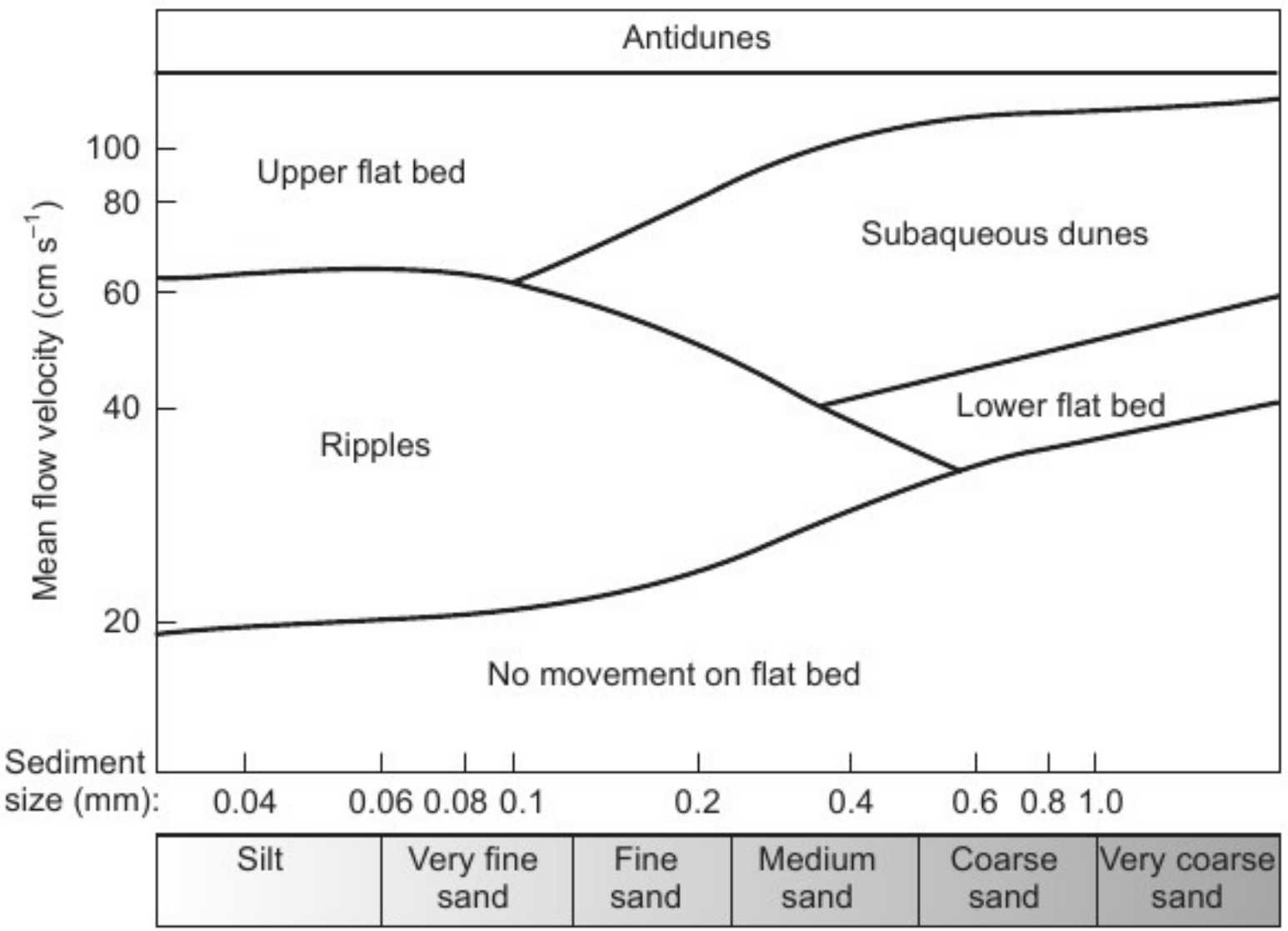
Antidunes
Upper flat bed
Subaqueous dunes
Lower flat bed
Ripples
No movement on flat bed
Mean flow velocity (cm s^{-1})
100
80
60
40
20
Sediment size (mm):
0.04
0.06
0.08
0.1
0.2
0.4
0.6
0.8
1.0
Silt
Very fine sand
Fine sand
Medium sand
Coarse sand
Very coarse sand

Filmes

Anti-dunas

Leito Plano

Migração de formas de leito e formação de estratificações

Leito plano

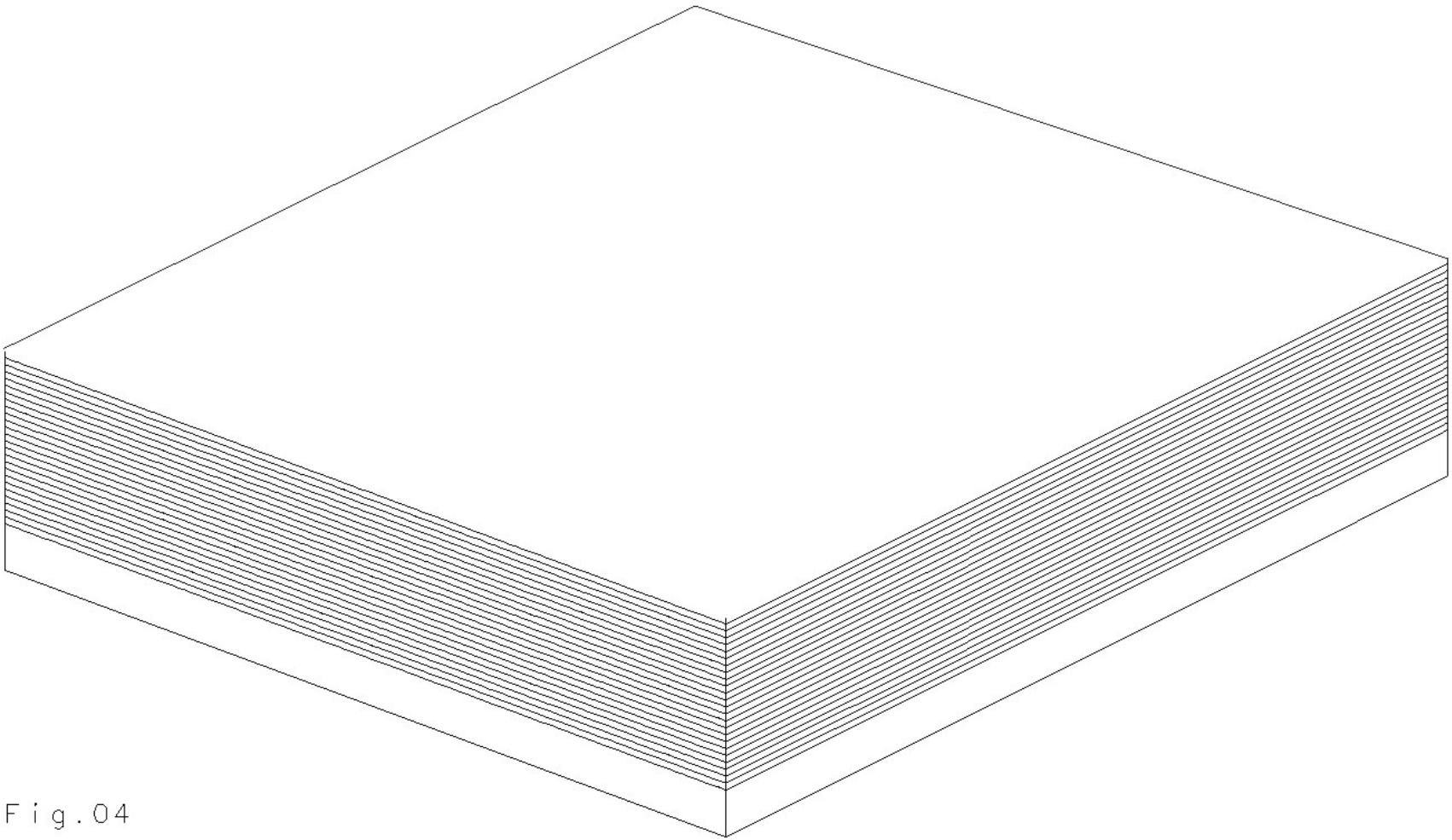

Fig.04

Stoss- and lee-depositional climb

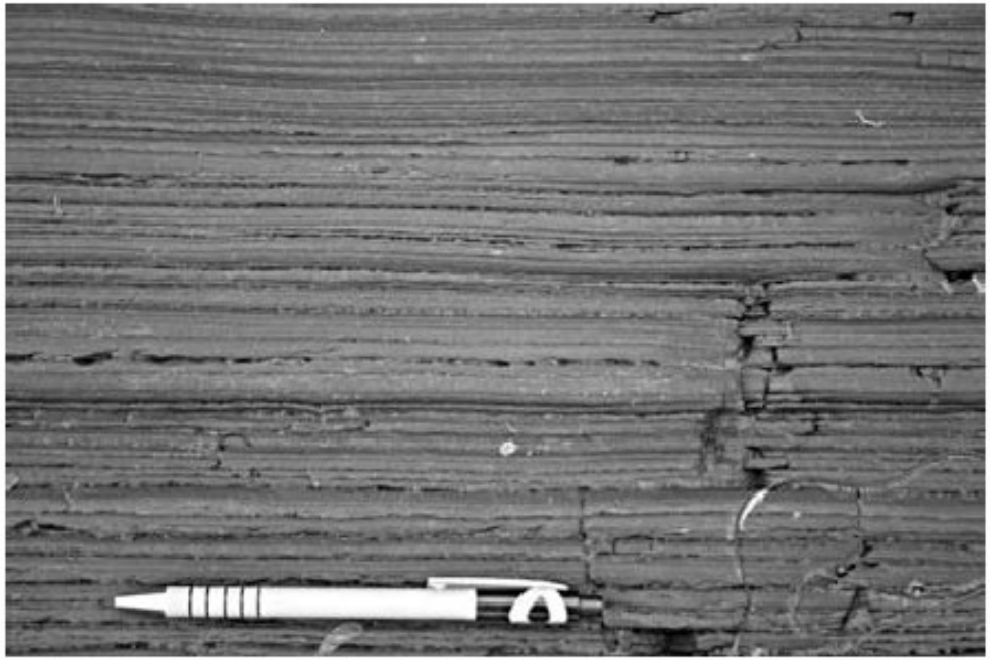

Fig. 4.19 Horizontal lamination in sandstone beds.

Lineação de corrente

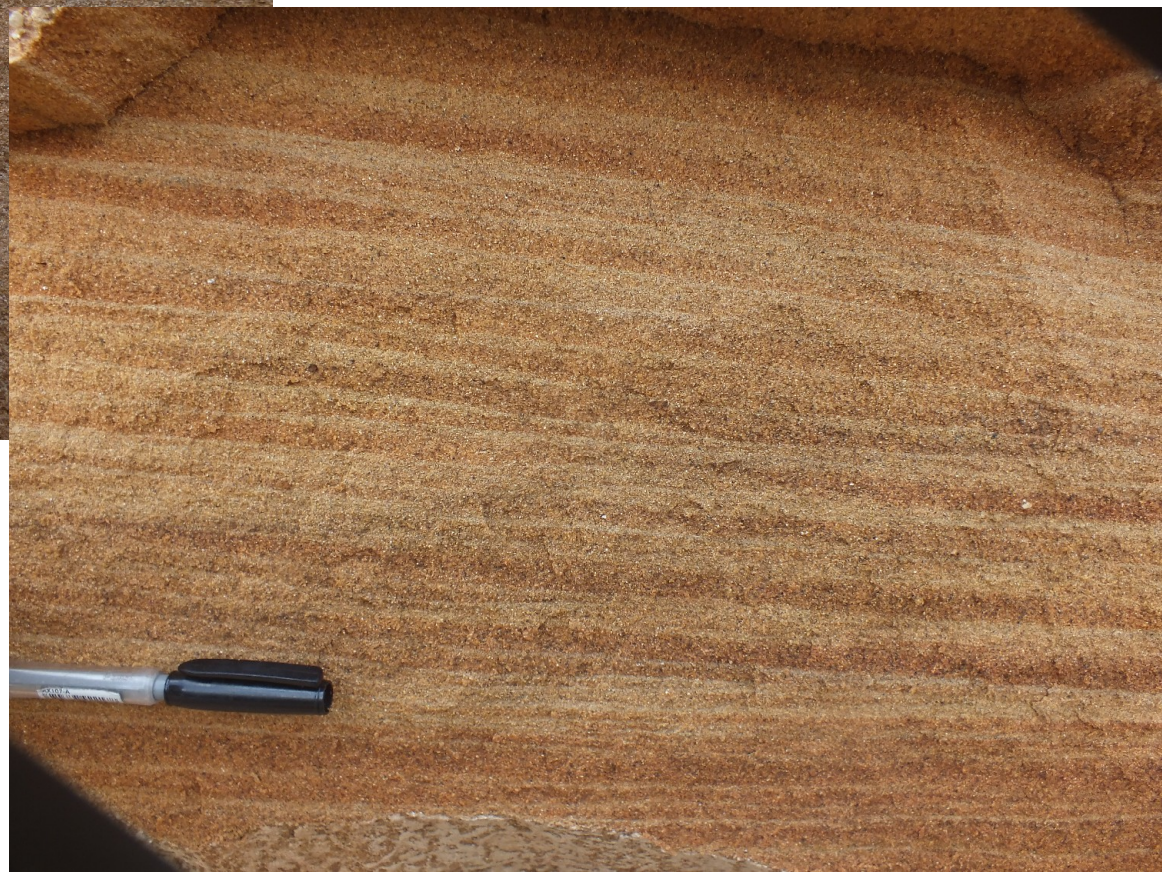


Como ocorre a segregação?

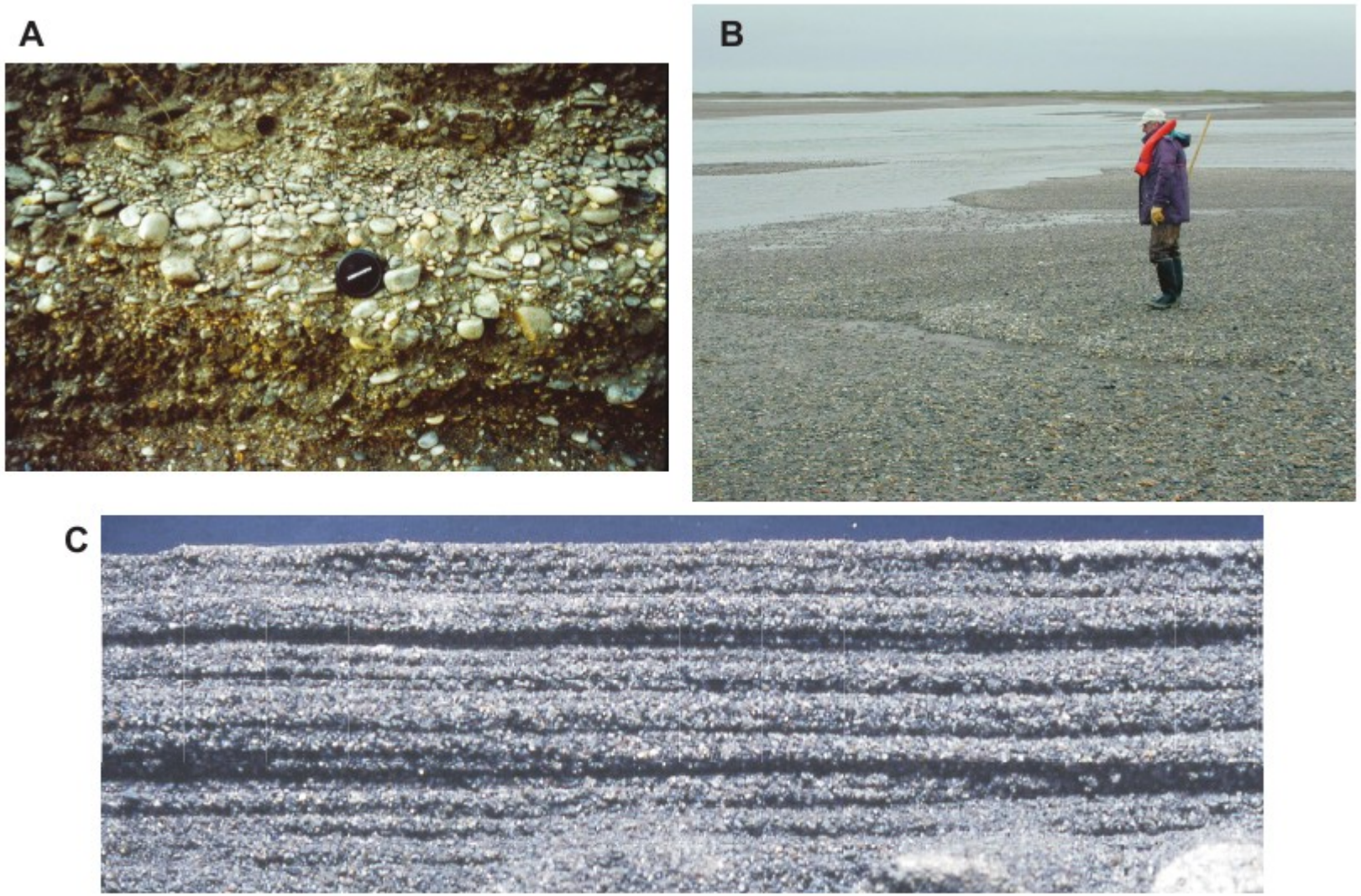

FIG. 3—**A)** Planar strata in gravel formed by migration of bedload sheets. A planar stratum composed of open-framework gravel occurs in the middle of the photo. The base of this stratum is relatively coarse grained and contains imbricated pebbles dipping to the left. The upper part of the stratum is finer grained and contains pseudo-imbricated pebbles dipping to the right. **B)** bedload sheets on a bar in the Sagavanirktok River, Alaska. **C)** Planar strata in sand formed by migration of low-relief bed waves (bedload sheets) on upper-stage plane beds. Section is 30 mm thick. The dark boundaries of the planar laminae are formed of relatively fine-grained sediment deposited from suspension in the troughs of bed-load sheets. From experiments of J.S. Bridge and J.L. Best.

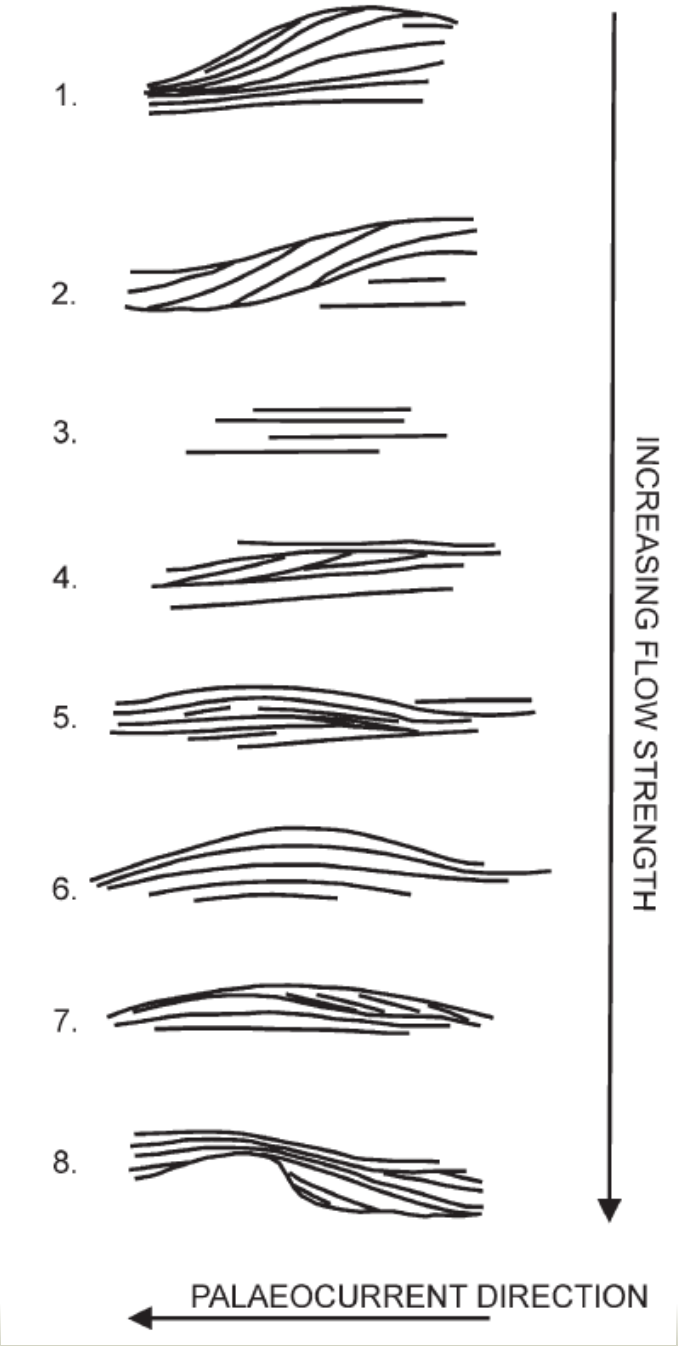

Transição entre os regimes de fluxo e estruturas de RFS

Line drawings to show an interpreted spectrum of sedimentary structures representative of the upper flow regime, from transitional dunes, through plane bed, transitional antidunes and antidunes, to chute and pool bedform states. Note that the drawings are intended to be scale-independent. Parting lineation is present on the bedding planes of many if not all of these structures.

Fielding (2006)

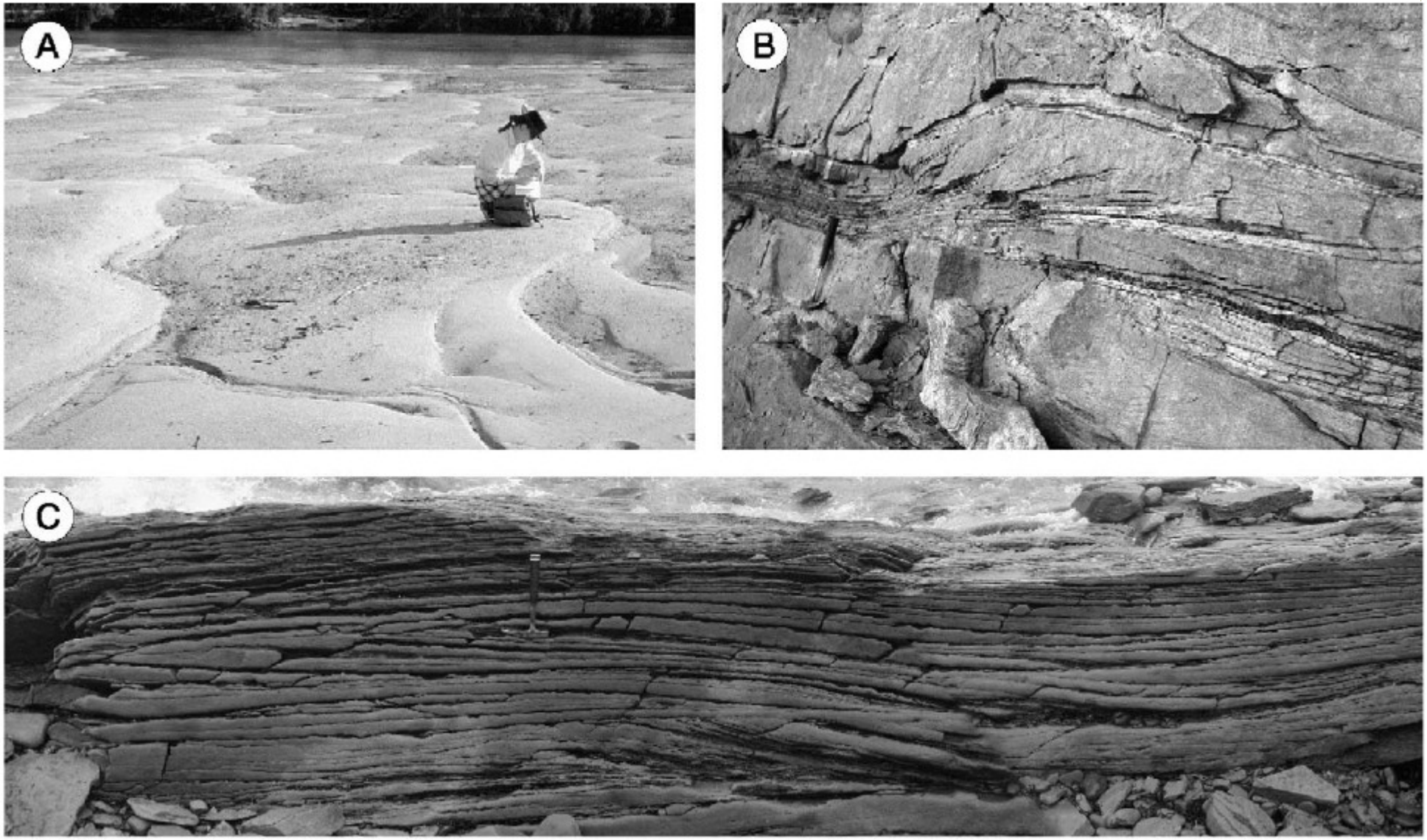

Photographs of cross-bedding structures considered representative of the transition from dune to upper plane bed phase. A) Small-scale, washed out dunes, showing flat, eroded tops. B) “Humpback cross-bedding” set, showing preservation of the complete bedform, reworking of the stoss side by small dunes or ripples, sigmoidal foreset geometry and flattening out of the lee side into an extensive bottomset. C) Example of humpback cross-bedding transitional to flat lamination, showing flattening out of foreset bedding downdip and upward through the set, culminating in a convex upward (hummocky) bedform.

Bacia do Tucano

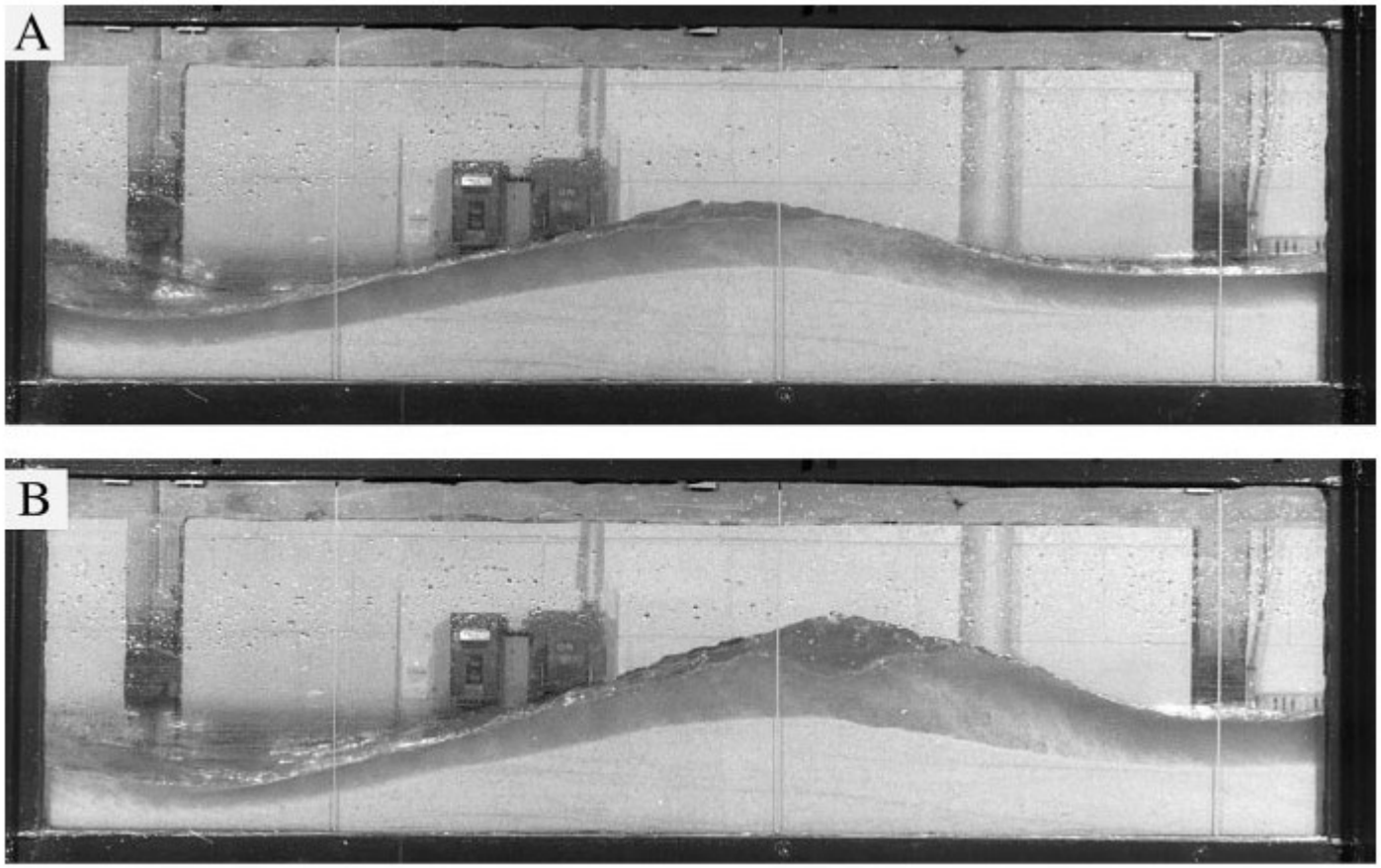

Photographs of test section (1á5 m wide) in Run 2 with water ¯ow from right to left. (A) standing water-surface wave and developing antidune, (B) asymmetrical water-surface wave and antidune, with ¯ow separation zone on upstream side of antidune prior to wave breaking,

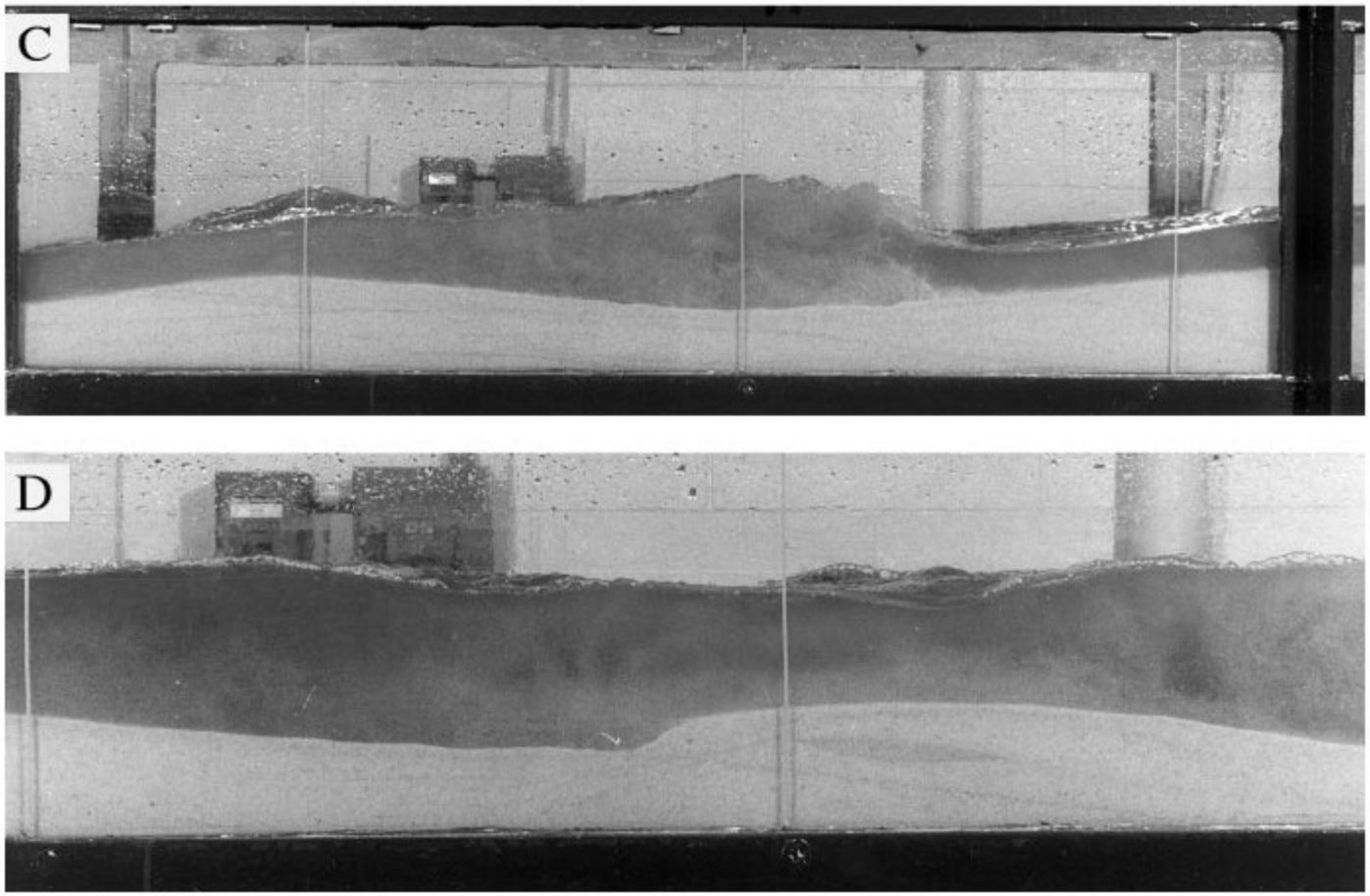

(C) a breaking wave and (D) asymmetrical bedform migrating into antidune trough after wave breaking.

Alexander et al. (2001)

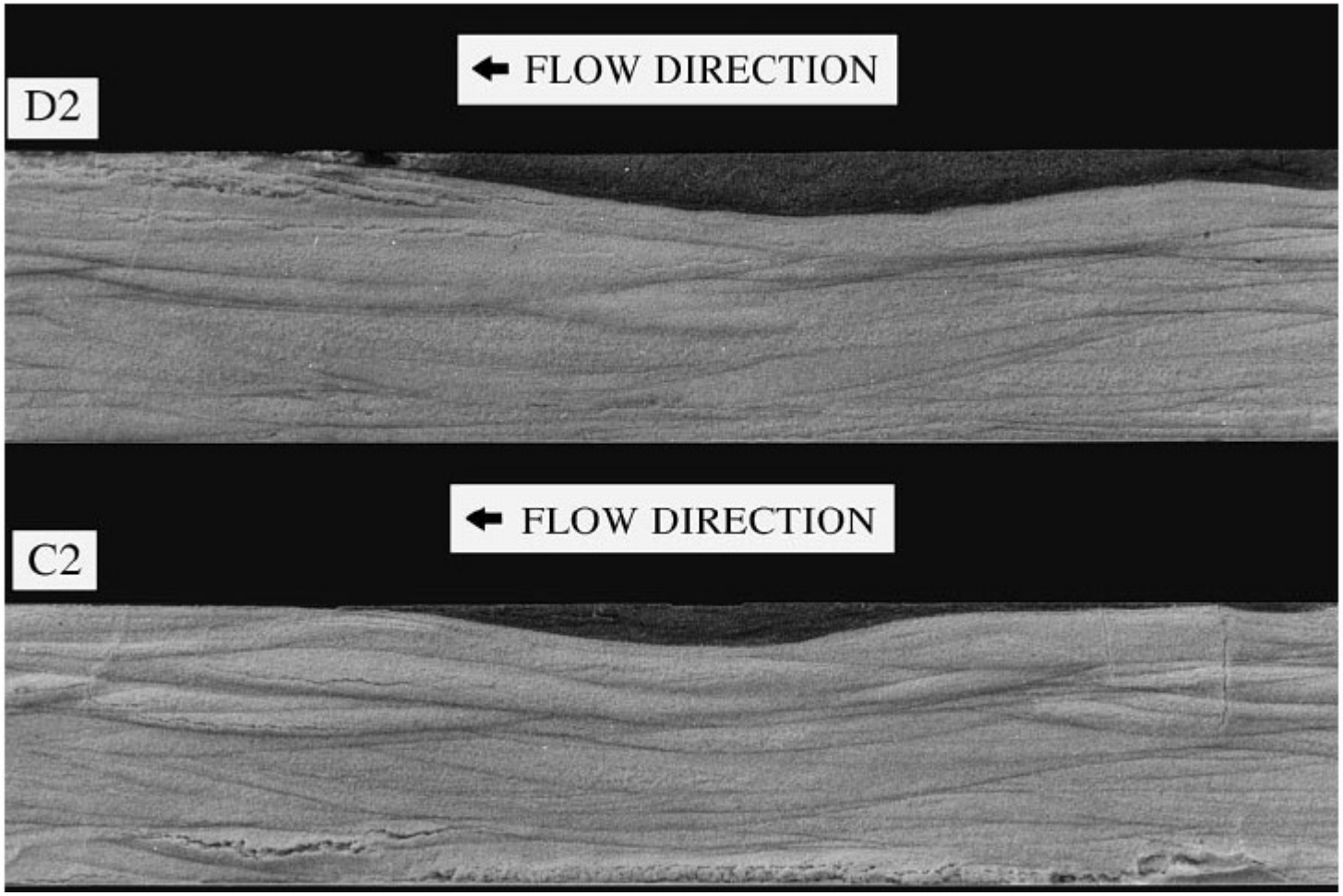

Estratificação por desestabilização de antidunas (Alexander, 2001)

Alexander, J.; Bridge, J. S.; Cheel, R. J. & Leclair , S. F. (2001), 'Bedforms and associated sedimentary structures formed under supercritical water ¯ows over aggrading sand beds', *Sedimentology* **48**, 133- 152.

Bridge, J. & Demicco, R. (2008), *Earth Surface Processes, Landforms and Sediment Deposits*, Cambridge University Press.

Eriksson, P.; Banerjee, S.; Catuneanu, O.; Sarkar, S.; Bumby, A. & Mtimkulu, M. (2007), 'Prime controls on Archaean-Palaeoproterozoic sedimentation: Change over time', *Gondwana Research* **12**(4), 550--559.

Eriksson, P.; Catuneanu, O.; Nelson, D. & Popa, M. (2005), 'Controls on Precambrian sea level change and sedimentary cyclicity', *Sedimentary Geology* **176**(1-2), 43--65.

Eriksson, P.; Martins-Neto, M.; Nelson, D.; Aspler, L.; Chiarenzelli, J.; Catuneanu, O.; Sarkar, S.; Altermann, W. & de W. Rautenbach, C. (2001), 'An introduction to Precambrian basins: their characteristics and genesis', *Sedimentary Geology* **141**, 1-35.

Eriksson, P. G.; Catuneanu, O.; Sarkar, S. & Tirsgaard, H. (2005), 'Patterns of sedimentation in the Precambrian', *Sedimentary Geology* **176**, 17â€“42.

Eriksson, P. G.; Condie, K. C.; Tirsgaard, H.; Mueller, W. U.; Altermann, W.; Miall, A. D.; Aspler, L. B.; Catuneanu, O. & Chiarenzelli, J. R. (1998), 'Precambrian clastic sedimentation systems', *Sedimentary Geology 120 (1998) 5–53* **120**, 5-53.

Eriksson, P. G.; Mazumder, R.; Catuneanu, O.; Bumby, A. J. & Ountsché Ilondo, B. (2006), 'Precambrian continental freeboard and geological evolution: A time perspective', *Earth-Science Reviews* **79**(3-4), 165--204.

Fielding, C. R. (2006), 'Upper flow regime sheets, lenses and scour fills: Extending the range of architectural elements for fluvial sediment bodies', *Sedimentary Geology* **190**, 227-240.

Nichols, G. (2009), *Sedimentology and Stratigraphy*, Wiley-Bleckwell.

Selley, R. C. (2000), *Applied Sedimentology*.

Sistema fluvial - macroformas

FIG. 14.—Sagavanirktok (northern Alaska, U.S.A.) channel belt with compound braid bars and point bars associated with braided and meandering channels, and anastomosing, braided–meandering channels separated by a bar assemblage. Compound bars have accretion topography indicating downstream translation and lateral growth, and channel fills are also evident. Channel belt is 2 km wide.

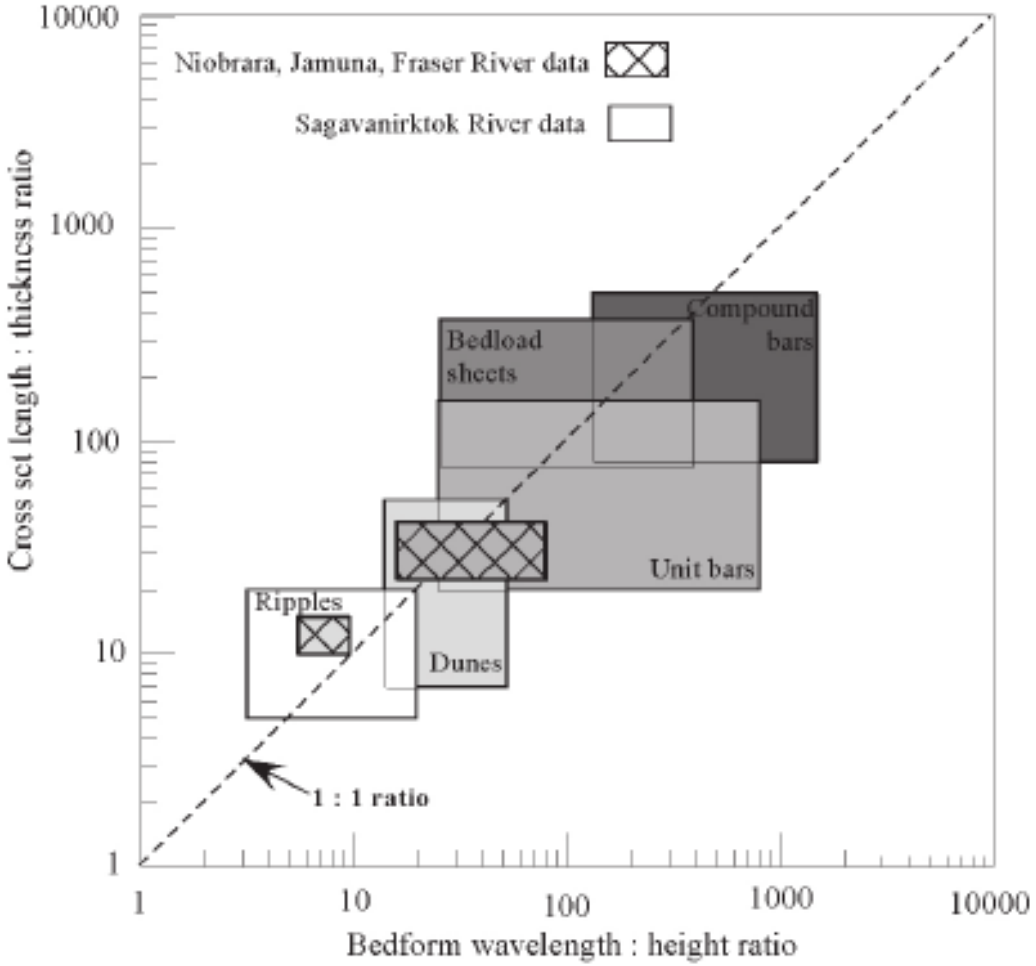

FIG. 6.—Scales of bedforms and associated stratasets from modern rivers. From Bridge and Lunt (2006).

Barra Unitária
Escalada
com a largura

Barra Composta Escalada
com a largura

Rio Surutu Bolívia

Barras unitárias

Rio Sone (Índia) próximo ao encontro com o Ganges

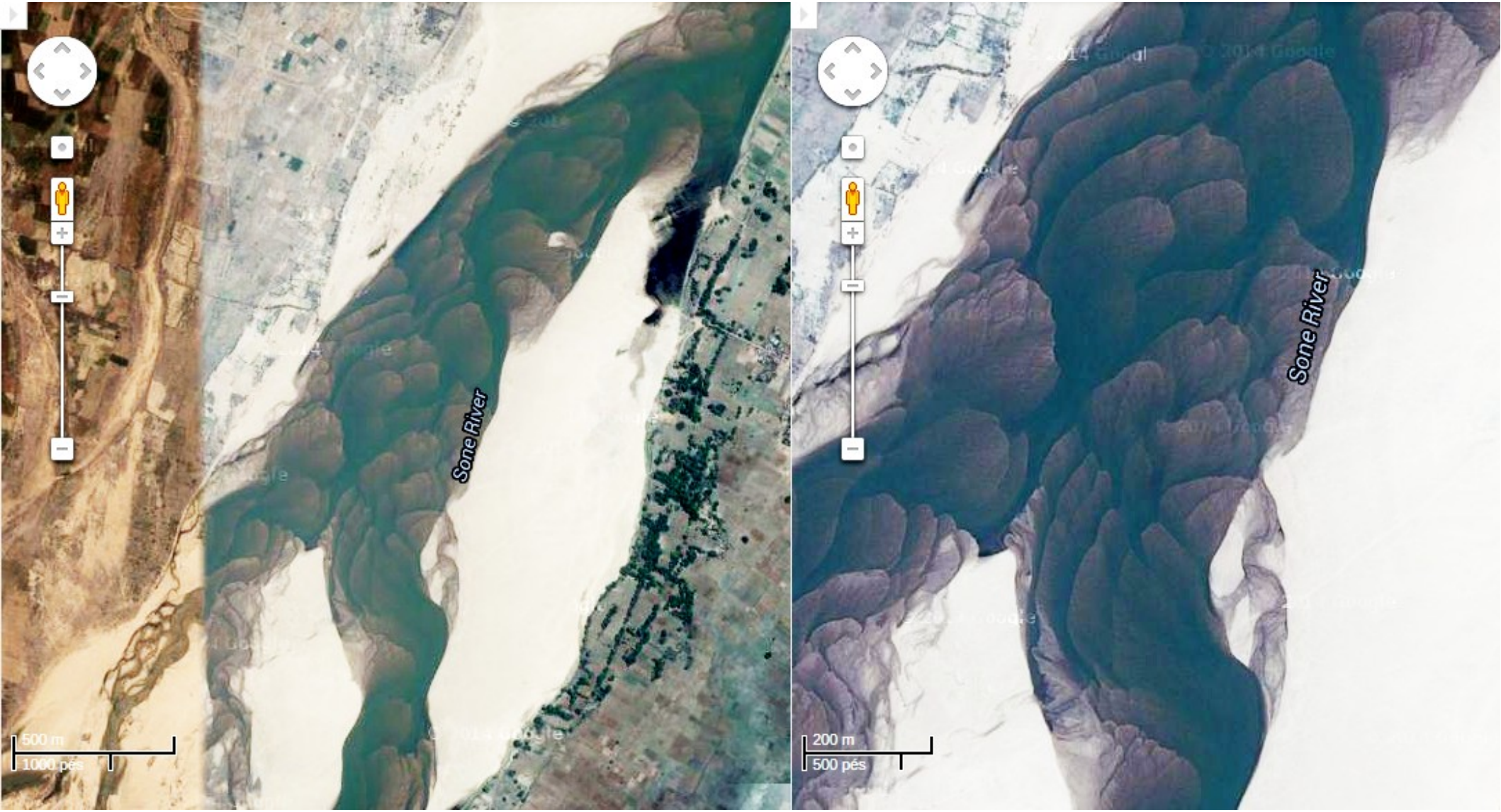

Barras unitárias

Rio Surutu Bolívia

Barras unitárias e dunas compostas.

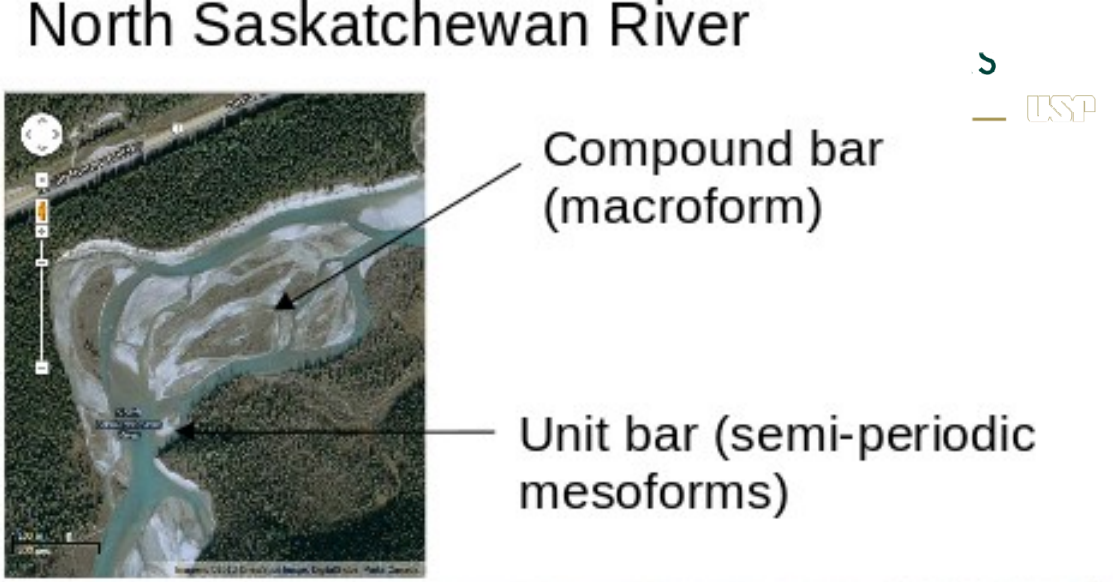

Rio Ghangara (entrelaçado, Índia) próximo ao encontro com o Ganges

Rio Ghangara (entrelaçado, Índia) próximo ao encontro com o Ganges

Rio Ghangara (entrelaçado, Índia) próximo ao encontro com o Ganges

Barra unítaria com dunas simples sobrepostas em rio de médio porte

Rio Brahmaputra próximo a Guwahati

Rio Brahmaputra próximo a Guwahati

Barra unitária sobreposta por dunas compostas em
Ri de grande porte

Rio Solimões

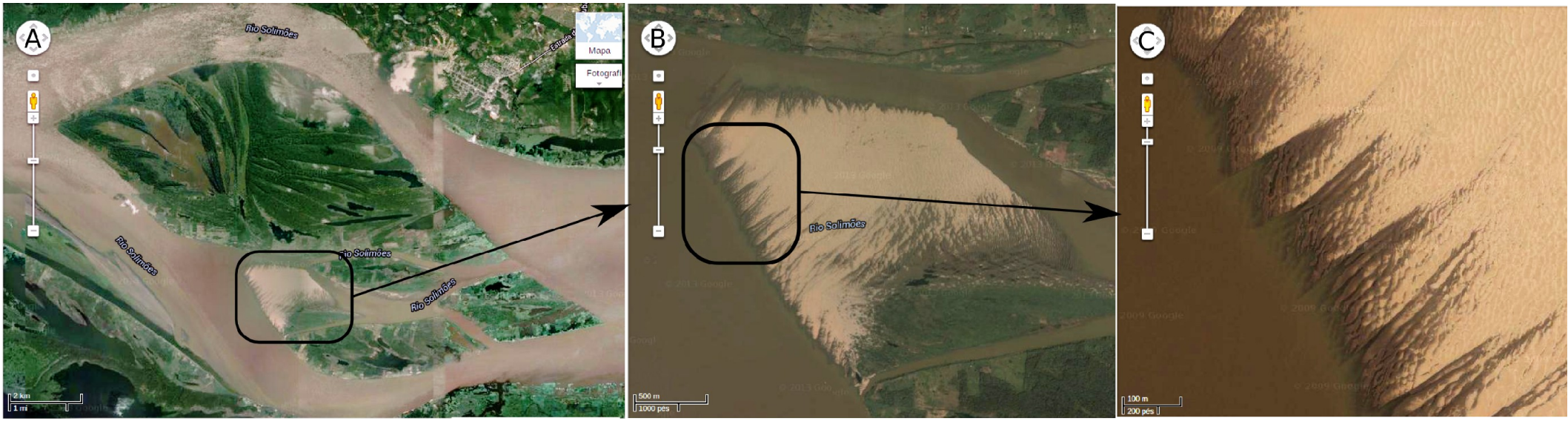

Fig 2. Example of complex unit bars in large river deposits. A- Compound bar in the Solimões River, Brazilian Amazon. B- Detail of exposed unit bar covered by large dunes. C- Detail of these large dunes, revealing superposition of smaller dunes. The presence of large compound dunes forming unit bars adds complexity to the patterns of cross-stratification and to the hierarchy of bounding surface in unit bar

Barra unitária sobreposta por dunas compostas em
Ri de grande porte

Rio Niger (retilíneo)

Rio Niger (retilíneo)

Rio Niger (retilíneo)

Rio Niger (retilíneo)

Barra unitária sobreposta por dunas compostas em
Ri de grande porte

GEOCIÊNCIAS
USP

Barras Compostas

Rio Brahmaputra próximo a Guwahati entrelaçado

GEOCIÊNCIAS USP

Barras Compostas

Rio Brahmaputra próximo a Guwahati

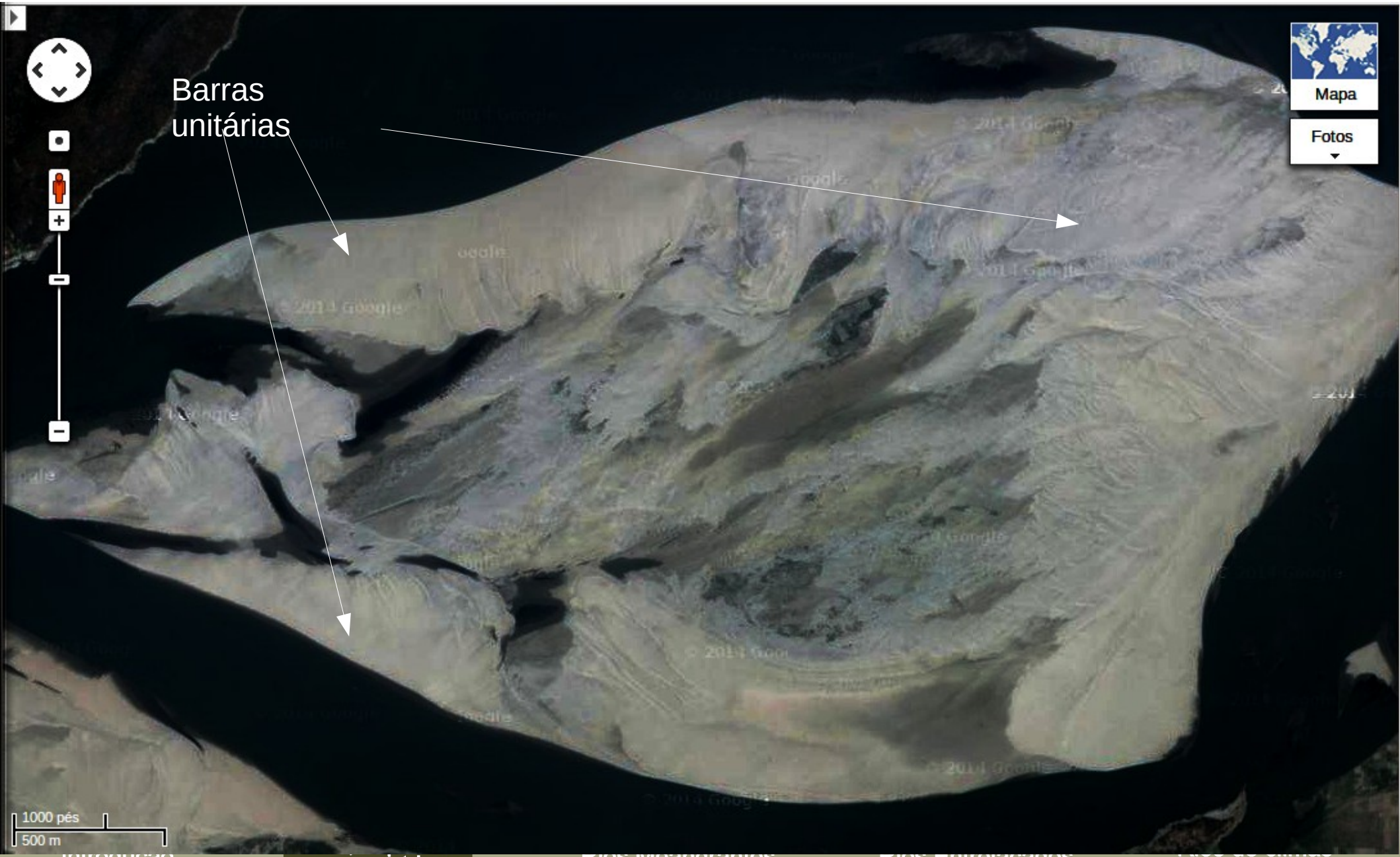

GEOCIÊNCIAS USP

Barras Compostas

Rio Brahmaputra próximo a Guwahati

Dunas sobre barras unitárias

GEOCIÊNCIAS USP

Barras Compostas

Rio Solimões

Rio Ucayali Peru

Rio Solimões (wandering)

RioKaratal (Meandrante)

Asymmetrical preservation of abandoned meanders due to tectonic tilting
Senguerr River, Argentina.

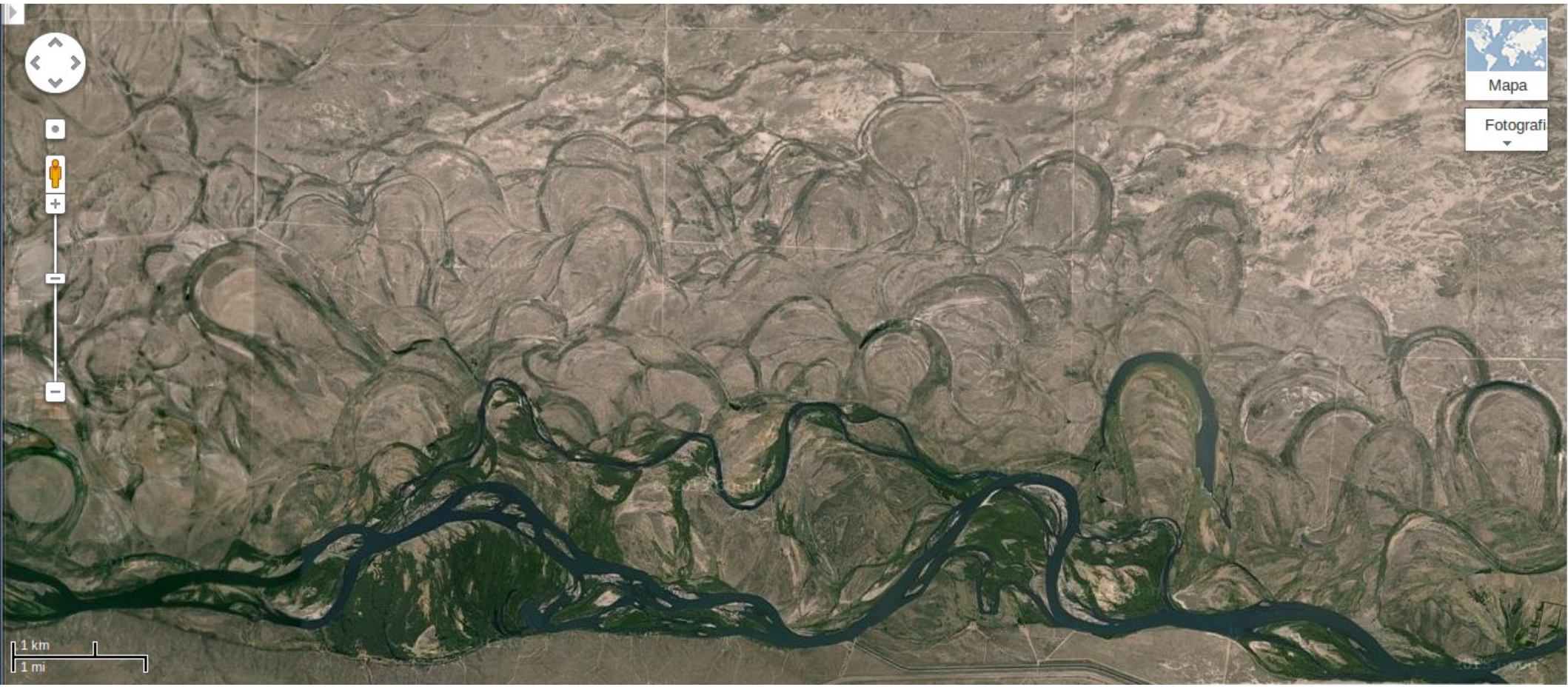

GEOCIÊNCIAS USP

Rio Brahmaputra próximo a Guwahati

Rio Brahmaputra próximo a Guwahati

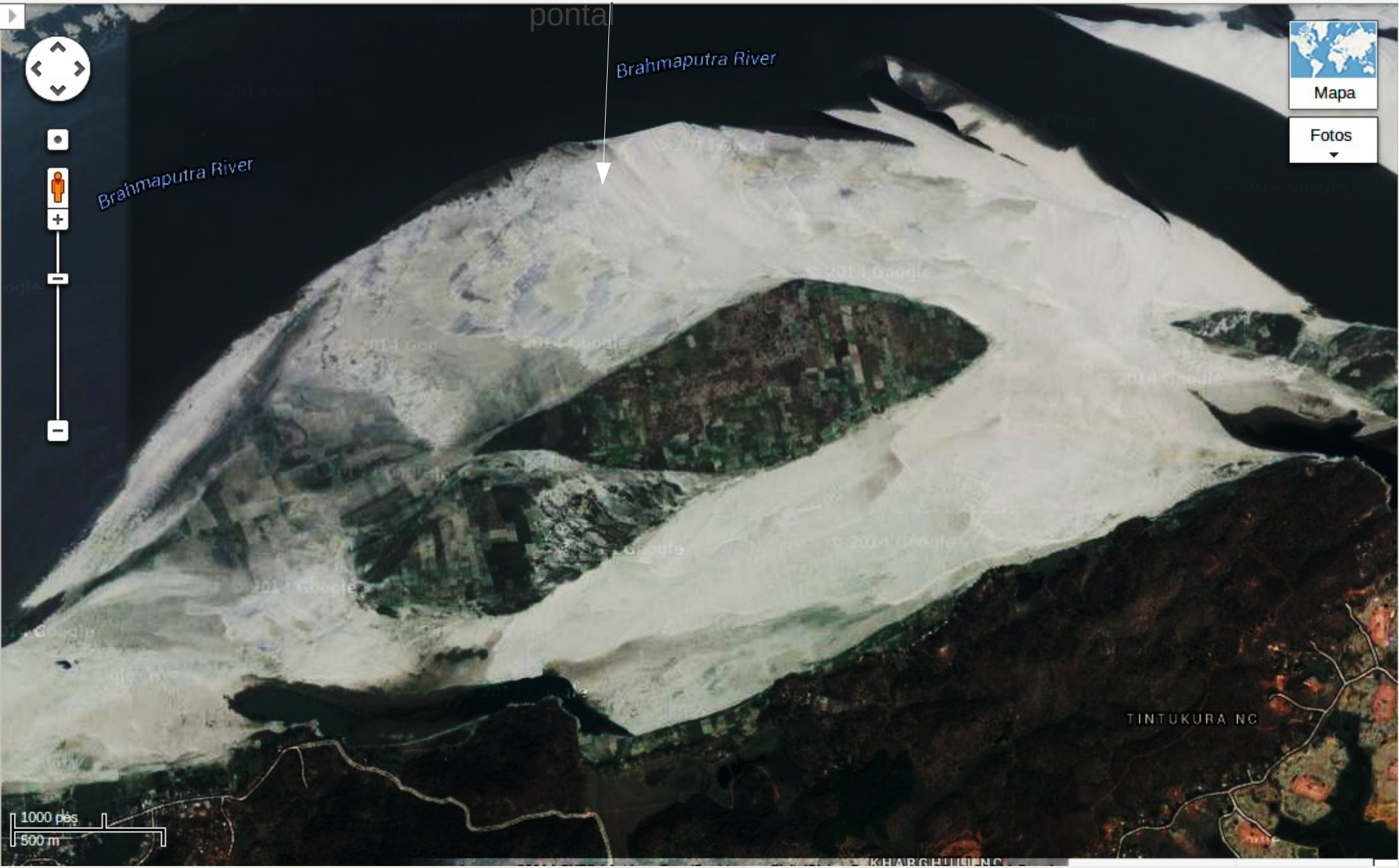

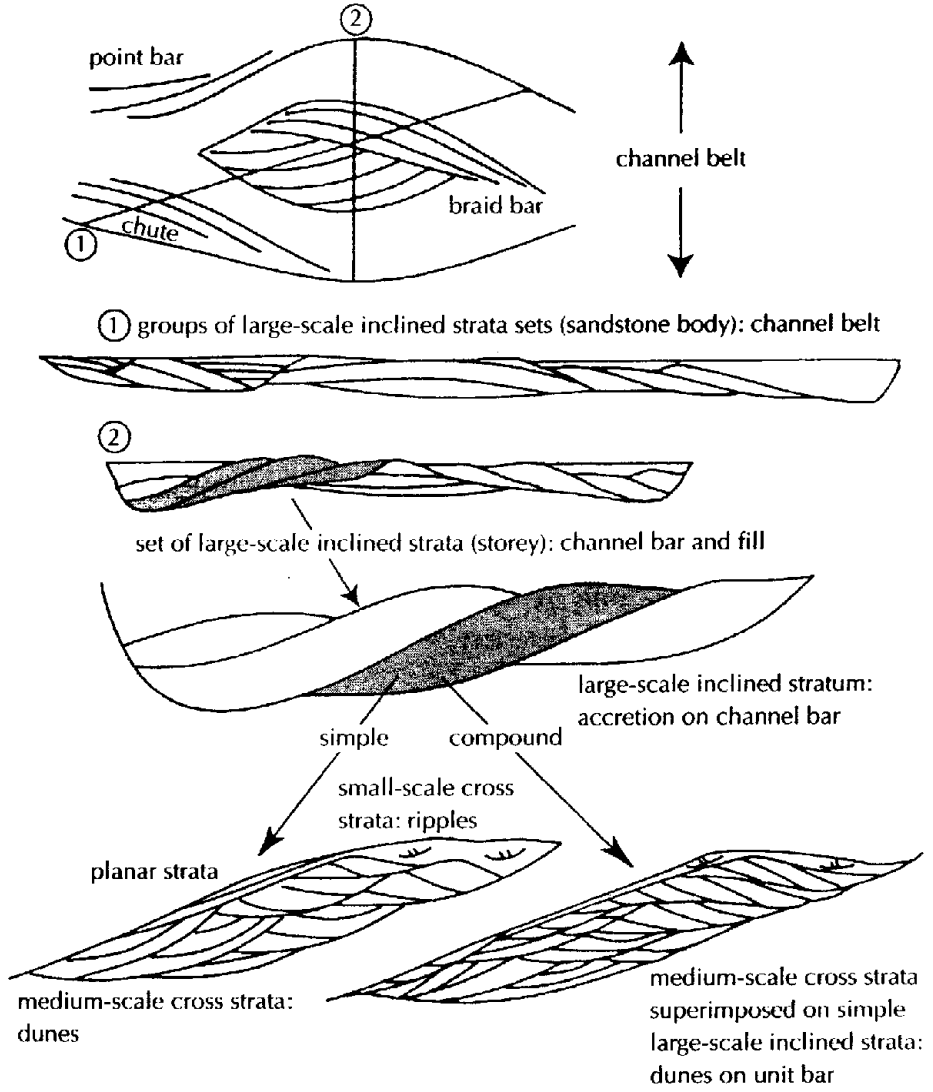

Fig. 5.42 Different scales of river deposits, illustrated with a cross section through a braided river. Upper section is a complete channel belt composed of several sets of large-scale inclined strata (storeys). The shaded storey (formed by incremental deposition on a channel bar) is expanded below to show detail of large-scale inclined strata. A large-scale inclined stratum (shaded) can be simple (formed during a single flood) or compound (associated with deposition on a unit bar over one or more flood periods). Large-scale inclined strata encompass smaller scale stratasets associated with passage of discrete bed waves moving over bars such as dunes, ripples, and bed-load sheets.

Distribuição de velocidades em canais meandrantes

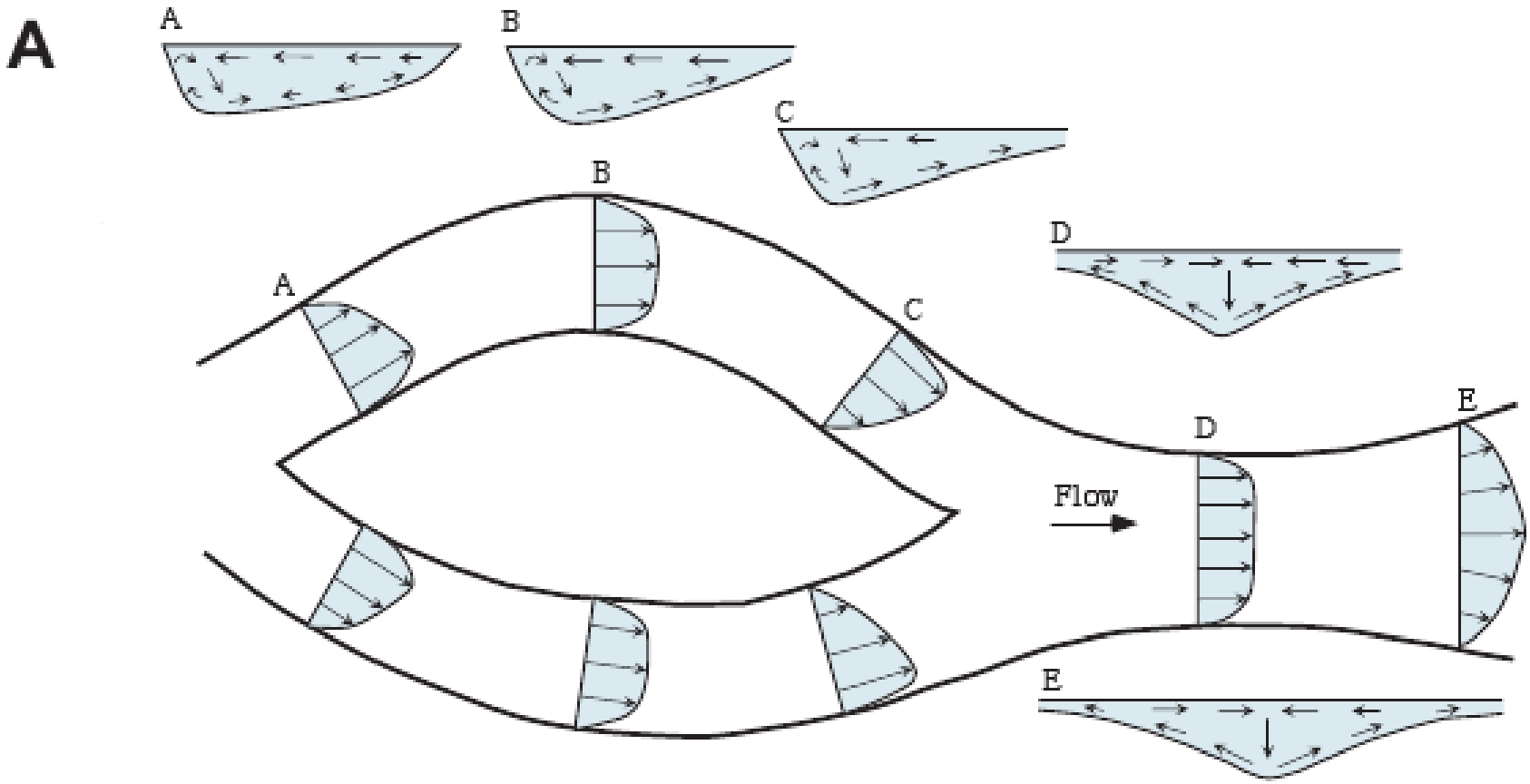

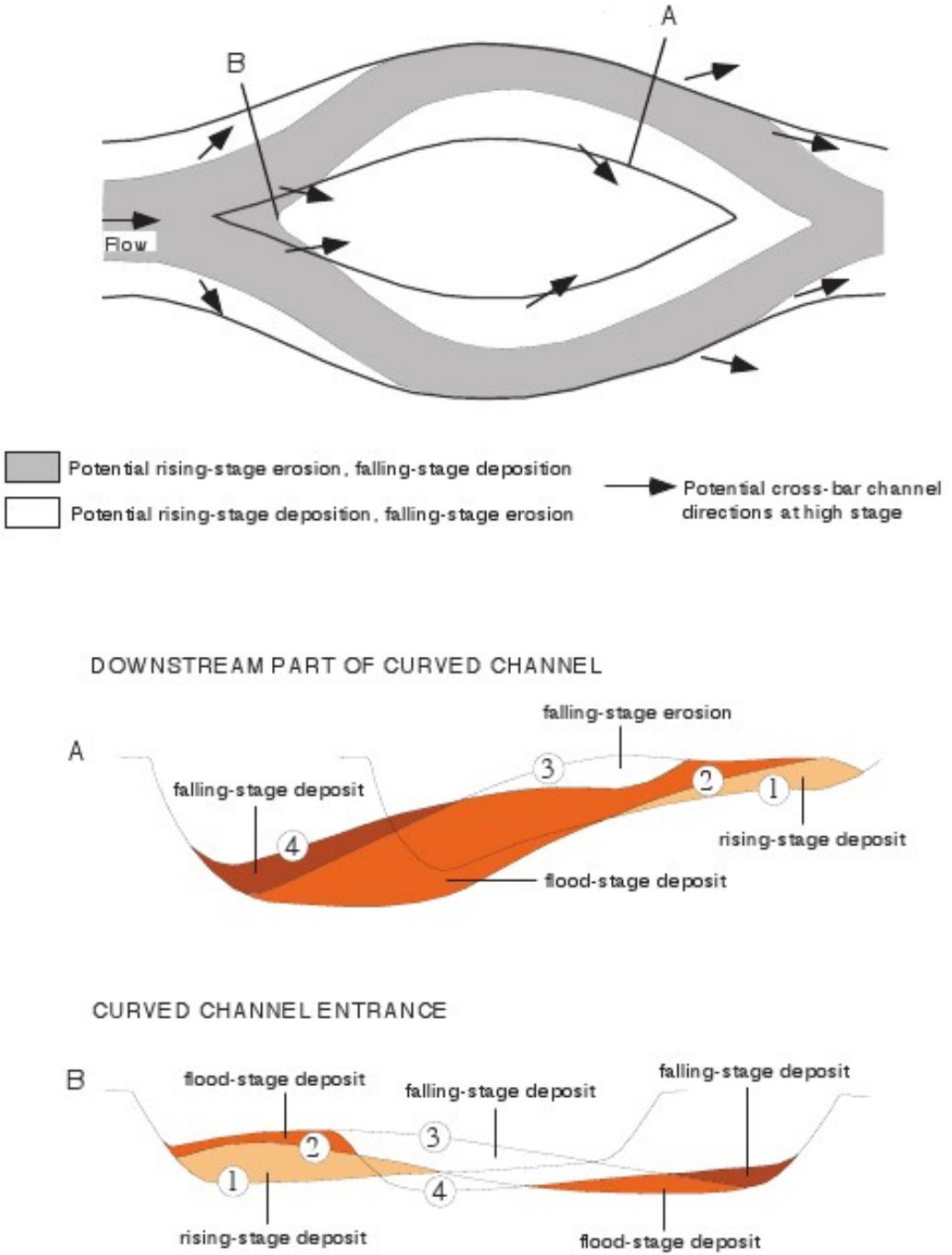

FIG. 12.—Typical pattern of erosion and deposition at the channel bar and bend scale for the case of a symmetrical braid bar (modified from Bridge, 1993). Cross sections show channel geometry during the course of a flood: (1) pre-flood low stage; (2) flood stage; (3) flood stage after bank erosion and bar deposition; (4) post-flood low stage.

Evolução de Barras longitudinais

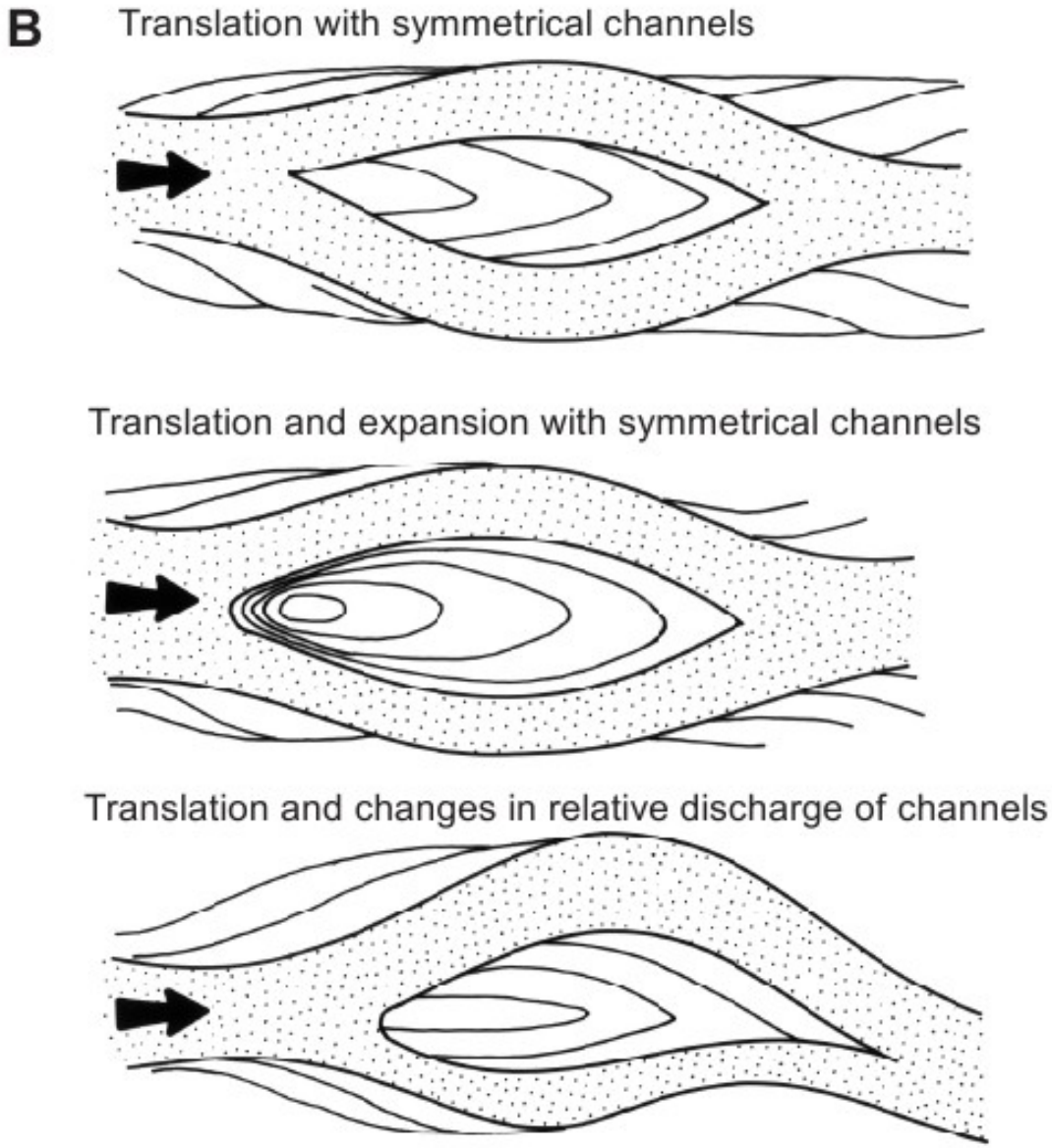

FIG. 13 (continued).—**B)** Typical modes of channel migration for simple braided-river patterns (from Bridge, 2003). Simplified accretionary units on braid bars (separated by lines) are actually composed of unit bars (bar-head lobes and bar-tail scrolls). The braid bar grows asymmetrically in the case where discharge in one channel is increasing at the expense of the other channel. Photo (Sagavanirktok River, northern Alaska, U.S.A.) shows braid bar with accretion topography, active channel to left and filling channel to right. Filling channel (about 120 m wide) contains lobate unit bars.

Fácies de barra longitudinal e barra transversal

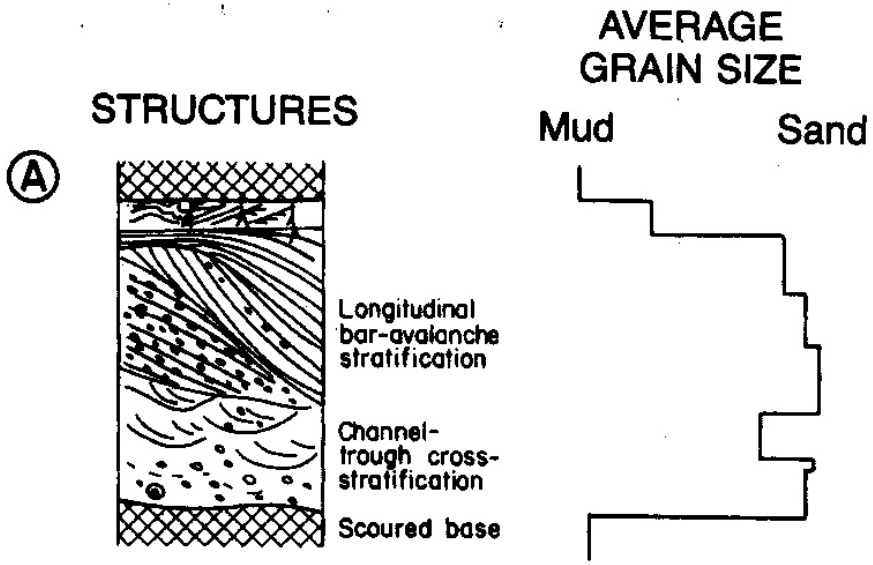

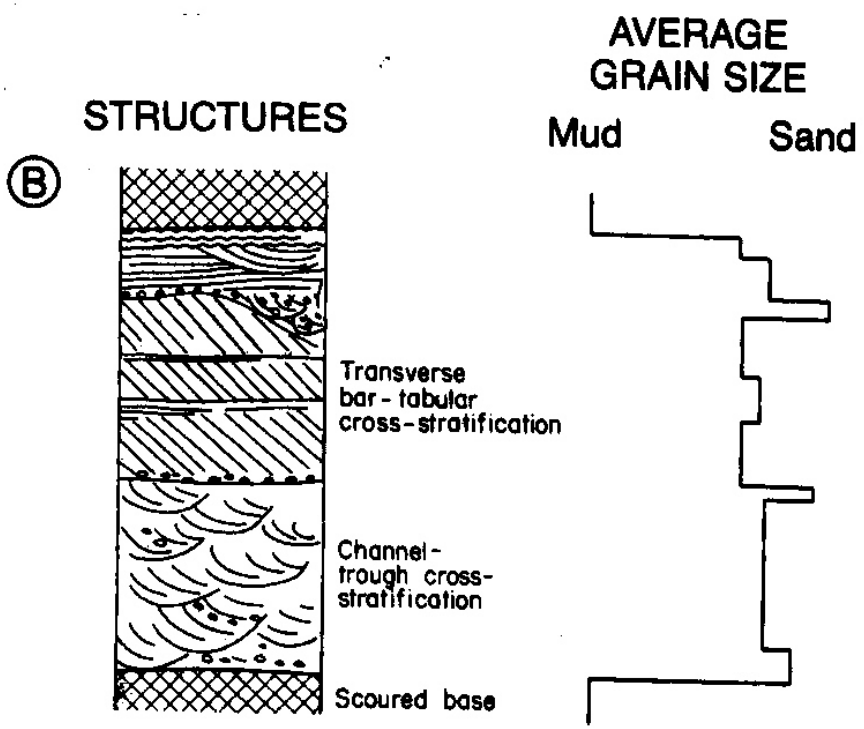

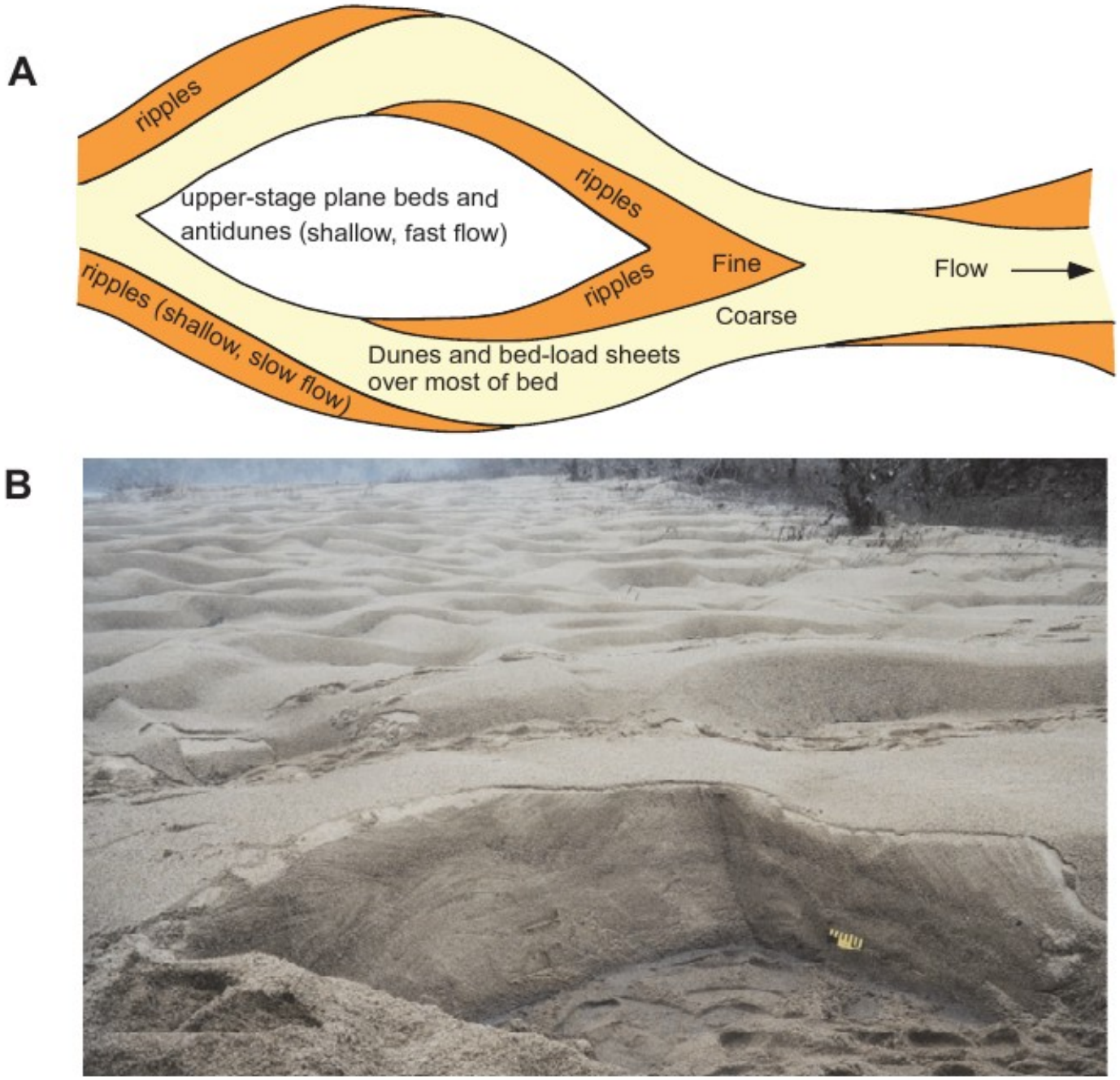

FIG. 11.—**A)** Schematic distribution of bedload grain size and sub–bar-scale bed forms in sandy and gravelly rivers at bankfull flow stage. Ripples occur only in sands with diameter less than about 0.7 mm. The boundary between coarse and fine sediment is actually gradational. **B)** Dunes preserved on the upper part of a point bar (Congaree River, South Carolina, U.S.A.) following a flood. Medium-scale trough cross strata exposed in trench in foreground. The scale in the trench is 0.15 m long, and the trench is about 0.75 m deep.

B Across-stream view of compound braid bar that migrated over a confluence

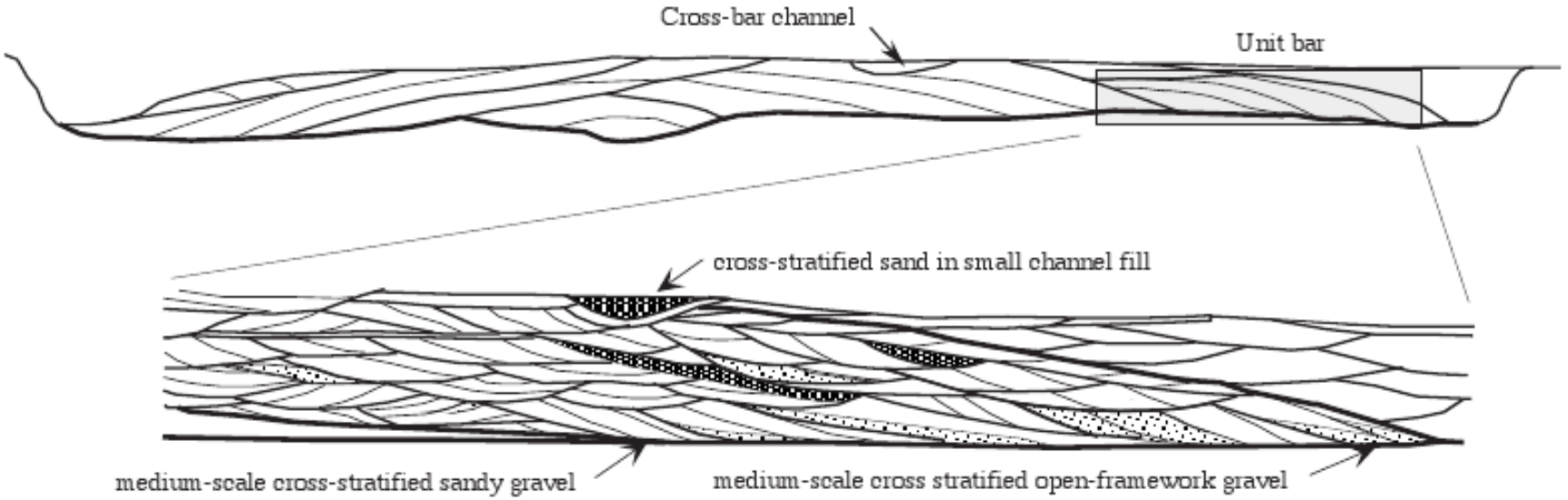

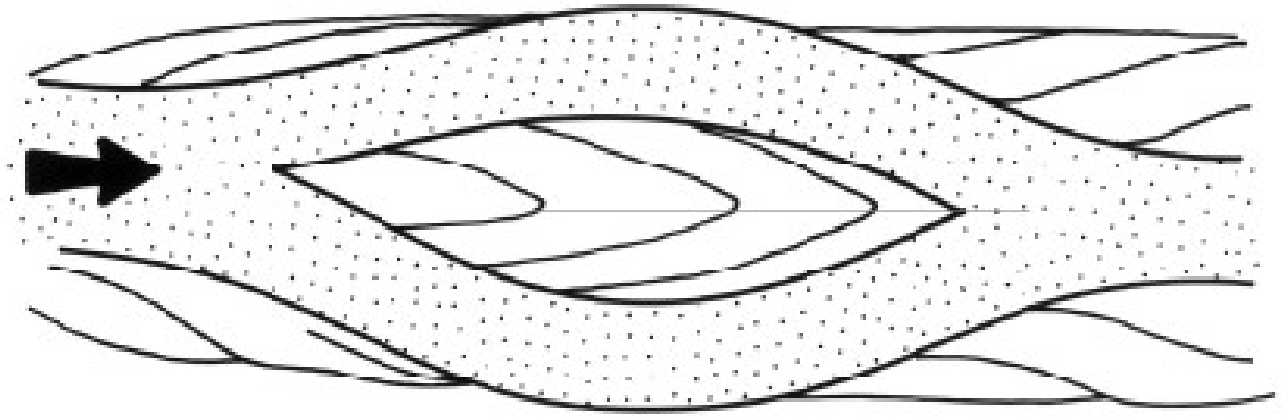

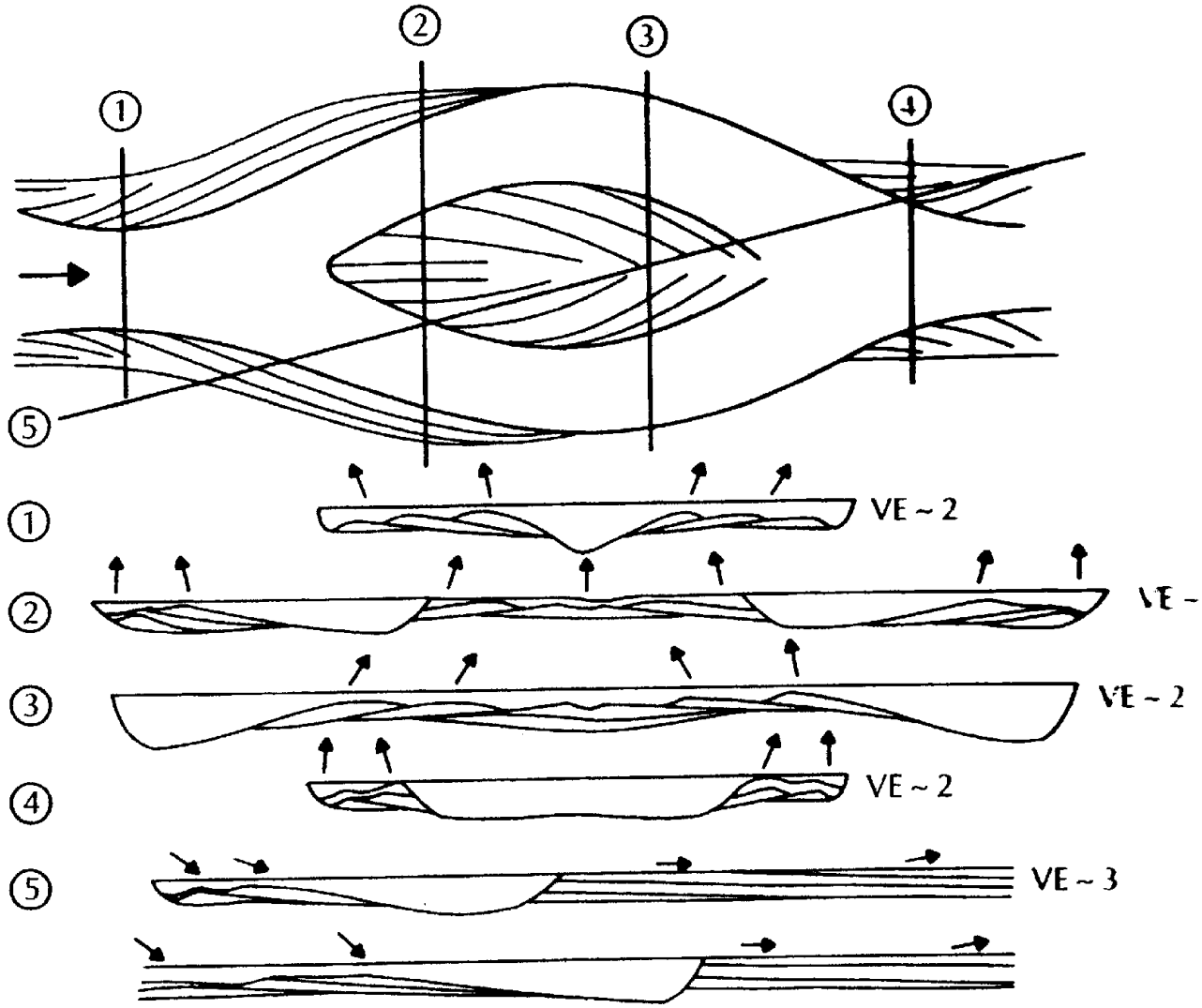

Fig. 5.46 Qualitative depositional model for simple braided channel, showing downstream bar migration but no vertical deposition (typical of gravelly rivers). Lines in plan and cross section are smoothed boundaries of large-scale inclined strata (no mesoforms or cross-bar channels shown). Arrows represent channel orientation during deposition of uppermost strata in the cross section (lower strata will have different orientations). Vertical exaggerations (VE) are approximately 2 to 3, and channel belt widths in nature will range from tens to thousands of meters. (From Bridge 1993a.)

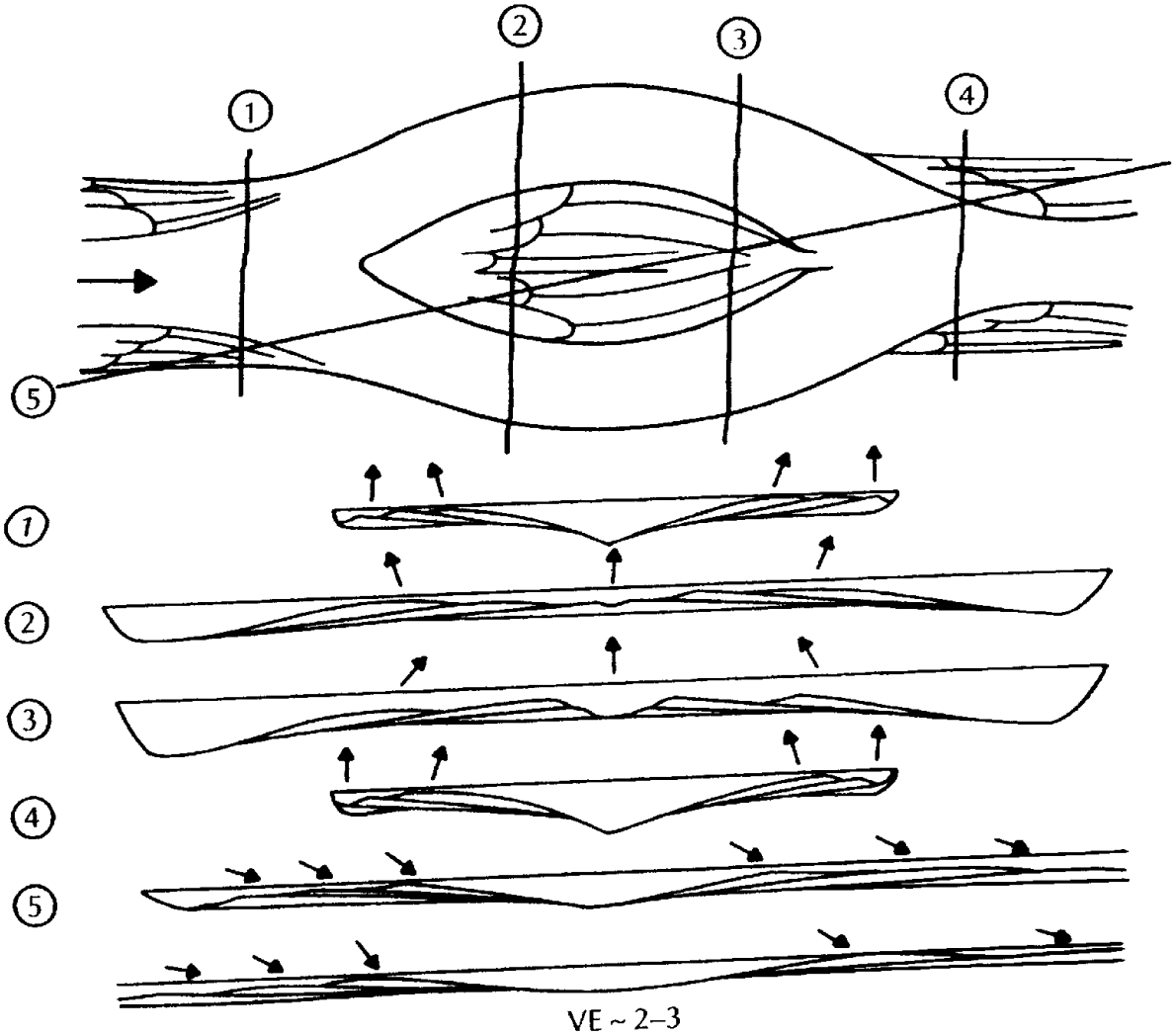

g. 5.47 Qualitative depositional odel of simple braided channel with ownstream bar migration and bend xpansion (typical of sandy rivers). ee caption for Fig. 5.46. (From Bridge 993a.)

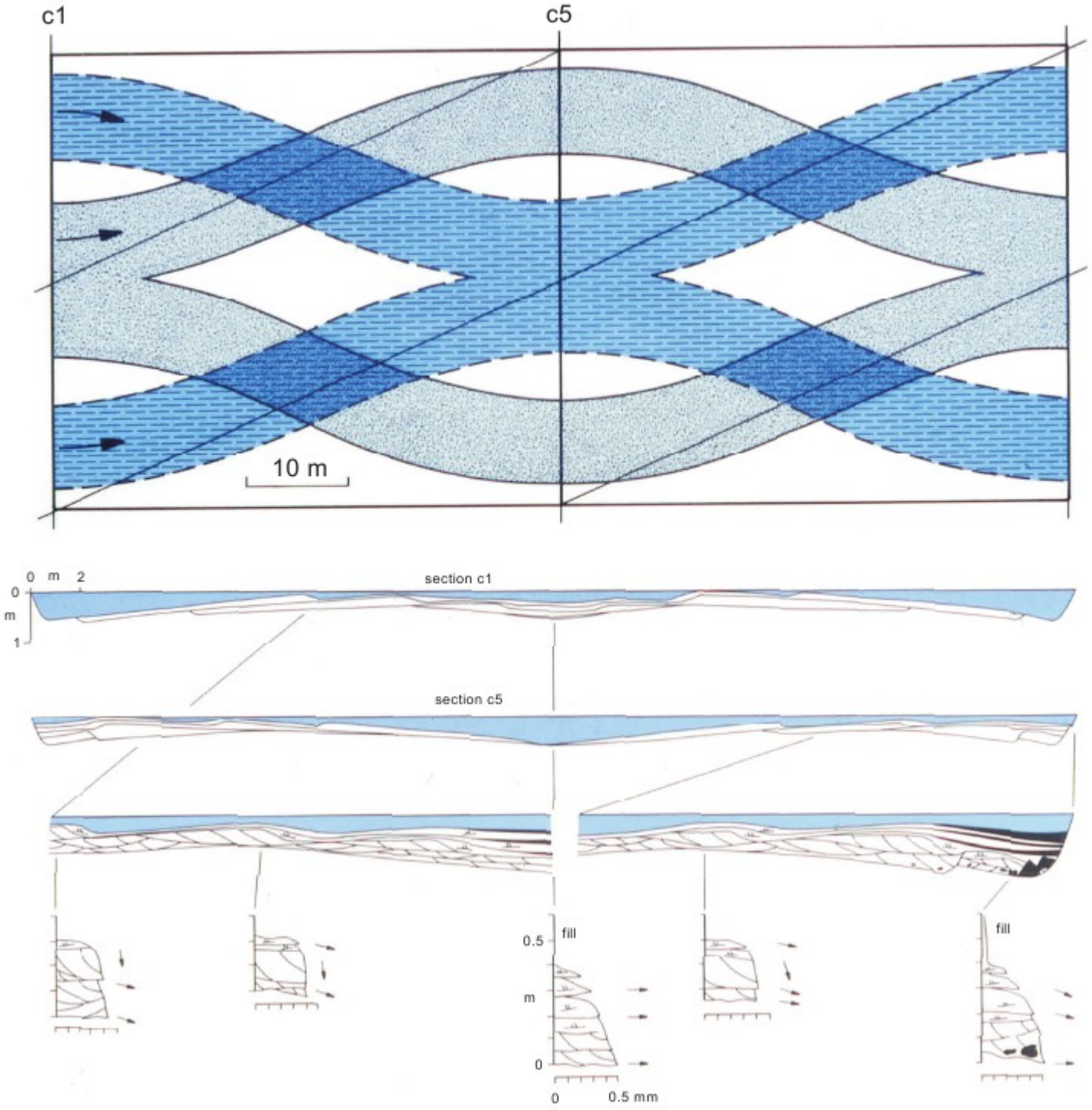

FIG. 16.—Example of quantitative model of braid-bar deposits (Bridge, 1993). Upper figure shows plan geometry of initial braided channels (stippled) and migrated channels (dashed). The braid bar migrated downstream in four discrete increments. Cross sections show basal erosion surface of bar deposits, large-scale inclined strata due to incremental deposition, and details of spatial variation in deposit thickness, grain size, sedimentary structure, and paleocurrents. Deposit thickness and inclination of large-scale inclined strata vary systematically. Bar sequences generally either fine upwards or have little vertical variation in grain size. The dominant internal structure in this example is medium-scale trough cross strata (formed by dunes), with subordinate small-scale cross strata (formed by ripples).

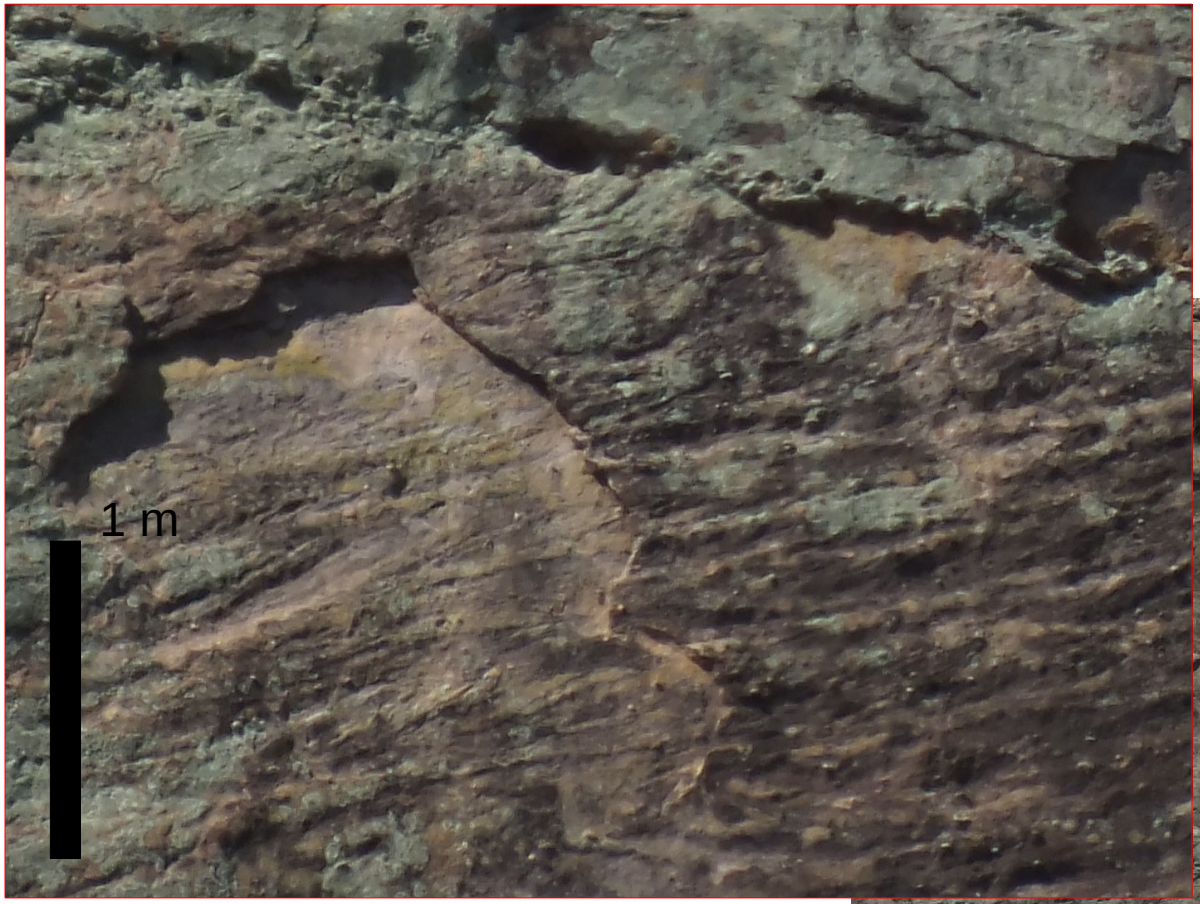
1 m

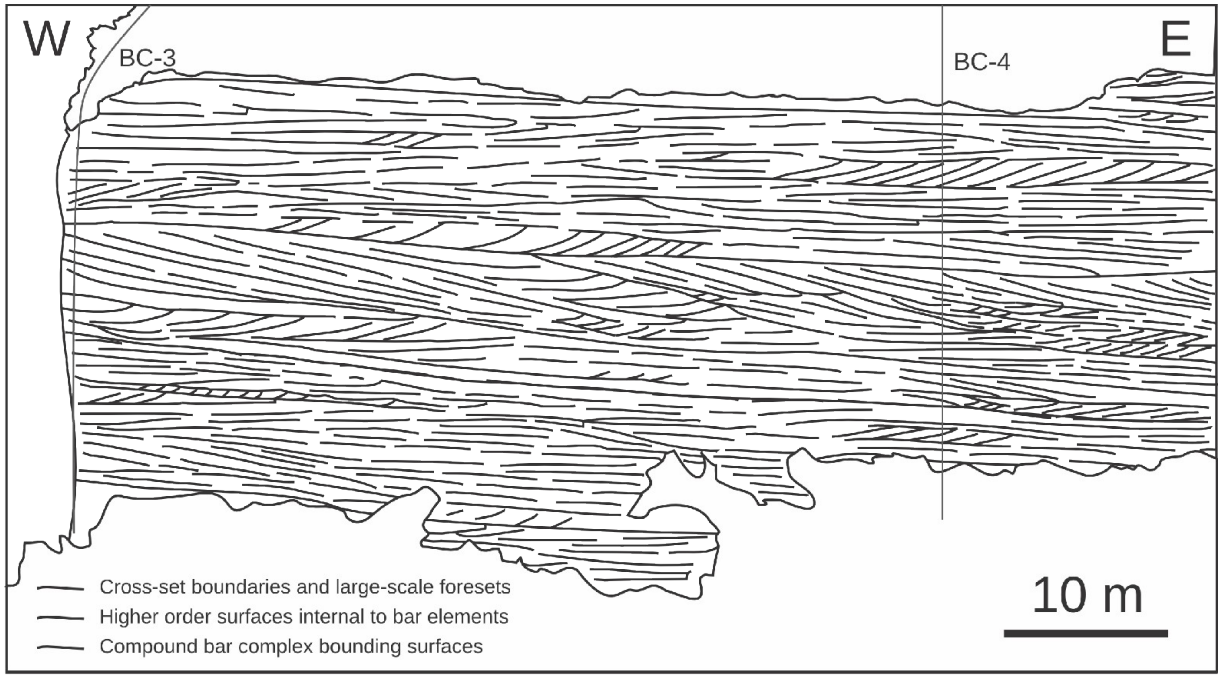
W
BC-3
BC-4
E
Cross-set boundaries and large-scale foresets
Higher order surfaces internal to bar elements
Compound bar complex bounding surfaces
10 m


BC-3 palaeocurrents
n = 51
a.d. = 180°
BC-3 cross-set boundaries
n = 23
a.d. = 305°
BC-4 palaeocurrents
n = 75
a.d. = 215°
BC-4 cross-set boundaries
n = 35
a.d. = 185°

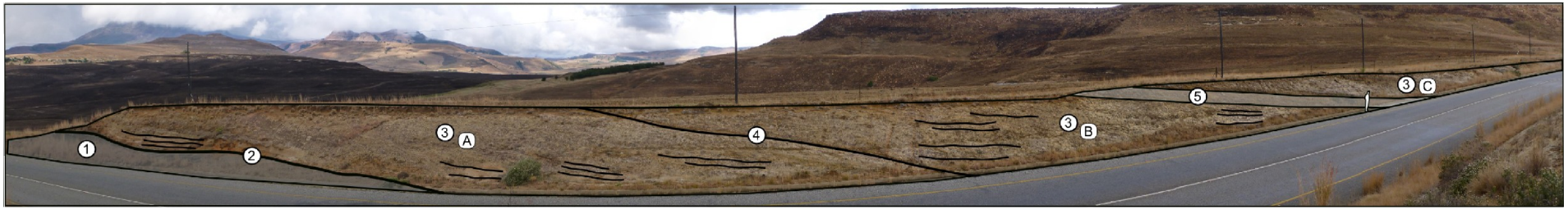

NE SW

1. Thin intercalation of rippled fine sand and organic rich mud
2. Erosional surface with intraclasts (channel base)
3. Coarse sand with compound through cross-strata, cosets tens cm thick
4. Drape of mud
5. Fine sand to silty heterolithic climbing ripples

A- cross-beds and set boundaries

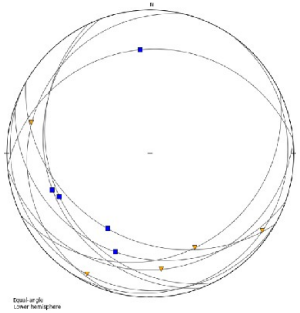

4 - Flood increment surface

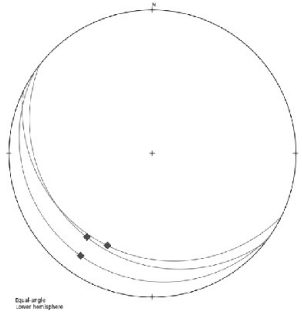

B- cross-beds and set boundaries

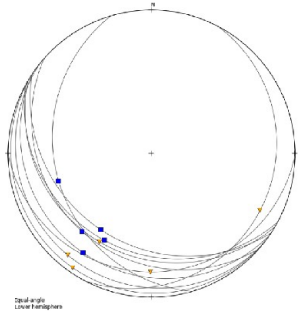

5 - Flood increment surface

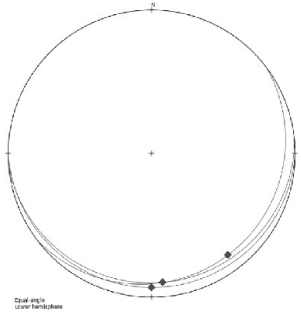

Calculated bar surfaces for A

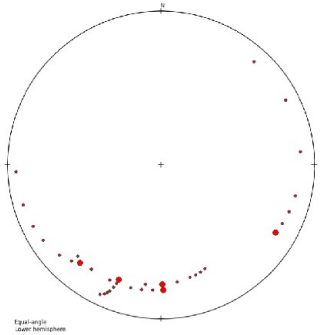

Calculated bar surfaces for B

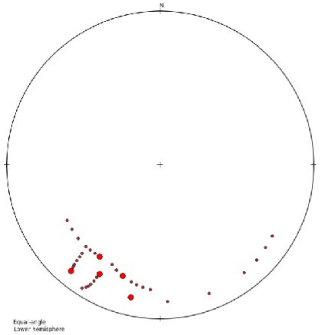

Calculated palaeocurrents (all)

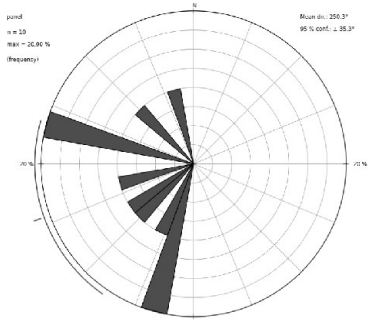

Sistema fluvial – palnícies de inundação

Planícies de inundação fluvial

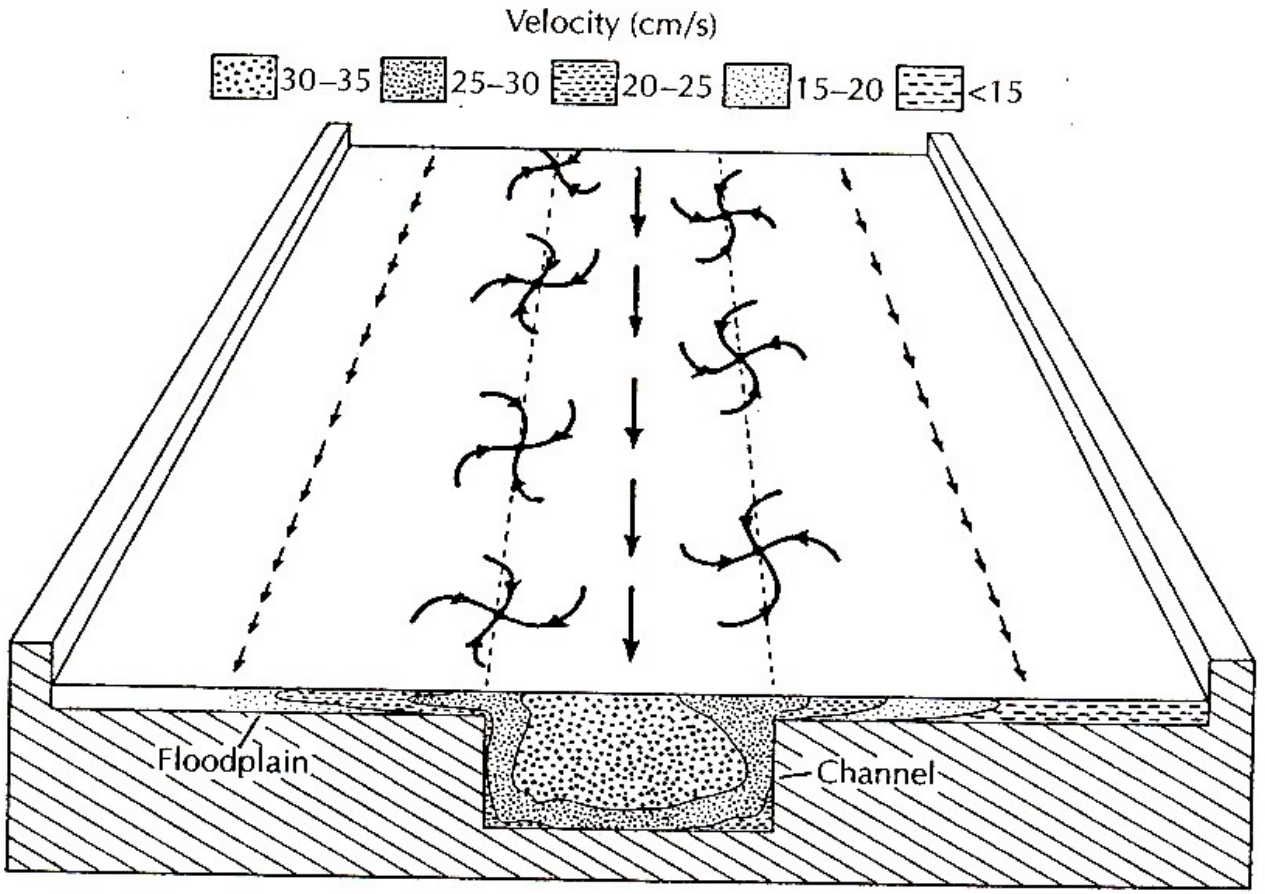

Padrão de fluxo durante enchente em experimento em escala. Notar diminuição da velocidade para as bordas, e formação de redemoinhos na superfície para acomodar a diminuição de velocidade. Extraído de Bridge (2003).

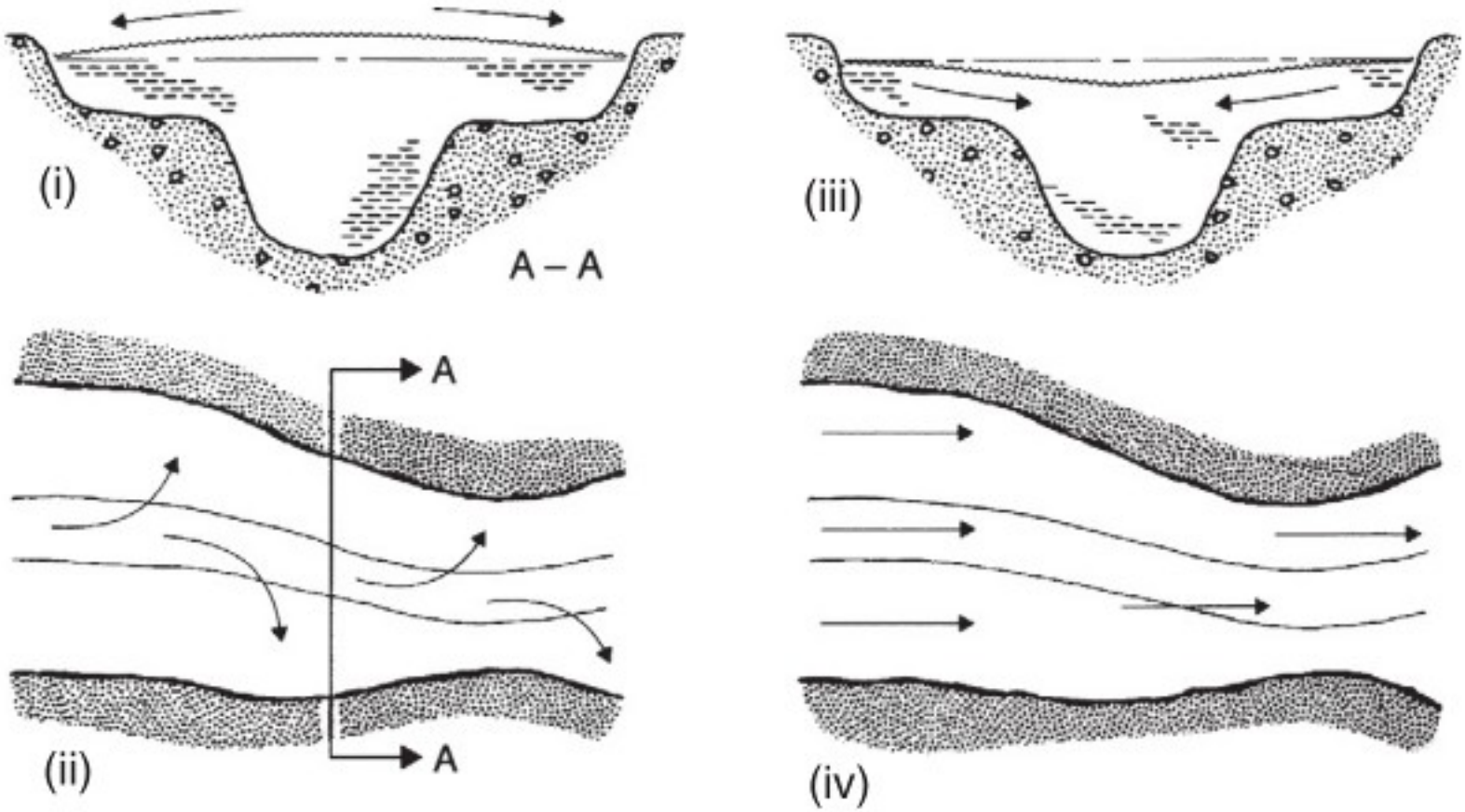

Mudanças de direção de fluxo durante cheia além do canal. (i) Seção e (ii) visão em planta de um canal durante o início da enchente; (iii) seção mostrando o fluxo retornando ao canal acompanhando a queda da descarga; (iv) visão em planta mostrando fluxo a jusante unidirecional, cruzando o canal submerso, durante cheia da enchente (North & Davidson 2012).

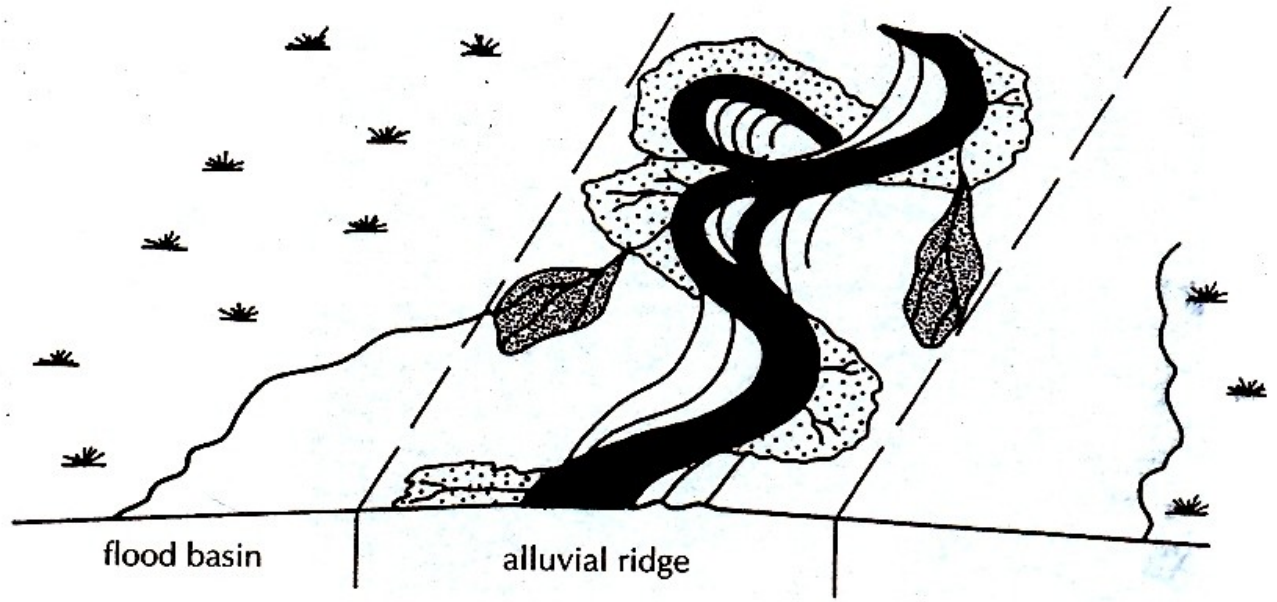

Principais elementos de planícies de de inundação. (Bridge 2003)

Depósito de dique marginal Formação São Sebastião Cretáceo BA

Planícies de inundação lamosas
Mississipiano- Permiano

FIG. 7.—Perennial fluvial style. **A)** Channel incised into floodplain deposits; note the stepped nature of the channel margin. Story boundaries are characterized by intraformational conglomerate–breccias overlying lower contacts of individual stories (white arrow). This sandbody is composed of two laterally amalgamated but vertically offset channel bodies; a second channel margin is observed to the right (black arrow). Hammer (circled) is 0.28 m. Ragged Reef Formation. **B)** View of two multistory sandstone bodies that display an extensive sheet-like architecture separated by well-drained floodplain deposits. Sandstones can be traced > 2 km along strike. The upper story in the lowermost sandstone body is composed of several lateral-accretion surfaces dipping to the left. A crevasse channel occurs in the floodplain deposits and pinches out to the right. Cliff is oriented approximately normal to paleoflow. Geologist is 1.85 m tall. Ragged Reef Formation. **C)** Erosionally based multistory sandstone body with heterolithic lateral-accretion surfaces in the upper story. Springhill Mines Formation.

Journal of Sedimentary Research, 2013, v. 83, 847–872
Research Article
DOI: 10.2110/jsr.2013.58

Planícies de inundação lamosas
Mississipiano- Permiano

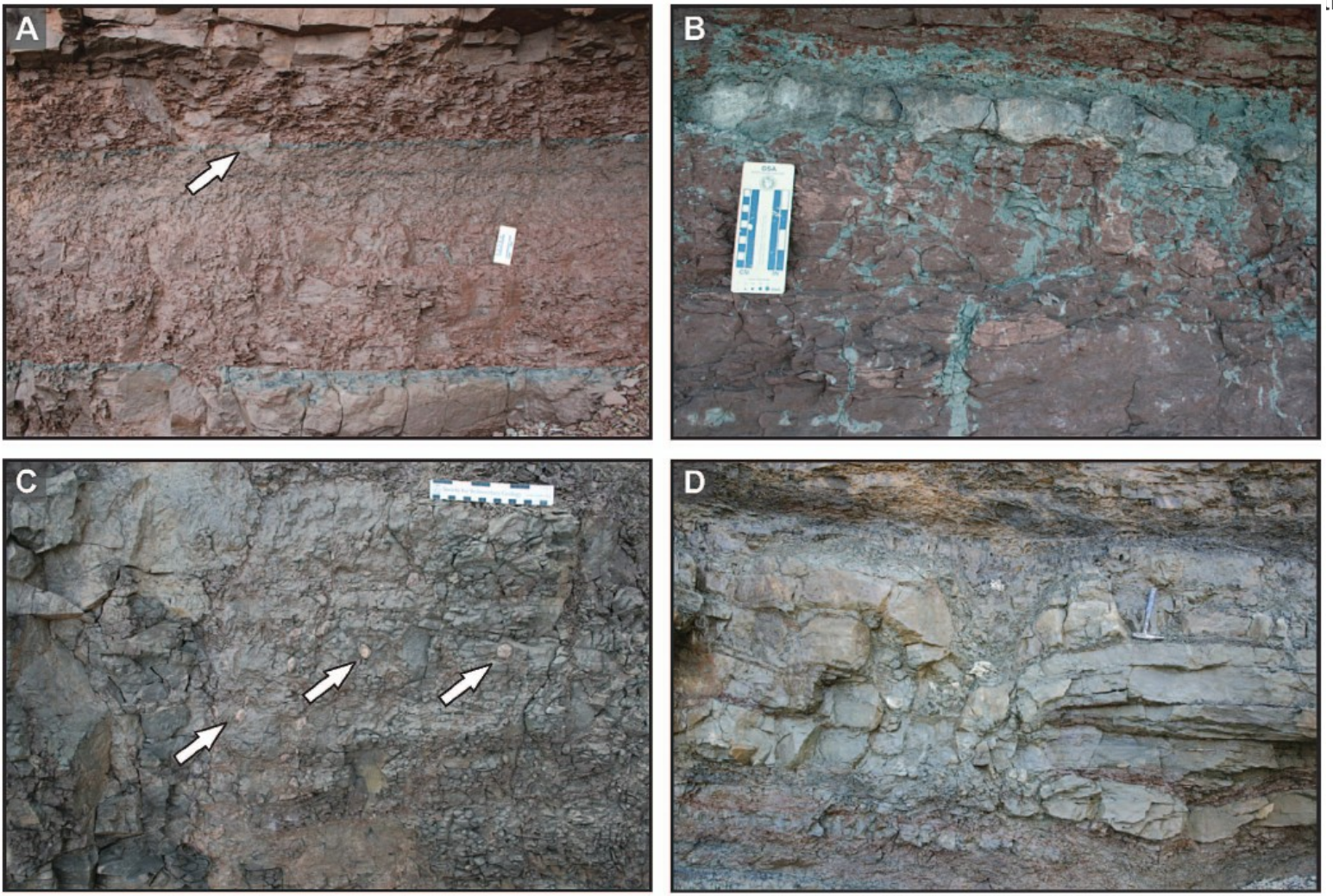

J.P. ALLEN ET AL.
Journal of Sedimentary Research, 2013, v. 83, 847–872
Research Article
DOI: 10.2110/jsr.2013.58

FIG. 9.—Fine-grained facies associations. **A)** Well-drained floodplain deposits (FA B2) with characteristic blocky texture. Mudstones are color mottled and root-penetrated. Note the laterally persistent drab horizon (arrowed) separating the more weakly stratified mudstones below from the stratified mudstones above. Scale card is 0.15 m. Boss Point Formation. **B)** Nodular limestone (calcrete) in red calcic mudstones. Nodules are elongate to bedding and separated by drab claystone. Mudstones are root penetrated and have a more brecciated appearance near the contact with the nodular limestone. Dispersed carbonate accumulations increase upwards. Scale card is 0.15 m. Cape John Formation. **C)** Poorly drained floodplain deposits (FA B1) with a blocky texture and sideritic rhizoconcretions (arrowed). Scale is 15 cm. Boss Point Formation. **D)** Downturned beds around a mud-filled hollow representing a lycopsid tree which decayed, after which the hollow was filled with mud (See Rygel et al. 2005). Hammer is 0.3 m. Springhill Mines Formation. **E)** Carbonaceous nonmarine mudstones (FA D1) with a prominent nodular limestone bed overlain by very carbonaceous poorly drained floodplain deposits (FA B1). Hammer is 0.28 m. Boss Point Formation. **F)** Alternating well-drained floodplain deposits with poorly drained and open-water deposits. Prominent carbonaceous limestone bed (arrowed) overlain by coarsening-upward sequence capped by a sharp-based sheet sandstone interpreted as shallow-water delta deposits (FA D2). Geologist is 1.65 m tall. Joggins Formation.

Planícies de inundação lamosas
Mississipiano- Permiano

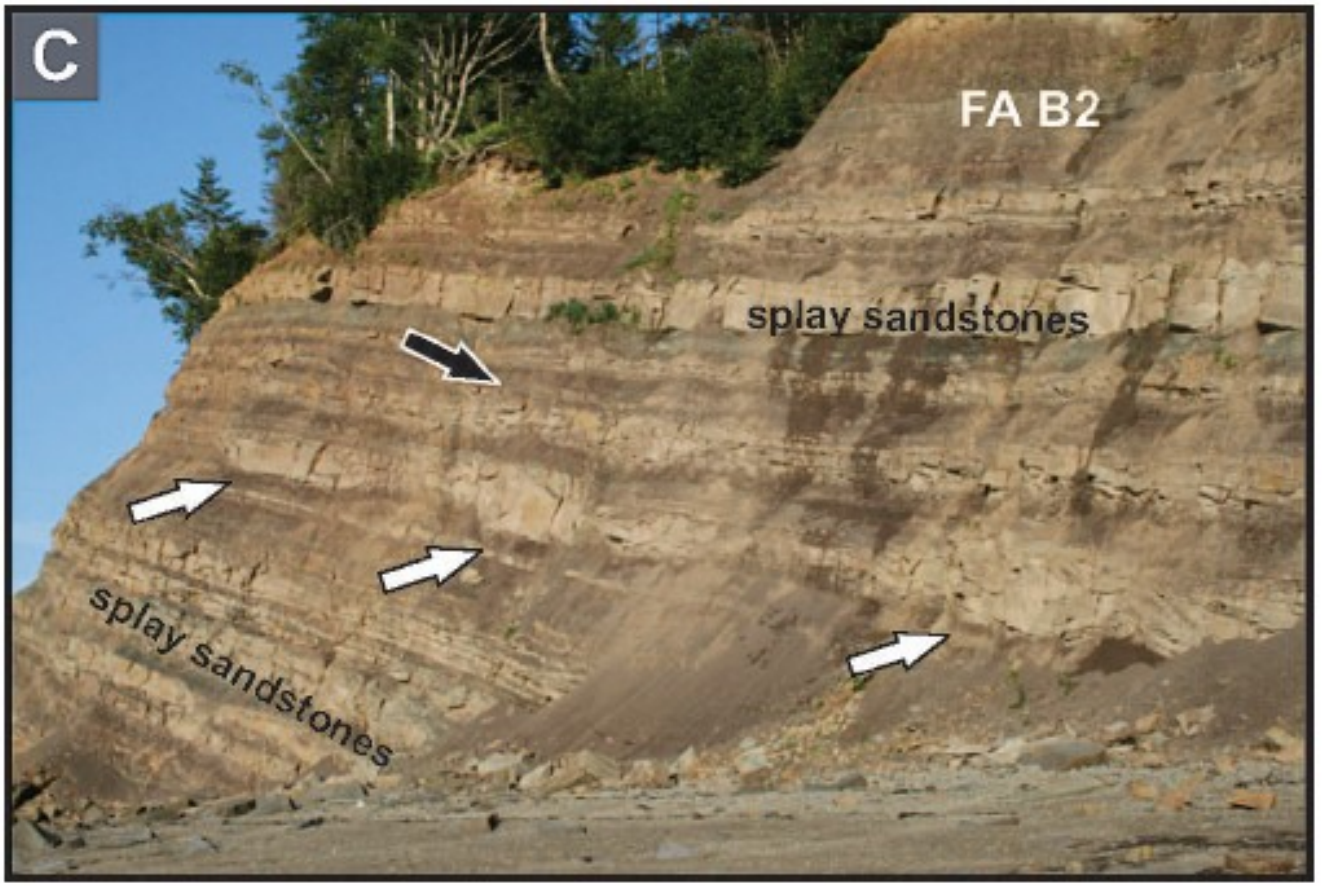

FIG. 11.—Fixed fluvial style. **A)** Single-story, isolated sandbody (at the shore level) with a large heterolithic abandonment fill (white arrow), connected to its associated splay deposits. A second channel body (black arrow) can be seen higher in the cliff face. Geologists are c. 1.6 m tall. Joggins Formation. **B)** Sandstone body displaying minor amounts of lateral accretion with a concentrically filled abandonment fill. Sandstone margin passes into a sandy wing (arrowed) that abruptly pinches out into poorly drained floodplain deposits. Geologist is 1.85 m tall. Springhill Mines Formation. **C)** Several ribbon-shaped sandstone bodies (white arrows) incised into well-drained floodplain deposits from the same stratigraphic horizon. Overlying sandstone body displays subtle levee topography (black arrow). Cliff is 10 m high. Springhill Mines Formation.

J.P. ALLEN ET AL.
Journal of Sedimentary Research, 2013, v. 83, 847–872
Research Article
DOI: 10.2110/jsr.2013.58

Canais em planície de inundação. Formação Marizal

Corpos arenosos retrabalhados por ondas Formação Marizal

Planícies de inundação arenosas – Rio Burdekin Australia.

Ver descrição er

J. ALEXANDER AND C.R. FIELDING Journal of Sedimentary Research, 2006, v. 76, 539–556

Planícies de inundação arenosas

Formação Marizal

Rios de climas secos

- Perene – intermitente – efêmero
- Desconfinado?
- Importância das enchentes
- Ausência de equilíbrio entre forma e processo
- Mito da enchente em lençol e elemento de *sand-sheet*

Examples of extreme rainfall events in drylands (based on Cooke et al., 1993)

Location	Date of event	Mean annual precipitation (mm)	Storm precipitation (mm)
Chicama, Peru	1925	4	394
Aozou, central Sahara	May 1934	30	370/3 days
Swakopmund, Namibia	1934	15	50
Lima, Peru	1925	46	1524
Sharja, Trucial Coast	1957	107	74/50 min
Tamanrasset, central Sahara	Sept. 1950	27	44/3 h
Mt. Dare, central Australia	March 1967	126	149/1 day
Bisra, Algeria	Sept. 1969	148	210/2 days
El Djem, Tunisia	Sept. 1969	275	319/3 days
Alice Springs, central Australia	March 1988	275	205/1 day

Tooth (2000)

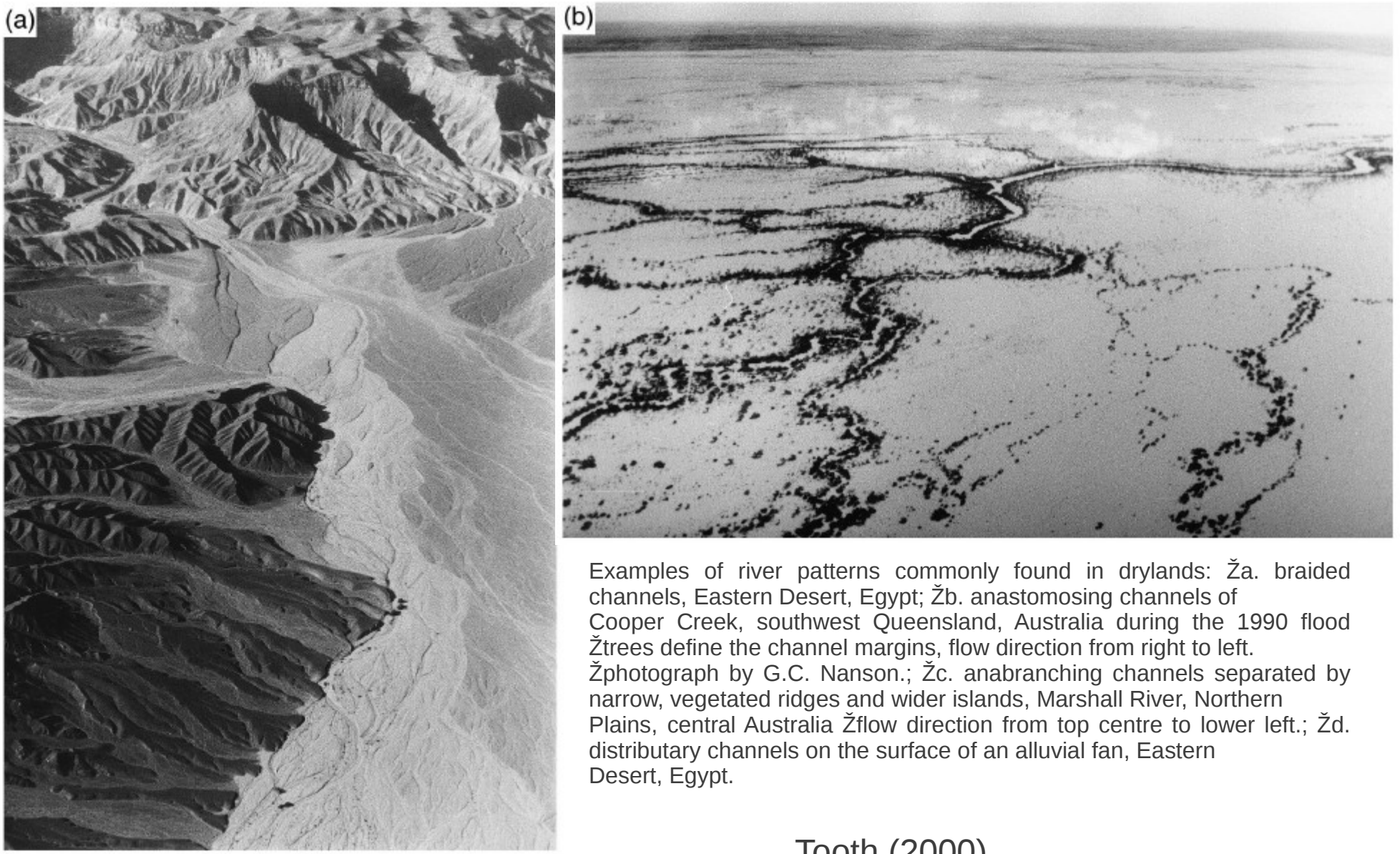

Examples of river patterns commonly found in drylands: Ža. braided channels, Eastern Desert, Egypt; Žb. anastomosing channels of Cooper Creek, southwest Queensland, Australia during the 1990 flood Žtrees define the channel margins, flow direction from right to left. Žphotograph by G.C. Nanson.; Žc. anabranching channels separated by narrow, vegetated ridges and wider islands, Marshall River, Northern Plains, central Australia Žflow direction from top centre to lower left.; Žd. distributary channels on the surface of an alluvial fan, Eastern Desert, Egypt.

Tooth (2000)

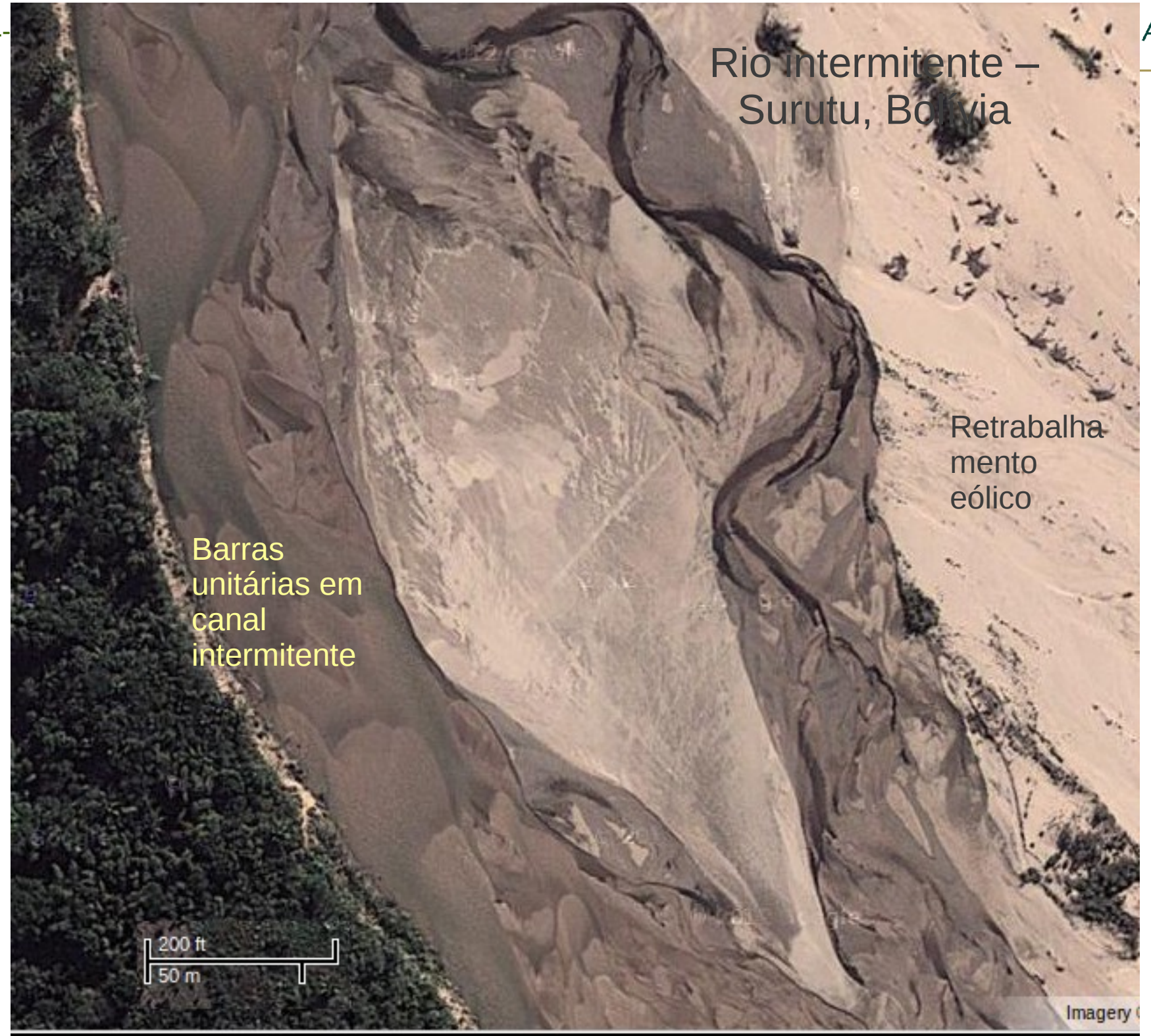
Rio intermitente – Surutu, Bolivia
Retrabalha mento eólico
Barras unitárias em canal intermitente
200 ft
50 m
Imagery

Rio Bolan, Paquistão – efêmero entrelaçado

Rio Bolan, Paquistão – efêmero entrelaçado (zoom)

Rio Leni, Paquistão – efêmero meandrante

Rio Leni, Paquistão – efêmero meandrante (zoom)


(c)

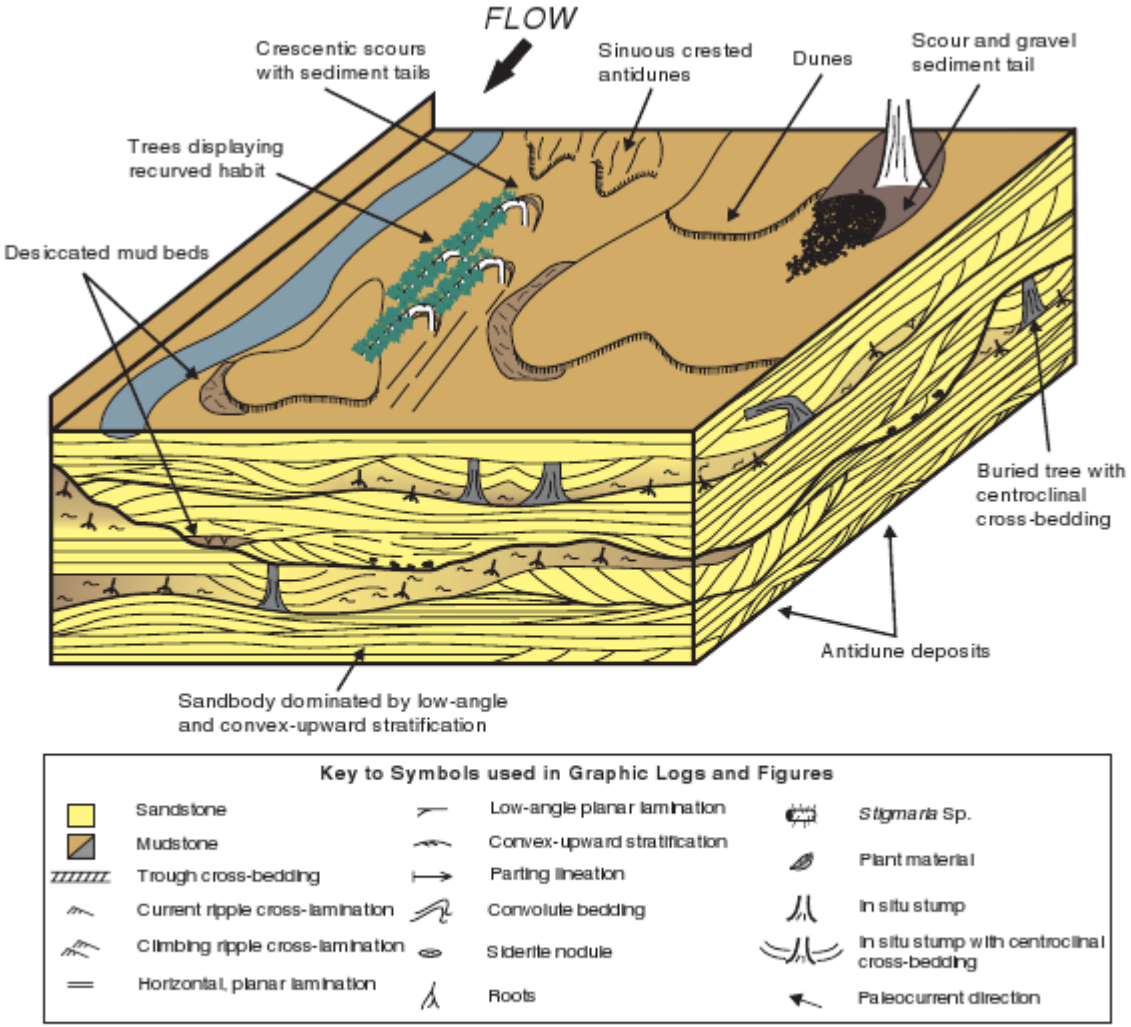

Figure 4. Annotated block diagram summarizing essential elements of proposed facies model for subhumid to semiarid tropical and subtropical fluvial deposits, and key to symbols used.

Fielding et al. (2009)

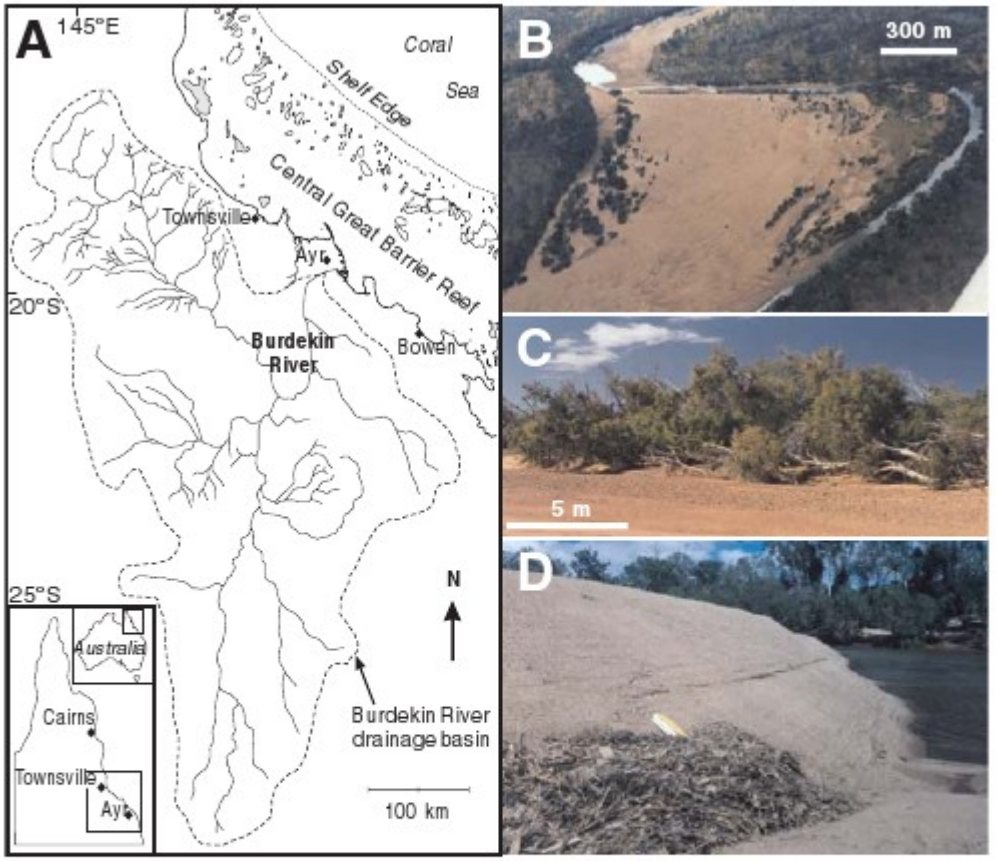

Figure 1. Sedimentological characteristics of modern Burdekin River in subhumid to semi-arid northeastern Australia. A: Map showing location of Burdekin River drainage basin in northeastern Australia. B: Aerial view looking downstream to Big Bend, near Charters Towers, showing mostly dry sandy river bed at low stage, covered by dunes, plane beds, large gravelly antidunes (dark traces in lower center), and linear groves of *Melaleuca argentea*. Sandy river bed is a maximum of 1500 m wide at the near-bend apex. C: View of linear *M. argentea* grove forming the nucleus of a linear bar. Field of view is ~20 m. D: Plant litter against lower foreset of dune near the low-stage channel. Notebook (above plant litter) is 15 cm long.

Fielding et al. (2009)

Fig. 15. Proximal equivalent of playa-lake deposits of the Bitche outcrop (after Bourquin & Durand, 2007). See Fig. 1C for location. Persons for scale are approximately 1.8 m tall.

Bourquin et al. (2009)

- Lamitos maciços = decantação?

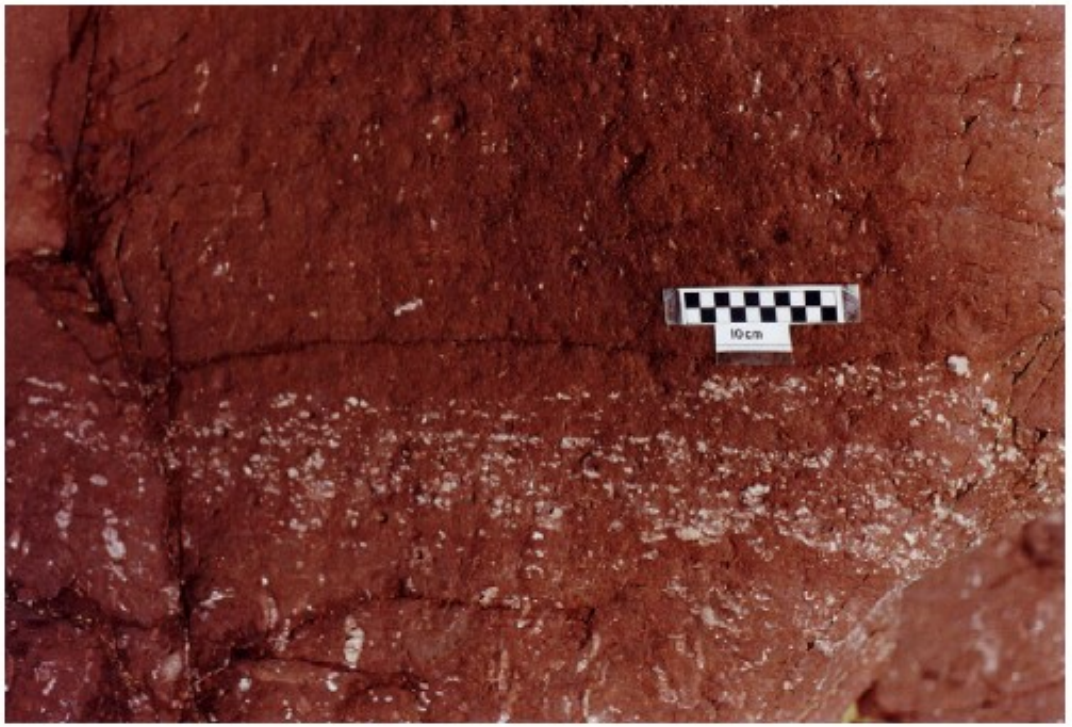

Fig. 8. Mudrock overlying intraformational calcrete clast conglomerate lenses showing low-angle cross bedding from the Moor Cliffs Formation, Freshwater East (Fig. 1; Table 1).

Wright & Marriott (2007)

Alexander, J. & Fielding, C. R. (2006), 'Coarse-grained floodplain deposits in the seasonal tropics: towards a better facies model', *Journal of Sedimentary Research* **76**, 539-556.
Bourquin, S.; Guillocheau, F. & Péron, S. (2009), 'Braided rivers within an arid alluvial plain (example from the Lower Triassic, western German Basin): recognition criteria and expression of stratigraphic cycles', *Sedimentology* **56**, 2235-2264.
Bridge, J. S. (), *Facies Models Revisited*, SEPM (Society for Sedimentary Geology), chapter Fluvial Facies Models, pp. 85-170.
Bridge, J. S. (2003), *Rivers and Floodplains: Forms, Processes, and Sedimentary Record*, Oxford: Blackwells.
Fielding, C. R. (2006), 'Upper flow regime sheets, lenses and scour fills: Extending the range of architectural elements for fluvial sediment bodies', *Sedimentary Geology* **190**, 227-240.
Fielding, C. R.; Allen, J. P. & andMartin R. Gibling, J. A. (2009), 'Facies model for fluvial systems in the seasonal tropics and subtropics', *Geology* **37**(7), 623-626.hitectural elements for fluvial sediment bodies', *Sedimentary Geology* **190**, 227-240.
Mackin, J. H. Concept of the graded river Bulletin of the Geological Society of America, 1948, 59, 463-512
Miall, A. D. (1996), *The Geology of Fluvial Deposits: Sedimentary Facies, Basin Analysis and Petroleum Geology*, Springer. Berlin.
Miall, A. D. (1991), Hierarchies of architectural units in terrigenous clastic rocks, and their relationship to sedimentation rate, *in* A. D. Miall & N. Tyler, ed.,'The three-dimensional facies architecture of terrigenous clastic sediments and its implications for hydrocarbon discovery and recovery', pp. 6-12.
Miall, A. D. (1985), 'Architectural-element analysis: a new method of facies analysis applied to fluvial deposits', *Earth Sciences Reviews* **22**, 261-308.
Miall, A. D. (1974), 'Palaeocurrent analysis of alluvial sediments: a discussion of directional variance and vector magnitude', *Journal of Sedimentary Petrology* **44**(4), 1174-1185.
Nichols, G. J. & Fisher, J. A. (2007), 'Processes, facies and architecture of fluvial distributary system deposits', *Sedimentary Geology* **195**, 75-90
North, C. P. & Warwick, G. L. Fluvial Fans: Myths, Misconceptions, and the End of the Terminal-Fan Model JOURNAL OF SEDIMENTARY RESEARCH, 2007, 77, 693-701
Shanley, K. W. & McCabe, P. J. Perspectives on the sequence stratigraphy of continental strata American Association of Petroleum Geologists Bulletin, 1994, 78, 544-568.
Tooth, S. (2000), 'Process, form and change in dryland rivers: a review of recent research', *Earth-Science Reviews* **51**, 67-107.
Wright, V. P. & Marriott, S. B. (2007), 'The dangers of taking mud for granted: Lessons from Lower Old Red Sandstone dryland river systems of South Wales', *Sedimentary Geology* **195**, 91-100.